Isolation, characterization, and cargo-loading of small extracellular vesicles

by

Hermon Abraham

Submitted in fulfilment of the academic requirements of

Master of Science

Discipline of Biochemistry

School of Life Sciences

College of Agriculture, Engineering and Science

University of KwaZulu-Natal

Pietermaritzburg

South Africa

February 2025

PREFACE

The research presented in this dissertation was conducted by the candidate within the Discipline of Biochemistry, School of Life Science of the College of Agriculture, Engineering and Science at the University of KwaZulu-Natal, Pietermaritzburg, South Africa. The research was financially supported by the Medical Research Council of South Africa.

The content of this work is entirely original and have not been submitted in any form to another university and, except where the work of others is acknowledged in the text, the results reported are due to investigations by the candidate.

Signed: Hermon Abraham

Date: 07 August 2025

As the supervisor, I agree to the submission of this dissertation by the candidate.

Professor C.U. Niesler

Date 12/08/2025

DECLARATION 1: PLAGIARISM

Note that two declaration sections are required if there are papers emanating from the dissertation/thesis. The first (obligatory) declaration concerns plagiarism and the second declaration specifies your role in the published papers.

I, HERMON ABRAHAM, declare that:

(i) the research reported in this dissertation, except where otherwise indicated or acknowledged, is my original work;

(ii) this dissertation has not been submitted in full or in part for any degree or examination to any other university;

(iii) this dissertation does not contain other persons' data, pictures, graphs or other information, unless specifically acknowledged as being sourced from other persons;

(iv) this dissertation does not contain other persons' writing, unless specifically acknowledged as being sourced from other researchers. Where other written sources have been quoted, then:

a) their words have been re-written, but the general information attributed to them has been referenced;

b) where their exact words have been used, their writing has been placed inside quotation marks, and referenced;

(v) where I have used material for which publications followed, I have indicated in detail my role in the work;

(vi) this dissertation is primarily a collection of material, prepared by myself, published as journal articles or presented as a poster and oral presentations at conferences. In some cases, additional material has been included;

(vii) this dissertation does not contain text, graphics or tables copied and pasted from the Internet, unless specifically acknowledged, and the source being detailed in the dissertation and in the References sections.

Signed: Hermon Abraham
Date: 07 August 2025

DECLARATION 2: PUBLICATIONS

Details of contributions to publications/conferences that form part and/or include research presented in this thesis.

Snyman C, Mkhize S, **Abraham H,** Adams T, Ibrahim U, Niesler C. (2025) *Proteins associated with human umbilical cord blood serum small extracellular vesicles (hUCBS sEVs): An investigation to explore the mechanism of their regenerative potential.* Placenta (submitted)

Snyman C, Mkhize S, **Abraham H**, Adams T, Ibrahim U, Niesler C (2024) "*Isolation and characterization of human umbilical cord blood serum extracellular vesicles (hUCB sEVs)"* Joint Meeting of the Extracellular Vesicles Societies in Austria and Czech Republic (ASEV-CzeSEV), 16-17 September, Vienna, Austria

Signed: Hermon Abraham

Date: 07 August 2025

ACKNOWLEDGEMENTS

First and foremost, I would like to express my deepest gratitude to God Almighty for His abundant blessings, guidance, and strength throughout this journey. Without His grace, completing this thesis would not have been possible.

I extend my heartfelt thanks to my supervisor Prof. Carola Niesler. for her exceptional support, insightful guidance, and constant encouragement throughout my research. Your expertise and belief in my potential have been a source of inspiration, and I am truly fortunate to have worked under your mentorship.

I would also like to express my appreciation to lab 44 for their valuable feedback, kindness, and moral support. Sharing this journey with you made even the toughest moments rewarding.

Above all, to my family, I owe the deepest gratitude for their unconditional love, sacrifices, and unshakable faith in me. Your prayers and encouragement have been my constant strength and motivation throughout this journey.

Finally, I thank everyone who contributed to this work, directly or indirectly, for their support and kindness. Your help and encouragement will always be cherished.

ABSTRACT

Small extracellular vesicles (sEVs) are natural lipid-enclosed vesicles that are secreted from living cells and act as mediators of intercellular communication. They are biocompatible nanovesicles that can transport a range of bioactive molecules, including nucleic acids, to target tissues. mRNA-loaded sEVs deliver functional expression of encoded proteins *in vitro* and *in vivo*. They are therefore emerging as promising alternatives to synthetic lipid nanoparticles for the delivery of therapeutic compounds such as mRNA. The current study aimed to isolate and characterize sEVs generated from human embryonic kidney (HEK293) cells and evaluate their potential to delivery mRNA *in vitro*.

Vesicles were isolated from the conditioned media of HEK293 cells using a polyethylene glycol (PEG 6000) based precipitation approach and characterized using tunable resistive pulse sensing (TRPS), transmission electron microscopy (TEM) and western blotting. sEVs with a mean diameter of 119 ± 16 nm and an average concentration of 349,14 x 10^9 particles/ml were successfully isolated and found to have a cup-shaped morphology and contain specific sEV proteins, including CD63, TSG101, and flotillin-1. Cytotoxicity was assessed using the MTS assay to confirm lack of vesicle toxicity for subsequent mRNA delivery. Lipofectamine, a widely used transfection reagent, was used as a positive control to introduce eGFP mRNA into HEK293 cells and compare GFP expression to that following incubation and delivery with sEVs. sEVs were able to deliver mRNA as evidenced by GFP expression in recipient cells at 24-hour post-incubation; strong expression was evident until 48 hours.

In conclusion, HEK293-derived sEVs represent a feasible and minimally cytotoxic mRNA delivery system. The use of PEG 6000 for sEV isolation provided a scalable and cost-effective approach, enabling further exploration of sEV therapeutic potential. The characterization methods and optimized mRNA loading protocols in this study provide valuable insight for advancing sEV-based therapeutic applications. Further studies should focus on optimizing cargo loading to improve delivery efficiency and evaluating long-term *in vivo* safety.

Table of Contents

LIST OF FIGURES

LIST OF TABLES

LIST OF ABBREVIATIONS

ABBREVIATION	EXPANSION
AD	Alzheimer's disease
APCS	Antigen-presenting cells
BCA	Bicinchoninic acid
BBB	Blood-brain barrier
BDMSCS	Bone marrow-derived mesenchymal stem cells
BSA	Bovine serum albumin
BDNF	Brain-derived neurotrophic factor
CNS	Central nervous system
CMOS	Complementary metal-oxide-semiconductor
HCL	Hydrochloric acid
CM	Conditioned media
CTLS	Cytotoxic T lymphocytes
DCS	Dendritic cells
DGC	Density gradient centrifugation
DMD	Duchenne muscular dystrophy
DLS	Dynamic light scattering
ECL	Enhanced chemiluminescence
EGFP	Enhanced Green Fluorescent Protein
EM	Electron microscopy
HEK293	Embryonic Kidney 293
ESCRT	Endosomal Sorting Complex Required for Transport
EVS	Extracellular vesicles
SEVS	Small extracellular vesicles
FCS	Flow cytometry scattering
FBS	Foetal Bovine Serum
FSC	Forward scatter
HNRNPS	Heterogeneous nuclear ribonucleoproteins
HDL	High-density lipoproteins
IA	Immunoaffinity
ILVS	Intraluminal vesicles
LNPS	Lipid nanoparticles
LNCRNAS	Long non-coding RNAs
VLDL	Low-density lipoproteins

MRNA	Messenger-Ribonucleic Acid
MIRNA	Micro-Ribonucleic Acid
MADLS	Multi-angle dynamic light scattering
MVBS	Multivesicular bodies
NTA	Nanoparticle tracking analysis
NP	Nanopore membrane
PTX	Paclitaxel
PBS	Phosphate-Buffered Saline
PEG	Polyethylene glycol
PEI	Polyethyleneimine
PKH26	Paul Karl Horan 26
RNP	Ribonucleoprotein
RNAI	RNA interference
RT	Room temperature
SCM	Serum containing medium
SFM	Serum- free media
SSC	Side scattered light
SEC	Size-exclusion chromatography
SDS- PAGE	Sodium Dodecyl Sulphate Polyacrylamide Gel Electrophoresis
SNARE	Soluble N-ethylmaleimide-sensitive factor attachment protein receptor
SD	Standard deviation
SOP	Standard operating procedure
ISEV'S	The International Society for Extracellular Vesicles
TLR	Toll-like receptor
TEM	Transmission electron microscopy
TBS - T	Tris Buffered Saline - Tween
TAAS	Tumour-associated antigens
TSA	Tumour-specific antigens
TSG101	Tumour susceptibility gene 101
TRPS	Tunable resistive pulse sensing
UC	Ultracentrifugation
UF	Ultrafiltration
WB	Western blotting
WR	Working reagents

Chapter 1: Introduction

1. Extracellular vesicles

Extracellular vesicles (EVs) are lipid-bound nanoparticles released by cells of all species, from prokaryotes to eukaryotes. They are found in biological fluids, as well as conditioned media following their release from cells *in vitro* (Raposo & Stoorvogel, 2013; Yáñez-Mó et al., 2015). Depending on their biogenesis, size and content, EVs are classified into three broad categories: apoptotic bodies, microvesicles and exosomes (Figure 1.1). EVs were initially isolated 50 years ago, by Chargaff and West, from blood and observed as procoagulant platelets (Chargaff & West, 1946). Wolf later referred to them as "*platelet dust*" consisting of vesicles ranging between 20-50 nm in diameter (Wolf, 1967). Approximately 15 years later, small vesicles, released into the extracellular environment after fusion of multivesicular bodies (MVBs) with the plasma membrane, were observed via electron microscopy in rat reticulocyte (immature red blood cells) and later in sheep reticulocyte preparations (Harding et al., 1985; Pan et al., 1985). These were referred to specifically as "*exosomes*" because "*the process seemed to be akin to reverse endocytosis, with internal vesicular contents released in contrast to external molecules internalized in membrane-bound structures*" (Johnstone, 2005; Johnstone et al., 1987).

In contrast to exosomes, which form following inward budding of the plasma membrane through the endocytic pathway and classically have diameters between 50 and 150 nm, apoptotic bodies range in size from 1000 to 5000 nm and are formed following membrane blebbing during apoptosis, while microvesicles are released through outward budding from the plasma membrane and range in size from 100 to 1000 nm (Lu et al., 2018; Stoorvogel et al., 2002) (Figure 1.1). It is important to mention that, when first defined, "*exosomes*" referred to the vesicles in the pellet obtained following 100,000 x g ultracentrifugation (Johnstone et al., 1987). Although this pellet was likely enriched in exosomes, it most likely also contained other vesicles and protein aggregates. Due to this heterogenous nature, more recently it has been suggested that the vesicles in this pellet should be referred to as *small* EVs) (Kowal et al., 2016). Therefore, in this study we will use the term small extracellular vesicles (sEVs), rather than exosomes.

sEVs are now known to be secreted by many different tissues and cell types, including dendritic, tumour, epithelial, B and T cells (Mu et al., 2013; Théry et al., 1999). They have been successfully isolated from various liquid biopsies including blood plasma, serum, saliva, bronchial lavage fluid, urine, breast milk, synovial fluid, semen, and amniotic fluid

(Théry et al., 2018; Yáñez-Mó et al., 2015). Furthermore, they are now commonly isolated from conditioned media, following the culture of cells *in vitro,* highlighting their ubiquitous nature in both *in vivo* and *in vitro* system (Mu et al., 2013; Simpson et al., 2008).

sEVs were initially thought to act as a waste disposal mechanism, removing unwanted components from cells to maintain cellular homeostasis (Johnstone R. M. et al., 1987) (Baixauli et al., 2014) (Hessvik et al., 2016). However, they were later identified as crucial for intracellular communication whereby MHC class I, class II and RNA molecules could be transported to antigen-presenting cells (APCs), resulting in antigen presentation and T cell stimulation (Raposo et al., 1996). This was a pivotal discovery as it emphasized that sEVs actively contribute to immune regulation, rather than acting as passive bystanders. In addition, these vesicles were suggested as natural carriers of cargo that can regulate tissue repair processes, including angiogenesis (Gézsi et al., 2019). Cells were shown to communicate with each other through either the direct release of proteins, including growth factors, cytokines, hormones, into the extracellular environment or through the transport of these factors, as cargo within sEVs, to target cells (Simons & Raposo, 2009; Valadi et al., 2007). In addition, studies have shown that sEVs not only carried proteins, but also mRNA and miRNA as well as lipids which are important for cell-to-cell communication (Simons & Raposo, 2009; Valadi et al., 2007). Importantly, sEVs derived from cancer cells promote angiogenesis, alter the immune system and modify the surrounding parenchymal tissue, aiding tumour progression (Becker et al., 2016). sEVs generated from pancreatic cancer cells and injected via the tail vein of healthy mice induce liver metastasis, highlighting their role in forming the pre-metastasis niche (Kamerkar et al., 2017; Peinado et al., 2012).

Beyond their natural function in intercellular communication, sEVs have emerged as promising tools for therapeutic applications. Their biocompatibility, ability to cross biological barriers, and capacity to transport proteins, lipids, and nucleic acids make them attractive candidates for drug delivery (Somiya et al., 2018; Zeng, W. et al., 2023). Among these, their potential for mRNA delivery has gained significant attention as a promising strategy for gene therapy. mRNA-loaded sEVs could serve as natural carriers for gene delivery, overcoming challenges associated with synthetic nanoparticles, such as immunogenicity and rapid clearance (Mashouri et al., 2019). However, optimizing sEV isolation and characterization methods remains essential to ensure their effective use in RNA-based therapeutics. While various cell sources have been explored for sEV production, HEK293 cells represent an attractive model due to their high transfection efficiency and scalable production potential (Kowal et al., 2016; Théry et al., 2018).

In light of these considerations, this study aims to isolate and characterize sEVs derived from HEK293 cells and evaluate their potential as mRNA delivery vehicles. HEK293 cells were chosen due to their high transfection efficiency and scalable production potential, making them an ideal model for sEV isolation. The study focuses on optimizing the isolation process, followed by comprehensive characterization of the sEVs to confirm their identity based on size, concentration, morphology, and protein markers. The ability of these sEVs to successfully deliver mRNA into target cells will also be assessed to evaluate their suitability as a gene delivery platform. Through these objectives, this study seeks to contribute to the growing body of research on sEV-based RNA delivery, offering insights that could further the development of gene-based therapies.

1.1. sEV biogenesis

EV size, content and membrane composition are highly heterogenous and depend on cellular origin and cargo. For instance, sEVs derived from tumour cells may contain tumour-associated antigens (TAAs) or oncogenic mRNAs, while sEVs derived from healthy immune cells may contain cytokines, co-stimulatory molecules and miRNAs (Gao et al., 2019). The biogenesis of sEVs is a regulated process that ensure selective cargo packaging (Figure 1.1).

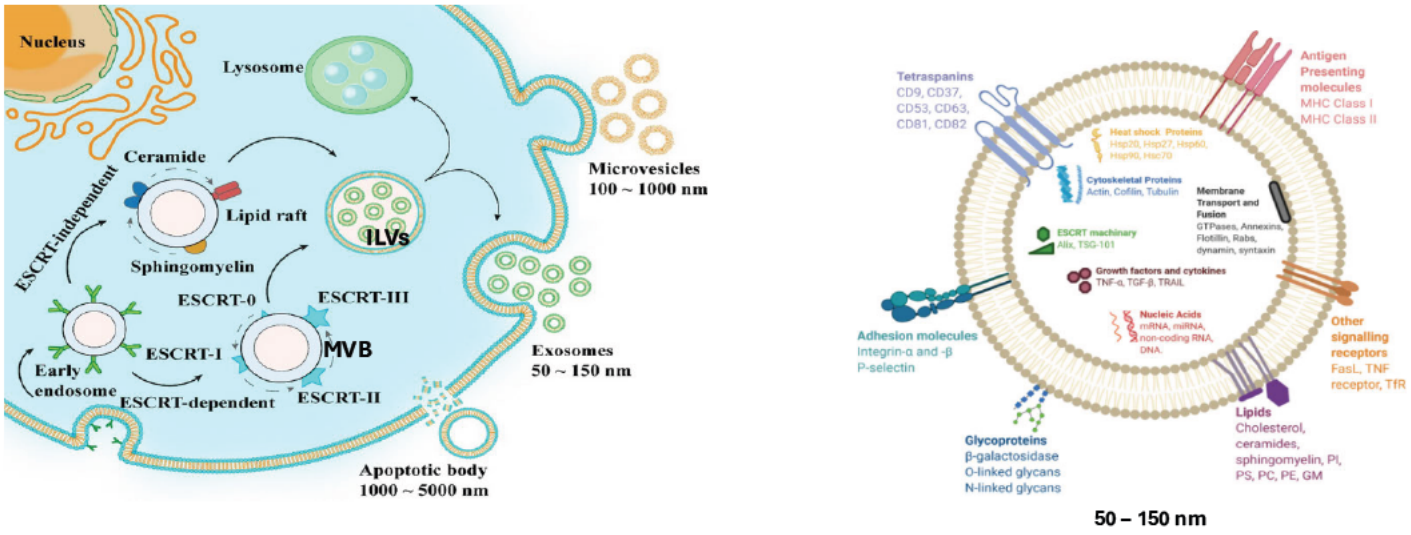

Figure 1. 1: A schematic diagram of the biogenesis and release of EVs. Exosome (small extracellular vesicles; sEVs) formation begins with the inward budding of the endosomal membrane, a process regulated by the Endosomal Sorting Complex Required for Transport (ESCRT) proteins. This leads to the formation of multivesicular bodies (MVBs), which contain intraluminal vesicles (ILVs). MVBs fuse with the plasma membrane, facilitating the release of ILVs (now referred to as exosome or sEVs) into extracellular space. ILVs can also be delivered to lysosomes for degradation. Microvesicles are released by outward budding of the plasma membrane into the extracellular space, while apoptotic bodies are released following membrane blebbing during apoptosis. (Du et al., 2023; Gurung et al., 2021).

During biogenesis sEVs are packed with various cargo components which originate through endocytosis, membrane fusion, and the cytoplasm of the cell of origin; these are transported to early endosomes (Hannafon et al., 2016). Early endosomes undergo maturation into late endosomes, a process that requires the recruitment of regulatory proteins, including Rab Ras-associated binding) GTPases, which control membrane trafficking, and tetraspanins (such as CD9, CD63, CD81), which are enriched in sEV membranes (Jeppesen et al., 2019). This process is critical in the formation of multivesicular bodies (MVBs), which act as a primary site for sEV biogenesis. MVBs are dynamic organelles that contain numerous intraluminal vesicles (ILVs), which serve as the precursors to sEVs (Yáñez-Mó et al., 2015). The formation of ILVs occurs via the inward budding of the MVB membrane, a process regulated by the Endosomal Sorting Complex Required for Transport (ESCRT) machinery. This machinery consists of four protein complexes (ESCRT-0, ESCRT-I, ESCRT-II, and ESCRT-III), which coordinate the budding and sorting of cargo into ILVs (Harris M.S. et al., 2020). In addition to the ESCRT complexes, proteins such as ALG-2-interacting protein X (Alix; which interacts with ESCRT-III) and tetraspanins (which organize membrane microdomains) are crucial for ILV formation and cargo selection (Hurley, 2015; Kowal et al., 2014).

Cargo is sorted into ILVs through the presence of membrane lipids (such as ceramide, cholesterol, sphingomyelin and phosphatidylserine) which are highly enriched in sEV membranes and play a key role in promoting vesicle budding while providing protection from degradation and micro-environment changes (e.g. osmolarity and pH) (Simons & Raposo, 2009; Zhang & Grizzle, 2014). In addition to proteins and lipids, recent research has highlighted a role for RNA-binding proteins, such as heterogeneous nuclear ribonucleoproteins (HNRNPs) and Toll-like receptor (TLR) proteins, in the selective packaging of RNA cargo into sEVs (Hessvik & Llorente, 2018). The lumen of EVs forms a perfect environment for biologically active components (Zomer et al., 2010). After the formation of MVBs, and the loading of their cargo, the next essential step in sEV biogenesis is the fusion of the MVB with the plasma membrane. The fusion process is facilitated by a complex network of proteins, including Rab GTPases and soluble N-ethylmaleimide-sensitive factor attachment protein receptor (SNARE) proteins and results in the release of ILVs into the extracellular space as sEVs (Liu et al., 2017). The MVB can also be degraded via lysosomes, in which case, sEVs are not released. This process is regulated by the ESCRT machinery, Rab GTPases (particularly Rab7), and autophagy-related proteins, which promote MVB-lysosome fusion (Trajkovic et al., 2008).

1.2. sEV structure

sEVs are therefore lipid bilayer-enclosed structures that serve as carriers of proteins, lipids, and nucleic acids, playing a crucial role in cell-to-cell communication. One of their defining features is their overall negative surface charge, primarily attributed to the presence of anionic phospholipids such as phosphatidylserine, as well as sulphated glycosaminoglycans and sialylated glycoproteins (van Niel et al., 2018; Yuyama & Igarashi, 2016). This charge influences their stability in biological fluids, their ability to evade immune clearance, and their interactions with target cells, often facilitating endocytosis or direct membrane fusion (Skotland et al., 2017; Zabeo et al., 2017).

Structurally, sEVs contain a distinct set of proteins essential for their biogenesis and function (Figure 1.1). Tetraspanins (CD9, CD63, CD81) are abundant and play a key role in vesicle formation, cargo sorting, and membrane dynamics (Andreu & Yáñez-Mó, 2014; Kowal et al., 2016). Additionally, proteins such as Alix and tumour susceptibility gene 101 (TSG101) regulate the ESCRT machinery, which is crucial for MVB formation and sEV release (Colombo et al., 2014; Mathieu et al., 2019). sEVs are also enriched in heat shock proteins 70 and 90 (HSP70, HSP90) which assist in protein folding, stress responses, and antigen presentation (Abramowicz et al., 2018). Moreover, cytoskeletal proteins (e.g., actin, tubulin) contribute to vesicle integrity and motility, while integrins mediate interactions with the extracellular matrix and recipient cells (Bebelman et al., 2018).

Lipid composition is another defining factor, with sEV membranes being enriched in cholesterol, sphingomyelin, ceramides, and glycosphingolipids, which contribute to membrane rigidity, stability, and the process of cargo sorting (Llorente et al., 2013; Skotland et al., 2017). Notably, ceramide plays a key role in vesicle budding and release by promoting membrane curvature and facilitating the sorting of cargo into vesicles (Trajkovic et al., 2008). These lipids not only impact vesicle formation but also influence how sEVs interact with recipient cells, often engaging in receptor-mediated endocytosis, macropinocytosis, or lipid raft-mediated uptake (de Gassart et al., 2003; French et al., 2017).

Beyond proteins and lipids, sEVs carry a wide range of nucleic acids, including messenger RNA (mRNA), microRNA (miRNA), long non-coding RNAs (lncRNAs), and DNA, which can be transferred to recipient cells to regulate gene expression (O'Brien et al., 2020; Valadi et al., 2007). The presence of miRNAs is particularly significant, as they can modulate post-transcriptional gene regulation in target cells, influencing processes such as proliferation, apoptosis, immune responses, and tumour progression (Tkach & Théry, 2016; Zhang, X. et al., 2015). The structural and molecular components of sEVs collectively determine their

stability, targeting specificity, and functional impact, ultimately shaping their role in intercellular communication.

1.3. sEVs as intercellular communicators

There are multiple mechanisms through which sEVs interact with their target cells to deliver their cargo as a means of intercellular communication (Figure 1.2). Direct membrane fusion is a major pathway, where sEVs merge with the plasma membrane of target cells, releasing their cargo into the cytoplasm. This process is mediated by surface proteins like tetraspanins (e.g. CD9 and CD63), to ensure efficient delivery (Zhang, J. et al., 2015). Macropinocytosis (which involves the engulfment of sEVs along with extracellular fluid into macropinosomes) and phagocytosis (which enables the internalization of sEVs into phagosomes for pathogen defence and tissue remodelling) both play a key role in immune surveillance and modulation (Swanson & Watts, 1995) (Jiang et al., 2022). Receptor-mediated endocytosis involves binding of sEV membrane proteins or lipids to specific receptors (such as integrins) on the target cell surface ensuring targeted internalization (Zhang, J. et al., 2015). Clathrin-mediated endocytosis involves clathrin-coated pits for sEV internalization; its exact role in sEV uptake remains unclear (Cocucci & Meldolesi, 2011). Caveolin-mediated endocytosis internalizes sEVs through lipid-rich caveolae, providing an alternative, non-clathrin pathway (Doherty & McMahon, 2009). Collectively, these different uptake mechanisms ensure efficient sEV cargo delivery, influencing immune modulation and tissue repair and also playing a role in cancer metastasis; understanding these interactions provide critical insights into sEV-mediated signalling that could address significant gaps in understanding disease progression and therapeutic intervention (Mashouri et al., 2019).

In recent years, due to properties such as low toxicity, good biocompatibility, ability to cross biological barriers and high *in vivo* stability, sEVs have emerged as promising drug delivery vehicles for a range of clinical applications, including cancer therapy, vaccine delivery and the treatment of neurodegenerative disorders and cardiovascular disease (Somiya et al., 2018; Zeng, W. et al., 2023; Zhu et al., 2017). Moreover, the delivery of cell-derived cargo by sEVs might provide tissue-specific biomarkers which would allow for diagnosis of a range of diseases at early stages (Théry et al., 2002). Given that sEVs protect cargo from enzymatic degradation, clinical trials are evaluating the usefulness and effectiveness of sEV-based delivery systems to increase the bioavailability of therapeutic agents (proteins, mRNA, miRNA, siRNA, and chemical drugs) for treating diseases (Lener et al., 2015). Despite technical difficulties in preparation and cargo-loading efficiency, sEVs hold significant potential as a new approach for drug delivery.

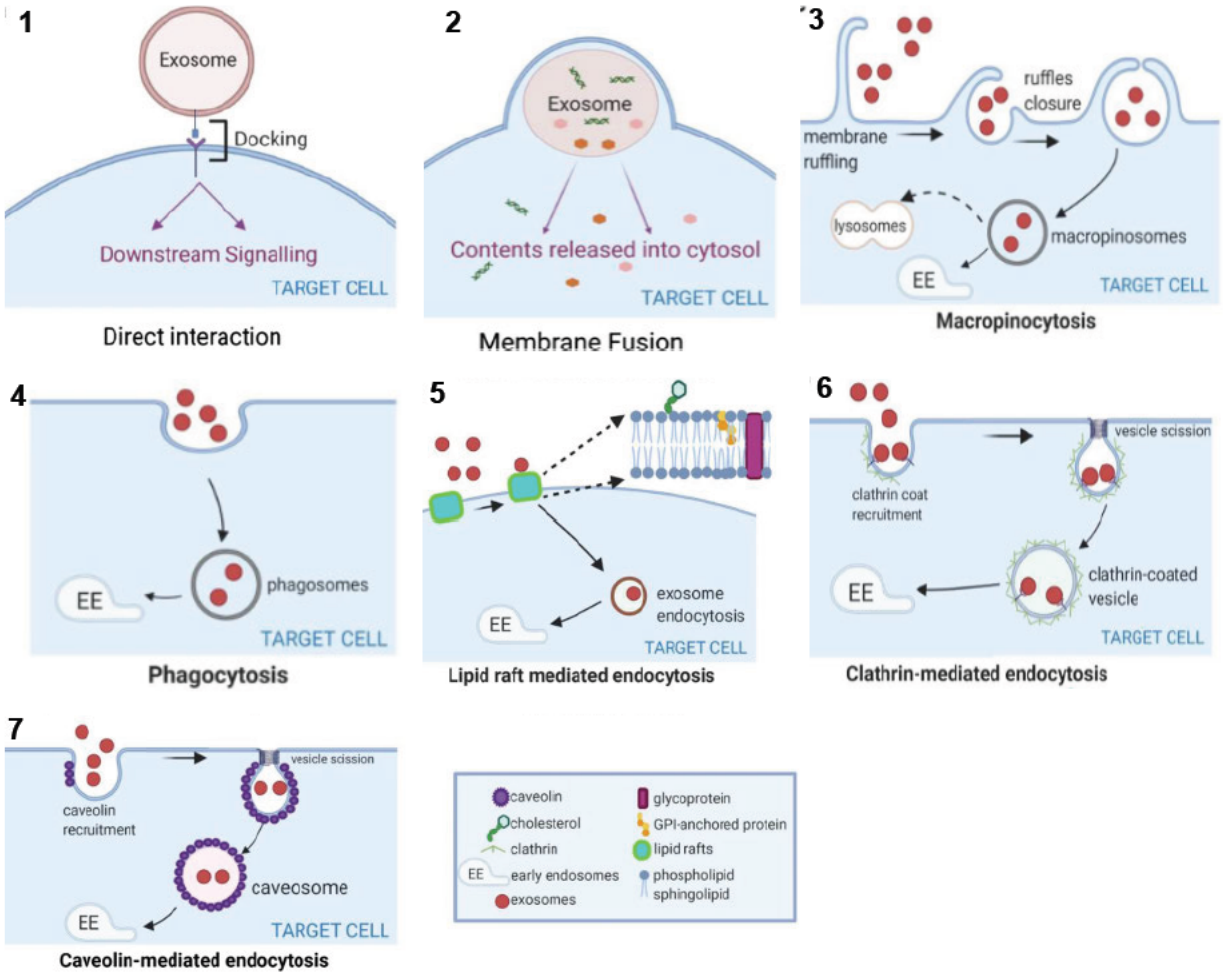

Figure 1. 2: Different mechanism whereby sEVs interact with target cells. 1) Direct interaction, 2) Membrane fusion, 3) Macropinocytosis, 4) Phagocytosis, 5) Receptor-mediated endocytosis, 6) Clathrin-mediated endocytosis, 7) Caveolin-mediated endocytosis. Adhesion molecules including integrins, ICAM-1, CD9 and CD81 on membranes are crucial for sEV binding and uptake (Gurung et al., 2021).

1.4. Isolation of sEVs

The isolation of sufficient, high-quality EVs for downstream purposes is a challenge, and is influenced significantly by the method used to separate sEVs from other nanoparticles (Lin et al., 2018; Shao et al., 2018). Ideal sEV isolation approaches would result in excellent purity and yield with high throughput, and reliable repeatability (Mathivanan et al., 2010). A range of isolation techniques exist, each with specific advantages and limitations (Table 1.1); these will be discussed below.

1.4.1. Ultracentrifugation

Ultracentrifugation (UC) is the '*gold*' standard technique that has been used widely for sEV isolation from complex biological samples (Gudbergsson et al., 2016). The principle of sedimentation relies on separation of particles by their size, shape and density using a series of centrifugal forces and duration of centrifugation (Livshits et al., 2016). Factors that affect the outcome of isolation are the time of centrifugation, acceleration (x g), rotor (*k*) specification and the viscosity of the solution (Sidhom et al., 2020). No universal ultracentrifugation protocol exists, as centrifugal forces and time depend on the volume and density of the solution.

The procedure however generally begins with the removal of higher density particles (such as cellular debris) at low-speed centrifugal forces of (300 - 2 000 xg) for 10-20 minutes (Alzhrani et al., 2021). This is followed by centrifugation of the supernatant at higher forces (10 000 - 16 500 xg) for 30 minutes to remove larger EVs (microvesicles, apoptotic bodies) (Gudbergsson et al., 2016). After this step, the supernatant is centrifuged at 100 000 xg for 2 hours or longer, followed by resuspension of the pellet in a buffer for downstream analysis (Kowal et al., 2017; Momen-Heravi, 2017). Throughout the process the temperature must be maintained at 4 °C to ensure that proteases, DNases, and RNases remain inactive (Wang et al., 2021).

Ultracentrifugation allows for the processing of a large volume of sample, thus increasing potential sEV yield and making it suitable for studies using cell culture media or easily accessible biofluids (Konoshenko et al., 2018; Zeringer et al., 2015). For instance, UC has been used to isolate sEVs from urine to subsequently analyse the presence of biomarkers in patients with prostate cancer and healthy controls (Bryzgunova et al., 2016). By using multiple centrifugation steps, at various speeds, UC can provide high sample purity; it also does not require specialized reagents or antibodies, which simplifies the process (Lobb et al., 2015; Théry et al., 2006). However, while UC is a relatively simple technique, several limitations including contamination of the final product with particles of a similar size to sEVs (e.g. lipoproteins) affect the purity and yield (Linares R. et al., 2015). One of the major drawbacks is the high cost of the ultracentrifuge and specialized rotors themselves; this can make UC less accessible especially for researchers in resource-limited environments (Théry et al., 2006; Witwer et al., 2013). Furthermore, high-speed centrifugation may result in EV aggregation and degradation as high forces can lead to fusion of sEVs, fission of larger EVs and can also lead to loss of their original bimolecular contents (Momen-Heravi, 2017). Additional purification methods such as a sucrose density gradient, size-exclusion chromatography or microfiltration (discussed below) have been applied to increase subsequent sEV purity (Onódi et al., 2018; Théry et al., 2006).

1.4.2. Density gradient centrifugation

Density gradient centrifugation (DGC) is commonly used in combination with ultracentrifugation to isolate sEVs from biological fluids (Karimi et al., 2018). This technique separates sEVs based on size, mass and density, and involves addition of the sample of interest onto a medium (such as sucrose, iodixanol or potassium bromide) with a range of densities that cover the particle densities in the sample (Kuo & Jia, 2017; Onódi et al., 2018). The process first uses filtration (0.22 μm or 0.45 μm) to remove debris and large particles from the sample, which is then layered on the top of a density gradient; a high-speed centrifugal force is applied to allow the different components of the sample to settle to their isodensity zones (Karimi et al., 2018). sEVs have a density of 1.10 – 1.19 g/ml on a sucrose density gradient (Rosado et al., 2019). Therefore, using this method, sucrose solutions of 10%, 20% and 40% (w/v) are layered in a tube, with the higher concentration at the bottom and the lower concentration at the top; the sample can then be layered on top of the gradient. Following ultracentrifugation (100 000 xg or greater) for 16 hours at 4^{o}C, the sEV fraction is collected, washed with buffer and can be subjected to ultracentrifugation at 110,000 xg for further purification (Momen-Heravi et al., 2014).

Compared with differential ultracentrifugation alone, sEV yield obtained by density gradient ultracentrifugation yields higher purity, although contamination with particles of similar density such as lipoproteins or protein aggregation does still occur (Théry et al., 2018; Yuana et al., 2014). For instance, the use of a sucrose density gradient ultracentrifugation on cardiomyocyte culture media successfully isolated sEVs, which were subsequently loaded with miR-133b for delivery to improve cardiac function(Zhang, X. et al., 2015). While this technique has recently gained great popularity for sEV separation, it has some limitations. Depending on the medium used, DGC requires an ultracentrifuge, specialized rotors and buckets, and it is time-consuming (more than 18 hours centrifugation to reach density equilibrium); this leads to DGC not being efficient enough for biomarker analysis in a clinical setting (Konoshenko et al., 2018). Furthermore, intermixing of gradient interfaces and fraction mixing may occur, leading to impurities and contributing to an increased contamination and low yield (Konoshenko et al., 2018).

1.4.3. Poly-ethylene glycol (PEG) Precipitation

One of the earliest approaches to isolate sEVs from complex biofluids was the use of hydrophilic polymers such as polyethylene glycol (PEG) to precipitate vesicles at lower centrifugal forces (Weng et al., 2016). PEG, due to its hydrophilic nature, causes system dehydration resulting in EV aggregation and precipitation due the lipophilic nature of the

vesicles; this produces a pellet of EVs leaving contaminants in the supernatant (Arakawa & Timasheff, 1985). The PEG precipitation method involves the addition of PEG to the sample, incubation and centrifugation at lower centrifugal forces than those needed in UC (Konoshenko et al., 2018). The resulting pellet can be resuspended in phosphate buffered saline (PBS) for further analysis or downstream applications(Abramowicz et al., 2016). Many commercial EV precipitation kits, such as ExoQuick® (System Biosciences), ExoPrep™ (HansaBioMed), Total EV Isolation Kit (Invitrogen), and miRCURY™ (Qiagen) also utilize PEG precipitation for their isolation process (Contreras-Naranjo et al., 2017) (Konoshenko et al., 2018). PEG 6000 itself gives similar results to commercial reagents and is significantly less expensive (Andreu et al., 2016).

Using precipitation for sEV isolation has increasingly gained popularity in recent years due to its simplicity, cost-effectiveness, and high EV yield (Konoshenko et al., 2018). However, PEG has limitations as it may not effectively remove all contaminants, particularly smaller particles (such as lipoproteins) as well as contaminating proteins such as albumin (Lobb et al., 2015; Shieh et al., 2022). For example, PEG-based EV precipitation from blood serum samples obtained from healthy donors yield both higher EV numbers as well as protein content. Which could suggest protein contamination (García-Romero et al., 2019). Additionally, PEG at concentrations above 10% can potentially damage sEV by disrupting the lipid bilayer (Baranyai et al., 2015). To increase the purity of sEV, methods such as size-exclusion chromatography, immunoaffinity or ultrafiltration can be used in combination with PEG precipitation (Lobb et al., 2015).

1.4.4. Size exclusion chromatography

Size-exclusion chromatography (SEC) separates EVs based on their size using a porous stationary phase such as ally dextran (Sephacryl), polyacrylamide, agarose (Sepharose) or cross-linked dextran (Sephadex) (Alzhrani et al., 2021; Kaddour et al., 2021). The sample is passed through the stationary phase of the chromatography column filled with porous beads of different sizes, and with the flow of the mobile phase allowing for the removal of larger contaminants and isolation of smaller EVs (such as sEVs) (Koh et al., 2018). Larger EVs passes through the large channels while smaller EVs get trapped in the pores of the resin and are eluted from the column later. The separated fraction is collected and analysed. Commercially available SEC kits, designed specifically for sEV isolation include the qEV columns (IZON Science). The separation of EVs from various biological fluids will depend on the column length, size, type of resin and flow rate of mobile phase (Ter-Ovanesyan et al., 2021)

SEC has been adapted as a single-step isolation process and over the years modified to support structural integrity, high level of purity, good yield and biological activity of EVs (Sidhom et al., 2020). The use of gravity rather than high g-forces (as required for UC or DGC) ensure that isolated EVs are of superior integrity and high quality (Mol et al., 2017). SEC can also partially remove co-separated contaminants, such as high-density lipoproteins (HDL) and small molecule proteins, however it is difficult to remove very low-density lipoproteins (VLDL) due to their overlapping size with sEVs (Liangsupree et al., 2021). To overcome this Guo *et al*. developed a simplified dichotomic SEC using the CL-6B column, optimizing bed volume and elution steps, making it more suitable for isolating sEVs and proteins from FBS, human serum, and FBS-free cell culture supernatants (Guo et al., 2021). A remaining drawback is that SEC cannot effectively differentiate sEVs from microvesicles of similar size (Sidhom et al., 2020). Additional limitations include of the need for small volumes and a requirement for specialized equipment (such as SEC column especially designed for sEV purification), limiting its practicality for eventual scale-up (Baranyai et al., 2015). Despite these limitations, SEC outperforms the UC and precipitation method in terms of purity and can also be used in combination with these methods to give both high sEV yield and purity (Shu et al., 2020; Ter-Ovanesyan et al., 2021).

1.4.5. Immunoaffinity isolation

Immunoaffinity (IA) is a more specific and targeted method of sEV isolation, which utilizes antibodies or affinity ligands coated on the surface of magnetic beads to capture and purify EVs (Konoshenko et al., 2018). Various magnetic bead-based approaches exist, including magnetic bead-based immunoaffinity chromatography and magnetic bead-based ligand affinity chromatography (Greening et al., 2015). Here, magnetic beads, coated with antibodies that specifically recognise factors on the surface of sEVs, are utilised (Greening et al., 2015; Konoshenko et al., 2018). The sample is incubated with these beads, and the EVs captured through specific protein binding interactions. The sample is then passed through a magnetic column, allowing for the separation of the sEVs from other vesicles. This technique uses antibodies against specific sEV surface markers such as CD9, CD63, CD81 or CD82 (all tetraspanins) or lipids (such as phosphatidylserine) known to be enriched in sEV membranes (Hong et al., 2014; Sidhom et al., 2020).

Immunoaffinity is advantageous as it enables the isolation of the sEV subpopulation with high specificity (Greening et al., 2015). However, the method has limitations as it can be time-consuming and expensive due to the need for specific antibody-based reagents; furthermore, surface markers used to identify sEVs are not completely specific to these

vesicles and therefore the technique may lead to inaccurate conclusions about the nature of the isolated particles (Zhu et al., 2020). It is therefore very important to optimize bead-based immunocapture of EVs as a successful validation can provide a powerful immune enrichment of EVs and can highly be adaptable to the clinic.

1.4.6. Ultrafiltration

Ultrafiltration (UF) can be used as a stand-alone technique or in addition to UC or SEC for isolation, based on the size of EVs. The process involves passing the sample through a membrane filter with a specific pore size (Liangsupree et al., 2021) to separate the sEVs from larger particles. UF, using 10 kDa regenerated cellulose membrane filters (Amicon Ultra-2 10k) yield the highest sEV numbers compared to Amicon Ultra-2 100k filters (Vergauwen et al., 2017). UF is advantageous as it is a relatively simple and fast method, requiring minimal equipment. However, this method has some limitation as it may result in loss of sEVs due to clogging of the filter or shear forces disrupting the integrity of sEVs (Alzhrani et al., 2021; Mathivanan et al., 2010).

Table 1. 1: A summary describing the advantages and limitations of sEV isolation techniques.

Separation approach	UC	DGC	PEG	SEC	A*	UF
Maximum sample volume (~0.1-500 ml)	M	M	H	L	L	H
sEV integrity	M	H	M	H	H	M
Time	H	H	L	M	H	M
Cost	L	H	L	M	H	M
Yield	H	M	H	M	L	M
Purity	M	H	L	H	H	M
Applicability to cell-type specific EV isolation	M	H	M	M	H	M
References	(Théry et al., 2006) (Baranyai et al., 2015; Deville et al., 2022; Lobb et al., 2015; Zhang, Y. et al., 2019)					

L = low; (undesirable for most categories, except cost and time where low is preferred); M = medium; (average); H = high (desirable for most categories, except cost and time where high is not preferred).
*Can be antibody dependent.

1.5. Characterization of EVs

It is critical to not only utilise reliable isolation protocols, but also to use appropriate characterisation techniques to study the size, morphology, concentration, cellular origin, and molecular composition of sEVs (van Niel et al., 2006). Common techniques used to characterise sEVs include nanoparticle tracking analysis (NTA), tunable resistive pulse

sensing (TRPS), dynamic light scattering (DLS), flow cytometry and electron microscopy. These techniques collectively contribute to a comprehensive understanding of sEV properties and facilitate their potential applications as biomarkers for diagnostics or therapeutic carriers to target various diseases.

1.5.1. Nanoparticle tracking analysis.

Nanoparticle tracking analysis (NTA) is a gold standard technique that tracks the Brownian motion of particles in suspension. By analysing the motion of each particle, NTA can provide information about particle size and concentration (Soo et al., 2012). This technique is particularly useful for studying nanoparticles with diameters ranging from 10 nm to 1000 nm. A typical NTA device consists of a laser module, a microscope connected to a sensitive charge-coupled device (CCD), or complementary metal-oxide-semiconductor (CMOS), camera, a hydraulic pump, and a measuring chamber. The measuring conditions (temperature and viscosity) should be specified in the NTA software before the actual measurement. The technique involves the use of a hydraulic pump to inject particles in suspension into the measuring chamber at a fixed flow rate, exposing them to a narrow laser beam. The particles, and their movement over time, are then recorded by a highly sensitive camera installed on an optical microscope (Figure 1.3A). From the acquired video recording, the displacement of each particle is tracked and plotted as a function of time, enabling the calculation of particle size distribution (Figure 1.3B) using the two-dimensional Stokes-Einstein equation. NTA is a powerful tool for calculation the concentration and size-distribution of particles, offering high resolution and sensitivity. If additional lasers are installed, fluorescence can be used to enable the detection of specific antigens on the sEVs (Saveyn et al., 2010). NTA does however face challenges with high-level aggregation when particle concentration is too high due to its reliance on tracking individual sample particles. Additionally, the Brownian motion principle can be distorted by the overlaying effect of larger vesicles masking smaller ones; as a result, the accurate measurements of polydisperse samples can therefore be challenging (Gardiner et al., 2013).

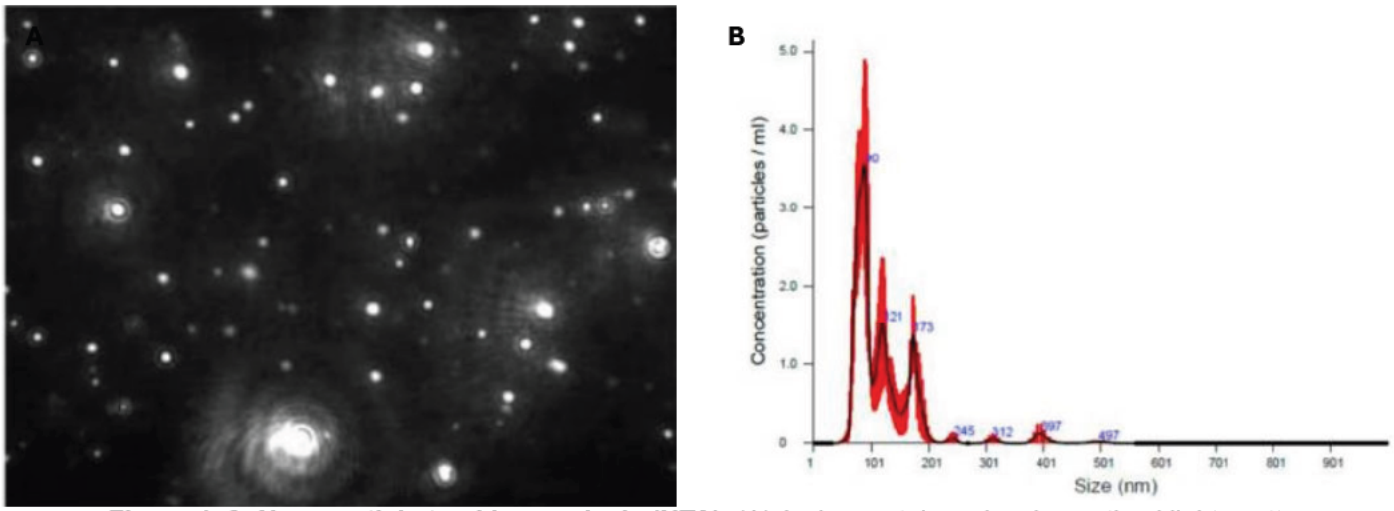

Figure 1. 3: Nanoparticle tracking analysis (NTA). (A) An image taken showing optimal light scatter of EVs of different sizes (white dots) during analysis using NTA video frames (B)The corresponding EVs size and concentration distribution in a graphical format (Serrano-Pertierra et al., 2020)

1.5.2. Tunable resistive pulse sensing (TRPS)

Tunable resistive pulse sensing (TRPS) is a technique that utilizes nanopores to analyse and measure particles based on their size and electrical properties. This technique involves single particles passing through pores while a voltage is applied across the size-tunable nanopore filled with electrolyte (Maas et al., 2014). As particles pass through the nanopore, they displace the electrolyte solution causing a measurable drop in current, known as a *blockade magnitude* (Figure 1.4A). While passing through the pore, the particle resistance increases, which in turn generates a pulse (blockade) that is directly proportional to the particle's size (www.izon.com). The magnitude and frequency of these blockade events provides detailed information on the size, concentration and distribution of EVs present in the sample (Figure 1.4B) (Vogel et al., 2011). TRPS is a valuable tool in the field of EV research as it allows for the accurate measurement of EV size, concentration, and surface charge (also referred to as zeta potential) in a small (35 µl) volume of sample (Vogel et al., 2016). By providing real-time calibration, TRPS helps to address the difficulties encountered when measuring EVs directly in fluid samples. The limitation of this technique includes the risk of pores getting clogged with repeated use of the membrane, and the short lifespan of the nanopore.

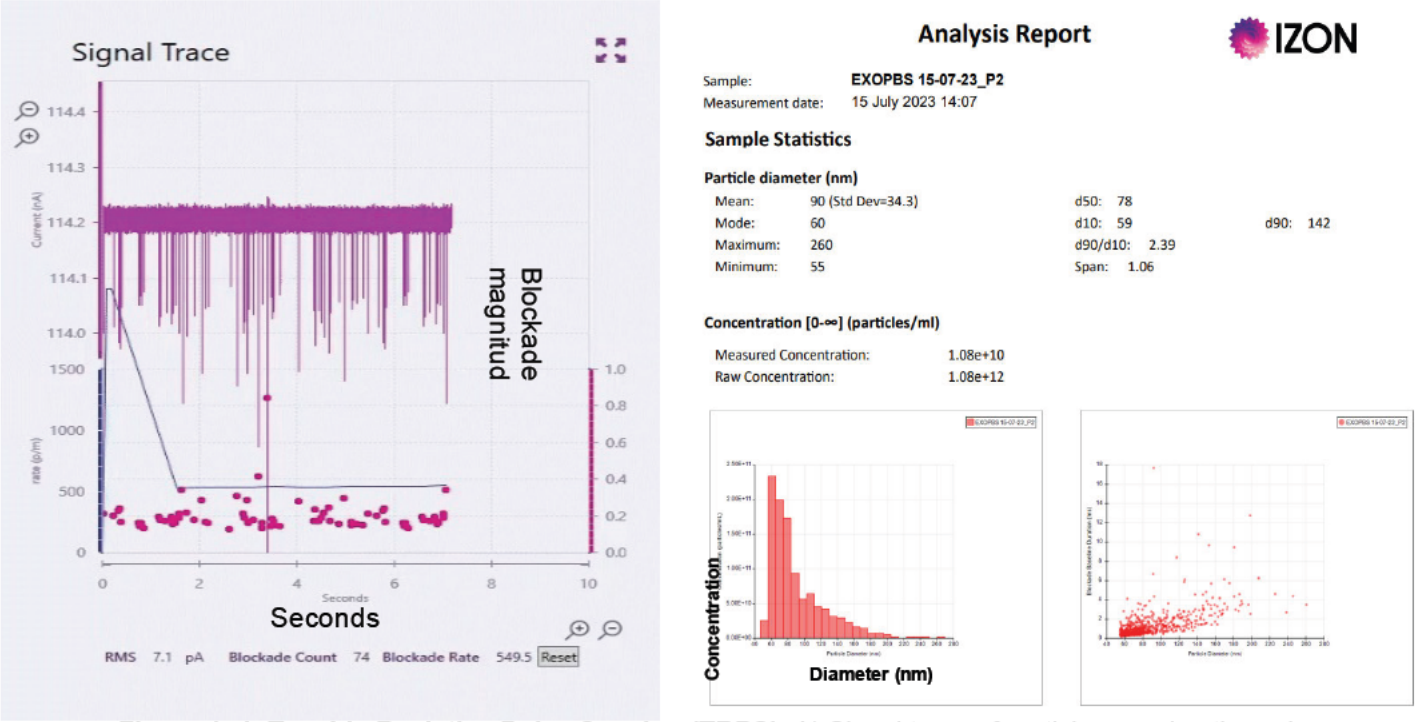

Figure 1. 4: Tunable Resistive Pulse Sensing (TRPS). A) Signal trace of particles passing through the nanopore indicating blockade magnitude (vertical pink lines). The more particles are present, the faster the blockade events will appear. B) Analysis of the size distribution and concentration of a sample following TRPS analysis. Information related to particle diameter (mean, mode, maximum and minimum) and size distribution within the sample (d90, d50, d10) is reflected. The concentration of the diluted sample (measured concentration) as well the original samples (raw concentration) is also indicated.

1.5.3. Dynamic light scattering

Dynamic light scattering (DLS), also known as photon correlation spectroscopy, is a technique where a monochromatic and coherent laser beam scatters through a suspension of particles (Shao et al., 2018). If a particle passes through the beam's path, the laser light is dispersed and scattered (Sitar et al., 2015). The intensity of the scattered light is recorded as a function of time, allowing for the observation of fluctuations due to Brownian motion of suspended particles. During Brownian fluctuations, the distance between scattered light beams constantly changes with time, leading to their interference, visible as minima (destructive interference) or maxima (enhanced interference) in the recorded spectrum. The autocorrelation function of the intensity spectra is generated to obtain a distribution of particle size, which is used for size determination. The analysis is relatively easy when suspended particles do not interfere with each other through collisions or electrostatic forces. The DLS method has the advantage of measuring particles ranging from 1 nm to 6 µm, but is less accurate in suspensions of particles varying in size (Hoo, C. M. et al., 2008). In such cases, even if larger vesicles are present in low quantity, they strongly influence the particle size profile as smaller events becomes difficult to measure due to the fact that larger

particles scatter more light (Maguire et al., 2018). This limitation can be overcome by using a technique called multi-angle dynamic light scattering (MADLS), which allows for more accurate measurements in suspensions with varying particle sizes. MADLS involves measuring the scattered light at multiple angles, which provides a more comprehensive analysis of the particle size distribution (Hoo, Christopher M. et al., 2008). Additionally, advanced data analysis algorithms can be employed to further improve the accuracy of particle size measurements in complex suspensions.

1.5.4. Flow Cytometry

Over the last two decades, flow cytometry scattering (FCS) has increasingly become an accepted technique for EV analysis, with the ability to determine the cellular origin, and morphology of single EVs. This technique involves directing a laser beam with a specific wavelength through a stream of sheath fluid containing suspended particles. The presence of particles causes light scattering; the studied particles can also be labelled with a fluorescent dye or antibody. The detection of small particles based on their light scattering signal is however a major challenge for conventional flow cytometers (van der Pol et al., 2014). Flow cytometers which can detect violet side scattered light (SSC) (15–150°) can however provide information about smaller particles and therefore enable the detection of nanoparticles, showing better detection sensitivity and a lower background than forward scatter (FSC) (Arraud et al., 2015). The CytoFlex flow cytometer is one of the few instruments that can therefore reliably detect particles as small as 100 nm, through the addition of fluorescent beads and the violet side scatter option (Morales-Kastresana & Jones, 2017).

1.5.5. Transmission electron microscopy.

Transmission electron microscopy (TEM) is a technique that creates images through electron interference when an electron beam crosses a sample. TEM requires specimens to be fixed and dehydrated before imaging, and image acquisition is performed under vacuum conditions for optimal resolution. Its high magnification and resolution capabilities facilitate direct visualization of EVs, allowing for detailed observation of their characteristic cup-shaped structure and morphology (Figure 1.5A; black arrow). It also offers the potential for collecting biochemical information through immuno-gold labelling techniques, providing insights into sEV composition (Pisitkun et al., 2004). By selectively labelling specific proteins with gold nanoparticles, TEM allows researchers to visualize their distribution and localization within the sEV structure (Figure 1.5A; yellow arrow). TEM also provides valuable

information about sEV size, shape, and morphology, aiding in their characterization and classification. Electron microscopy (EM) can however cause changes in sEV morphology and damage biological samples. To address these issues, cryo-EM is commonly used for sEV analysis. This method avoids invasive steps like dehydration or fixation, protects specimens from damage, and generates 3-D images, verifying the spherical morphology of sEVs based on cryo-electron tomography (Figure 1.5B) (Adrian et al., 1984; Glaeser & Hall, 2011)

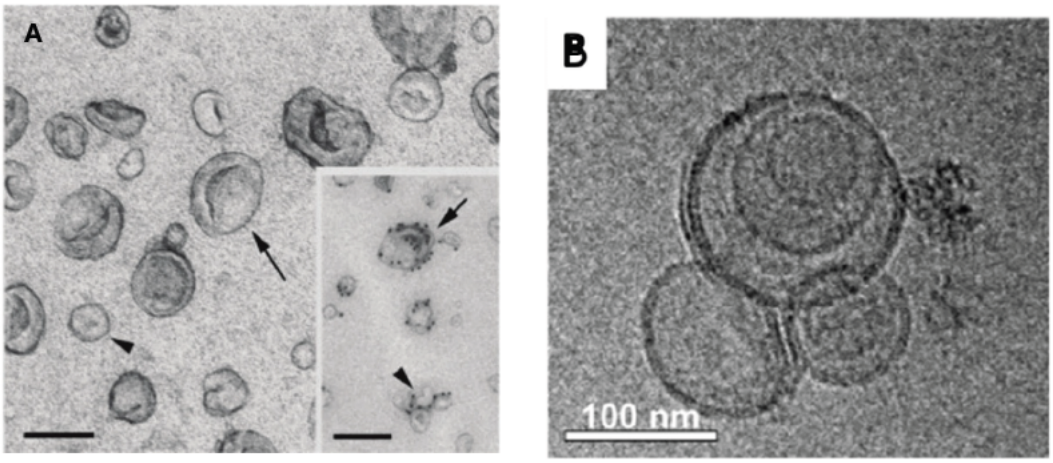

Figure 1. 5: Transmission electron microscopy (TEM) of sEVs. (A) Classical TEM reveals the cup-shaped morphology of unlabelled and gold-labelled sEVs. (B)Cryo- TEM image of sEVs purified from mouse dendritic cells. Black arrows indicate cup-shaped sEVs while yellow arrow indicates immune-gold labelled sEVs. Scale bar = 100 nm (Lima Moura et al., 2020);(Yang J. et al., 2018).

1.6. Cargo loading of sEVs

Efficient drug delivery systems are essential for ensuring the stability, bioavailability, and therapeutic efficacy of various biomolecules, including nucleic acids, proteins, and small-molecule drugs (Yerneni et al., 2022). Cargo loading into delivery vehicles is a fundamental process that enables targeted and sustained release of therapeutic agents, enhancing their stability and bioavailability while minimizing off-target effects (Tenchov et al., 2022). Lipid nanoparticles (LNPs) have been a standard platform widely employed for delivering mRNA, and other therapeutic compounds, due to their ability to encapsulate and protect cargo, as demonstrated by their success in COVID-19 mRNA vaccines (Baden et al., 2021; Polack et al., 2020). However, LNPs present limitations such as potential toxicity, rapid clearance, and challenges in achieving tissue-specific targeting (Jeong et al., 2023). In response to these limitations, small extracellular vesicles (sEVs) have emerged as a promising alternative to LNPs. sEVs are naturally occurring, offering a natural, membrane-bound vesicles that facilitates intercellular communication by transporting proteins, lipids and nucleic acids between cells (Kalluri & LeBleu, 2020). Their biocompatibility, stability, and ability to evade

immune detection make them attractive candidates for therapeutic applications (Patil et al., 2020)

Drug delivery technologies are essential for ensuring the stability, optimal delivery, and therapeutic efficacy of mRNA-based treatments. sEVs present a promising drug delivery vehicle to deliver RNAs, particularly mRNA due to their high biocompatibility, stability, and low immunogenicity (Tenchov et al., 2022). sEVs can provide a protective microenvironment for loaded cargo, protecting it from degradation by extracellular enzymes and macrophages, thereby ensuring its integrity, stability and extended circulation time during transit to target cells (Yerneni et al., 2022). sEV-based mRNA delivery holds great potential in several therapeutic areas, including COVID-19 vaccine development, cancer immunotherapy, and treatment of neurodegenerative disorders (Bebelman et al., 2018; Pang et al., 2020). sEVs, with their lipid bilayer membrane, acts as a natural barrier against cargo degradation and enhance drug utilization by increasing solubility of poorly water-soluble drugs and promoting the simultaneous delivery of drugs (Yerneni et al., 2022). Modified or unmodified sEVs effectively deliver drugs to intracerebral regions for treating central nervous system (CNS) disorders since they can cross the blood-brain barrier (BBB) (Terstappen et al., 2021). However, cargo-loading sEVs remains challenging since these vesicles may already hold endogenous content and the lipid bilayer may restrict loading of exogeneous cargo.

Loading of cargo into sEVs may occur passively during an incubation period or actively using techniques such as electroporation, sonication, extrusion, freeze-thaw cycling, and transfection. These approaches are discussed below, while their advantages and limitation are summarized in Table 1.2.

Table 1. 2: A summary of the advantages and limitations of various sEV cargo-loading approaches.

Methods	Cargo	Advantages	Limitations
Passive incubation	Small molecule drugs, such as doxorubicin and curcumin	Simple and convenient; can be adopted by most laboratories	Low loading efficiency; may affect the EV components
Electroporation	Small molecules drugs (doxorubicin and curcumin); biomolecules, including small RNAs, mRNA, DNAs and proteins	Potential to load macromolecules; loading efficiency is relatively high	Increase EV instability and aggregation; time-consuming
Sonication	Small molecules drugs (doxorubicin and curcumin); biomolecules, including small RNAs, mRNA, DNAs and proteins	Loading efficiency is relatively high	Increase EV aggregation
Extrusion	Small molecule drugs, such as doxorubicin and curcumin	Loading efficiency is relatively high	May lead to variations in zeta potential and

			changes in immunological aspects of EVs
Freeze-thawing	Small molecules drugs (doxorubicin and curcumin); biomolecules, including small RNAs, mRNA, DNAs and proteins	Loading efficiency is relatively high	Time-consuming and may not be ideal for large-scale manufacturing
Transfection	Biomolecules, including small RNAs, mRNA, DNAs and proteins	Load large cargos; efficiency is relatively high	Transfection reagent is required; loading efficiency of commercial transfection may be low

1.6.1. Passive loading via co-incubation

Co-incubation is a simple method that involves two forms of passive loading: incubating sEVs directly with the desired cargo or priming donor cells with the cargo and subsequently generating sEVs from these so-called *primed* cells. Co-incubation also includes cationic loading, where negative charged cargo is electrostatically complexed with cationic molecules such as polymers or cationic lipids, before incubation with sEVs. These approaches have been used to load sEVs with compounds (such as doxorubicin and curcumin) and nucleic acids (such as mRNA and miRNA).

1.6.1.1. Direct loading

It is possible to load sEVs by co-incubating them with the desired cargo at 37°C for a period of time (1-24 hours); this approach can include shaking at 500 xg (Goh et al., 2017). The increase in temperature is thought to increase the fluidity of the lipid membrane, which is beneficial for loading as the cargo interacts with the lipid bilayer of the vesicle. The loading efficiency of a drug is primarily determined by its hydrophobicity and concentration gradient in the solution (Haney et al., 2015). Gong *et al*. demonstrated increased loading of macrophage-derived sEVs with cholesterol-modified miR-159, compared with miR-159 alone (Gong et al., 2019). HEK293 cell- and breast cancer cell-derived sEVs have also been directly cargo-loaded with miR-497 (Jeong et al., 2020) and miR-126 (Nie et al., 2020) using commercial reagent kits. This approach has a high loading efficiency and good molecular stability.

1.6.1.2. Priming of donor cells

Priming involves co-incubation of the cargo with the donor cells such that the cargo is taken up by the cell and then packaged into the extracellular vesicles during endocytosis

(Gebeyehu et al., 2021). Wang *et al*. incubated macrophages with curcumin to generate curcumin-loaded sEVs and found these sEVs were able to cross the blood brain barrier (BBB) for potentially treating Alzheimer's disease (AD) (Wang et al., 2019). Research has demonstrated that co-incubation of mRNA with cells under optimized conditions (reflected in the mRNA concentration, incubation time and donor cell state) can result in successful encapsulation of mRNA in released sEVs (Zhang et al., 2010). Incubation of cells with mRNA has also been found to increase the secretion of sEVs from cells, particularly when cultured in serum-free media, thus enhancing the overall yield and quality of mRNA-loaded vesicles (Auber et al., 2019; Gudbergsson et al., 2019). The advantages of incubation of cargos and cells is that the protocol is easy, highly reproducible, and does not significantly affect the integrity of the sEVs. The drawback is that the loading efficiency is low, and the loading quantitation is challenging due to physicochemical properties of both cargo and sEVs.

1.6.1.3. Cationic Loading

Cationic loading is a passive method for incorporating negatively charged cargo, such as nucleic acids, into small extracellular vesicles (sEVs) using positively charged molecules, including cationic lipids, polymers, or peptides (Chang et al., 2022). This approach relies on electrostatic interactions between the cationic molecules and the negatively charged cargo, facilitating complex formation that promotes cargo incorporation into sEVs through natural diffusion or membrane association (Gurunathan et al., 2019). The primary advantage of cationic loading is its simplicity and efficiency, as it does not require specialized equipment or harsh treatment, thereby preserving sEV integrity. Additionally, cationic-loaded sEVs exhibit enhanced cellular uptake due to electrostatic attraction with negatively charged cell membranes, making this approach particularly suitable for drug and gene delivery applications (Elsharkasy et al., 2020). Despite its advantages, cationic loading presents certain challenges. Excessive positive charge can disrupt sEV membrane stability, alter biophysical properties, and affect biodistribution, potentially compromising the vesicles' functional integrity. Therefore, optimizing parameters such as charge ratio, incubation time, and buffer conditions is critical to balancing loading efficiency with sEV stability (Zakeri et al., 2018).

A commonly employed strategy for cationic loading involves polyethylenimine (PEI), a highly cationic polymer widely used for the passive encapsulation of nucleic acids, including siRNA, mRNA, and plasmid DNA. PEI-mediated loading relies on electrostatic interactions between the positively charged amine groups of PEI and the negatively charged phosphate backbone

of nucleic acids, forming stable PEI-cargo complexes (Uchida et al., 2020). These complexes are then incubated with sEVs, facilitating cargo incorporation either through spontaneous diffusion or membrane association (Mohammadi et al., 2024). The efficacy of PEI loading is highly dependent on the N/P ratio, which represents the ratio of positively charged nitrogen (N) groups in PEI to the negatively charged phosphate (P) groups in the nucleic acid cargo (Zakeri et al., 2018). Suboptimal N/P ratios (below 10:1 for small nucleic acids such as siRNA and mRNA) may result in incomplete complex formation, leading to inefficient loading. Conversely, excessively high N/P ratios can cause aggregation, vesicle destabilization, or cytotoxic effects (Zakeri et al., 2018). Unlike electroporation, a widely used active loading technique, passive PEI loading is ease of use, non-disruptive, preserving sEV morphology and function. However, passive methods generally exhibit lower encapsulation efficiency, particularly for larger or highly charged biomolecules, necessitating careful optimization of the loading conditions (Gurunathan et al., 2019).

1.6.2. Active Loading

1.6.2.1. Electroporation

Electroporation is a simple and efficient method for loading nucleotides (siRNA or miRNA), doxorubicin, and other drugs into sEVs and offers higher loading efficiencies compared to passive methods (Zhang, Y. et al., 2019). A short high-voltage pulse from an external electrical field distributes the phospholipid bilayer of the sEV to produce micro-pores in the membrane. This serves to enhance permeability and allows the cargo to penetrate into the sEV (Johnsen et al., 2014). One study by Momen-Heravi *et al.* tested different electroporation conditions to load miRNA-155 and found that higher voltages (between 0.14 kV to 0.2 kV) and a total sEV protein concentration between 500 µg/mL and 1000 µg/mL resulted in better loading yields for miRNA-155 into B cell derived-sEVs (Momen-Heravi et al., 2014). Rong *et al.* immobilized the target therapeutic peptide CAQK onto the sEV membrane, followed by incubation with siRNA, and then electroporation under specific conditions. Furthermore, induced neural stem cell-derived sEVs exhibited anti-inflammatory and neuro-reparative effects, and the co-delivery of siRNA enhanced the repair following spinal cord injury in mice (Rong et al., 2023). A main drawback of electroporation is however the aggregation and fusion of sEVs after electroporation. Additionally, this method has a low loading rate, may also negatively affects the sEV structure and activity. To reduces the likelihood of aggregation and fusion, the addition of 50 mM trehalose to a solution containing 50 ug total sEV protein results in improved colloidal stability of the sEV solution (Momen-Heravi et al., 2014; Reshke et al., 2020).

1.6.2.2. Sonication

Through sonication, cargo such as drugs, proteins and nanomaterials, can be loaded into sEVs. An ultrasound probe applies a mechanical shear force to deform the membrane of the sEV, which allows cargo to diffuse into the vesicle (Haney et al., 2020; Li et al., 2020). Haney *et al,* successfully incorporated paclitaxel (PTX) into sEVs following sonication, resulting in higher loading capacity than simple incubation strategies (Haney et al., 2020). Tao *et al*., isolated sEVs from milk, dispersed them in PBS, and added Bcl-2 siRNA at a mass ratio (sEVs to siRNA) of 5:1. These sEVs were capable of targeting cancer cells by upregulating apoptotic genes and downregulating metastasis-related genes, inducing apoptosis as well as suppressing tumour migration and invasion (Tao et al., 2020). Sonication is therefore highly effective in nucleic acid loading, but can damage the sEV plasma membrane, causing drug leakage and sEV aggregation.

1.6.2.3. Extrusion

Extrusion-based techniques are used to load drugs into isolated sEVs. This method involves passing a mixture of the drug and sEVs through a syringe-based lipid extruder with 100-400 nm porous membranes at controlled temperatures. This disrupts the sEV membrane and allows for efficient drug loading. Zhang *et al.* used this approach to load PTX into sEVs isolated from human umbilical cord-derived mesenchymal stem cells (huc-MSCs). They extruded the PTX solution mixed with sEVs through a lipid extruder with a pore size of 100 nm and achieved efficient PTX encapsulation into sEVs without any significant alteration in the lipid content of the loaded sEV membranes. The loading efficiency for PTX was recorded to be 14.23 ± 0.25%, higher than the efficiency obtained using the conventional freeze–thaw treatment (6.87 ± 0.4%). The drug-loaded sEVs were successful in inducing differentiation of neural stem cells into neurons (Zhang et al., 2021). Another study reported that sEVs derived from MDA-MB231 breast cancer cells could be loaded with porphyrin using the extrusion method (Fuhrmann G. et al., 2015). Although extrusion is a method with a high cargo loading efficiency, it may compromise the immune-privileged status of sEVs due to recombination of their surface structure (Fuhrmann et al., 2015).

1.6.2.4. Freeze-thawing

The freeze-thaw cycling method is a simple and effective method for loading drugs and nucleic acid into sEVs. It involves repeated cycles of freezing at low temperatures (-80°C or liquid nitrogen) and thawing at room temperature; this causes the sEV plasma membrane to rupture and repair multiple times. This continuous process (a minimum of 3 cycles) allows

the drug to enter the sEVs, achieving successful loading. The freeze-thaw cycle is simple, mild and suitable for mass production due to its stability at low temperatures. However, repeated freeze-thawing could inactivate proteins and induce sEV aggregation. Zhuang *et al*. utilized the freeze–thaw cycling approach, by adding ribonucleoprotein (RNP)solution to sEVs and incubating for 30 minutes at room temperature, followed by freezing with liquid nitrogen, and then thawing at room temperature. This process was repeated three times. Compared to ultrasonication (where an efficiency of 15.34% was reached) under the same conditions, the freeze–thaw cycle achieved a loading efficiency of 37.62%, making it well-suited for subsequent targeted delivery of sEVs (Zhuang et al., 2020). This technique has no significant impact on the structure of sEVs, but it may result in an uncertain loading efficiency therefore methods such as incubation is incorporated with freeze-thawing (Tran et al., 2019).

1.6.2.5. Transfection

Transfection has emerged as the most common strategy for stably loading nucleic acids, proteins, and peptides into sEVs. Transfection involves introducing specific plasmids into cells to express desired nucleic acids, proteins, or peptides, which are packaged into sEVs. Born et al., mixed the pCMV-HOTAIR plasmid with P3000 reagent, and added a liposome solution. Then human bone marrow-derived mesenchymal stem cells (BDMSCs) were incubated with the mixed solution, after which sEVs containing HOTAIR were collected through multiple rounds of centrifugation. The high amounts of HOTAIR in sEVs were effective in promoting angiogenesis and wound healing (Born et al., 2022). Similarly, BCR-ABL siRNA was transduced into human embryonic kidney 293 (HEK293) cells and sEVs subsequently collected from the culture medium (Bellavia et al., 2017). The siRNA-loaded sEVs were able to target chronic myeloid leukaemia cells *in vivo.* However, certain conventional transfection reagents are toxic and may pose safety issues (Xu et al., 2021). Additionally, the direct chemical transfection of sEVs regularly induces sample impurities (such as reagent residues and aggregated vesicles) (Shtam et al., 2013; Wahlgren et al., 2012). Lipofectamine and other lipid-based formulations are commonly used in this context and significantly increase the loading efficiency of mRNA into EVs (Didiot et al., 2016).

1.7. RNA-loaded sEVs

The efficient loading of RNA into sEVs is essential for maximizing their potential as RNA delivery vehicles, especially in therapeutic applications. Understanding how RNA associates with sEVs, either in the lumen, incorporated into the membrane, or bound to the outer surface, is crucial for optimizing both the efficacy and safety of RNA-based treatments (Jiang

et al., 2011; Liang et al., 2020). The lumen, being the internal compartment of the sEV, is the most common site for RNA encapsulation. RNA is typically loaded into the lumen using chemical treatments, such as surfactants and lipid-based agents, that transiently increase the membrane's permeability. These approaches allow RNA to be enclosed within the vesicle's interior, protecting it from external degradation and enhancing its stability for targeted delivery (Zhang, J. et al., 2015). Such encapsulation is particularly important for RNA therapies like mRNA vaccines and delivery of RNA interference (RNAi), where RNA integrity is essential for therapeutic success (Alvarez-Erviti et al., 2011). Techniques like electroporation and sonication have also been employed to improve RNA encapsulation within the lumen, providing further strategies for efficient loading (Lai et al., 2013) (Bobrie et al., 2011).

In addition to lumen loading, incorporating RNA into the membrane of sEVs holds considerable potential for targeted delivery. This method ensures RNA interacts directly with membrane proteins or receptors upon vesicle fusion, facilitating specific cellular interactions (Simons & Raposo, 2009). The use of lipid agents or lipid rafts can enhance this mechanism, ensuring that RNA remains integrated into the lipid bilayer. Alvarez-Erviti et al. (2011) demonstrated that lipid transfection methods effectively load RNA into EV membranes, improving the precision of cell targeting (Alvarez-Erviti et al., 2011). Membrane-associated RNA can be advantageous for therapies where receptor-mediated uptake is crucial, such as in the targeted delivery of RNAi agents or mRNA vaccines.

Although less commonly utilized, loading RNA onto the outer surface of EVs presents another promising strategy. Surface-bound RNA enables rapid recognition by cells, especially in applications like RNA-based vaccines and surface receptor binding. However, surface-bound RNA is more vulnerable to degradation by extracellular RNases, which can limit its stability compared to luminal or membrane-bound RNA (Borniego & Innes, 2023). Nevertheless, the rapid cell-surface recognition enabled by surface-bound RNA can be advantageous for immune activation, particularly in the context of vaccine development (Jiang et al., 2011). This approach facilitates immune system recognition, promoting quicker cellular uptake and enhancing therapeutic efficacy.

A comprehensive understanding of RNA loading mechanisms is essential for improving RNA delivery systems. The localization of RNA within EVs affects its stability, targeting efficiency, and ultimately its therapeutic potential. Despite significant progress, challenges remain in achieving high-loading efficiency, ensuring RNA stability, and optimizing delivery to target cells. Future research should focus on refining loading techniques, addressing the factors that govern RNA compartmentalization, and advancing methods for high-throughput,

scalable RNA loading. As RNA-based therapies continue to evolve, optimized loading strategies will play a pivotal role in enhancing the development of novel, effective delivery systems with improved therapeutic outcomes.

1.8. Therapeutic Applications of sEV-based RNA Delivery

1.8.1. mRNA Vaccines

One of the most significant recent advancements in nucleic acid-based therapeutics is the development of mRNA vaccines, most notably for the prevention of infectious diseases like COVID-19. Unlike traditional vaccines, which introduce attenuated or inactivated pathogens, mRNA vaccines deliver a synthetic mRNA encoding a pathogen protein (such as the spike protein from SARS-CoV-2), triggering an immune response. The Pfizer-BioNTech and Moderna COVID-19 vaccines are prime examples of mRNA vaccines, using lipid nanoparticles (LNPs) to deliver the mRNA encoding the SARS-CoV-2 spike protein to human cells (Baden et al., 2021; Polack et al., 2020). These vaccines have shown high efficacy in preventing severe illness, and death from COVID-19. Ongoing research is exploring mRNA vaccines for other diseases, including influenza, Zika virus, HIV and even cancer (Pardi et al., 2018) where they aim to stimulate a targeted immune response against tumour-specific antigens.

1.8.2. Cancer Immunotherapy

Cancer immunotherapy uses the immune system to fight cancer cells, and mRNA-based approaches are gaining traction. This can be achieved by using mRNA to either encode tumour-associated antigens (TAAs) or enhance their anti-tumour activity (Guevara et al., 2020).

sEVs are also emerging as a promising platform for cancer immunotherapy, particularly for delivering tumour-associated antigens (TAAs) to immune cells, thereby stimulating targeted anti-tumour immune response. By loading mRNA encoding TAAs into sEVs, these vaccines enable recipient cells to produce antigens, which then activate cytotoxic T cells to recognize and destroy tumour cells (Zhang, F. et al., 2019). Additionally, personalized cancer vaccines are being developed where mRNA is tailored to a patient's specific tumour mutations (Ott et al., 2017). Dendritic cells (DCs) are crucial for initiating immune responses, and researchers are exploring mRNA-based approaches within their role in cancer treatment. One strategy involves using sEV-based mRNA encoding tumour-specific antigens (TSAs) to deliver these antigens to DCs and activate cytotoxic T lymphocytes (CTLs) against tumour cells (Huang et al., 2013). sEVs are known for their ability to cross biological barriers and target specific

tissues enhances the effectiveness of mRNA vaccines. Clinical trials are ongoing to test the efficacy of mRNA-loaded DCs in treating cancers such as melanoma and glioblastoma (Sahin et al., 2017). In addition to directly encoding tumour antigens, mRNA can also encode immune stimulatory factors such as cytokines or co-stimulatory molecules. For example, encoding interleukin-12 (IL-12) in mRNA delivered to tumour cells can enhance local immune responses, making tumours more susceptible to immune attack (Nguyen et al., 2020).

1.8.3. Gene Therapy for Genetic Diseases

Gene therapy aims to correct genetic defects by introducing new genetic material into the patient's cells. While traditional gene therapy uses DNA, mRNA therapy offers advantages, such as avoiding permanent genetic modification and introducing the ability to control the duration of gene expression (Wallen et al., 2023).

mRNA therapy is being explored for genetic diseases as a way to replace a non-functional or absent protein in diseases like cystic fibrosis, Duchenne muscular dystrophy (DMD), and haemophilia (Gussoni et al., 1999). For cystic fibrosis, mRNA encoding the CFTR protein (which is defective in cystic fibrosis patients) can be delivered to airway epithelial cells to restore normal CFTR function (Munagala et al., 2021). sEV-based mRNA delivery of dystrophin is being studied for DMD to restore protein production in muscles and potentially target the central nervous system by crossing the blood-brain barrier (Liang et al., 2023).

mRNA therapies are also being developed for liver-related genetic diseases such as haemophilia or alpha-1 antitrypsin deficiency. By delivering functional copies to liver cells, this approach aims to restore the synthesis of missing protein, thereby offering a promising approach (Trepotec et al., 2019). In neurodegenerative diseases, sEVs can be used to deliver mRNA encoding neurotrophic factors, such as brain-derived neurotrophic factor (BDNF), which promote the survival and regeneration of neurons. This approach could help to repair damaged neural networks and slow the progression of diseases like Alzheimer's or Parkinson's (Alvarez-Erviti et al., 2011).

1.8.4. CRISPR-Cas9 Gene Editing

CRISPR-Cas9 gene-editing enables precise genome modification by making targeted cuts at specific locations. While plasmid DNA or viral vectors are commonly used to deliver CRISPR components, mRNA delivery of the Cas9 protein and guide RNA is emerging as a safer alternative, reducing the risks of DNA integration and providing better control over gene

editing. mRNA encoding the Cas9 protein and guide RNA can be delivered to somatic cells to perform precise edits at specific loci. This approach has shown promise for correcting mutations in diseases like sickle cell anaemia and cystic fibrosis, where the therapeutic goal is to edit the patient's own genome (Duan et al., 2021). sEVs could also be used to deliver mRNA encoding CRISPR-Cas9 components to correct genetic mutations in neurodegenerative diseases. For example, mRNA encoding the Cas9 protein together with guide RNA can be delivered to neurons to perform precise genetic editing of disease-causing mutations (Liang et al., 2023).

1.8.5. RNA Interference (RNAi) Therapies

RNA interference (RNAi) is a process in which small RNA molecules, such as small interfering RNAs (siRNAs) or microRNAs (miRNAs), inhibit the expression of specific genes (Hannon G.J., 2002). RNAi-based therapies have been developed to target and silence genes responsible for various diseases, including cancer, viral infections, and genetic disorders (Kim D.H. & Rossi J.J., 2007; Sledz C. A., & Gross C., 2003). In cancer, RNAi therapies can be used to target oncogenes. For example, siRNAs can be used to downregulate the expression of anti-apoptotic proteins or growth factors that drive cancer progression (Elbashir S.M., et al., 2001). Delivery of RNAi-based therapies to tumours can be achieved using lipid nanoparticles, sEVs, or other targeted delivery methods (Wang Y. & Yu. Y., 2020; Kalluri R. & LeBleu V.S., 2020). RNAi has also been explored as a therapeutic approach for viral infections, such as HIV and hepatitis B. By delivering siRNAs targeting viral RNA, it is possible to inhibit the replication of the virus and limit the spread of infection (Rivara M., et al., 2018). For example, siRNAs targeting the HIV-1 genome have shown promise in preclinical studies and early-phase clinical trials (Liu Y. & Zhang L. 2017).

1.9. Challenges and Future Directions

The delivery of nucleic acids, particularly mRNA, has vast therapeutic potential across a wide array of diseases, from infectious diseases and cancer to genetic disorders and diseases requiring protein replacement therapies. Despite the promising applications of sEV-based mRNA delivery, several challenges remain, including the need for efficient sEV isolation, cargo loading, and targeting specificity. Additionally, large-scale production of sEVs

remains a significant hurdle for ultimate clinical use. Research should therefore also focus on improving delivery efficiency of sEV-mediated mRNA, enhancing targeting accuracy to specific tissues, and evaluating the safety and efficacy of sEV-based therapies in clinical trials. sEVs have the potential to play a key role in mRNA-based therapeutics, particularly in personalized medicine and targeted cancer therapies.

1.10. Aims and objectives

The aim of the current study was to isolate small extracellular vesicles (sEVs) from HEK293 cells and evaluate their potential for mRNA delivery.

To achieve this, the objectives were set as follows:

1) Generation and isolation of extracellular vesicles from HEK293 cells
2) Characterisation of extracellular vesicles to confirm their sEV nature by analysing vesicle:
    a) Size and concentration
    b) Morphology
    c) Protein markers
3) Evaluation of the ability of sEVs to deliver mRNA into HEK293 cells.

Chapter 2: Materials and Methods

2.1. General lab reagents and procedures

2.1.1. Cell culture medium

Serum containing medium (SCM) was prepared using Dulbecco' Modified Eagle's Medium (DMEM, Capricorn Scientific, cat. DMEM-HPA; with L-Glutamine), containing 10% Foetal Bovine Serum (FBS) (Capricorn Scientific, cat. FBS-GI-12A) and 2% Penicillin-Streptomycin (Capricorn Scientific, cat. PS-B). SCM was stored at 4°C until use.

2.1.2. PEG 6000

PEG 6000 (3 g; uniLAB, cat. 504018) was dissolved in 10 ml distilled water containing 0.44 g NaCl (MERCK, cat. SAAR5822320M) to make a stock solution of 20% (w/v) PEG 6000 containing 0.5 M NaCl. The solution was vortexed thoroughly until fully dissolved and stored at 4°C until needed.

2.1.3. PBS

Phosphate-Buffered Saline (PBS) stock solutions were prepared free of Calcium and Magnesium by dissolving 0.2 g KCL (MERCK, cat. 104936), 0.2 g KH2PO4 (MERCK, cat. SAAR5043600EM), 8.0 g NaCl, and 1.15 Na2HPO4 (MERCK, cat. 7558794) in 1 L distilled water. The solution was sterilized by autoclaving at 120°C for 20 minutes and stored up to several months at 4°C.

2.1.4. TRPS reagents

The wetting solution was used at a dilution of 1:100 in filtered PBS. The calibration particles used for TRPS analysis are listed in Table 2.1 below:

Table 2. 1: Calibration Particles Carboxylate 100 (CPC100) Information

Reagent	Concentration (particles/ml)	Mean particle diameter (nm)	Batch ID
CPC 100	1.7 x 1013	100	12350B

2.1.5. TBS-T

Tris Buffered Saline - Tween (TBS - T) stock solution was prepared by dissolving 2.42 Tris (Sigma – Aldrich, cat. 648310-M) and 11.69 NaCl in 950 ml distilled water. The pH was adjusted to 7.4 with concentrated hydrochloric acid (HCL; Sigma–Aldrich, cat. 7647-01-0) and added 10% Tween 20 (MERCK, cat. 822184) before autoclaving at 120°C for 20 minutes and stored at room temperature until use.

2.1.6. Blotting buffer

In a large beaker, 6.05 g Tris, 14.4 g glycine (MELFORD, cat. 56406) and 1 g Sodium Lauryl Sulphate (SDS; MERK, cat. SAAR5823610EM) was dissolved in 700 ml distilled water and 200 ml methanol (MINEMA, cat. M5550). The volume was made up to 1000 ml and stored at room temperature until use.

2.1.7. Tris-HCl buffer

A 1M Tris-HCL buffer was prepared in a 1L beaker, 121.14 g of Tris was dissolved in distilled water and mixed using a magnetic stirrer. The pH was adjusted to 8.5 with concentrated hydrochloric acid (HCL) and the total volume adjusted to 1L. The solution was stored unopened at room temperature until use.

2.1.8. Stain stock solution

To prepare 1% (m/v) Coomassie Dye blue R-250 stain stock solution, 1 g of dye in 100 ml dH2O was dissolved and stirred for 1 hour at RT and subsequently filtered through Whatman No.1 filter paper. For a staining solution 62.5 ml stain stock solution was mixed with 250 ml methanol and 50 ml acetic acid and the volume adjusted to 500 ml with distilled water. Solution was stored at room temperature in a brown beaker to protect from direct light.

2.1.9. Destaining solution

In a 1L beaker, 70 ml acetic acid and 50 ml methanol was mixed, and the solution volume adjusted to 1L with distilled water.

2.1.10. Mowiol mounting medium

Mowiol (9.6 g; Sigma–Aldrich, cat. 81381) and glycerol (24 g; Sigma–Aldrich, cat. 49770) were mixed in a beaker with 24 ml distilled water and incubated at room temperature for 2 hours. Following this, Tris-HCl buffer (48 ml) was added and dissolved using a magnetic stirrer on a hot plate set to medium-low heat. Excess powder was pelleted using centrifugation at 5000 xg for 15 minutes. The supernatant was removed and stored in 500 µl aliquots in Eppendorf tubes at -20°C until use.

2.1.11 Uranyl acetate

A stock solution of 2% (w/v) uranyl acetate was prepared by dissolving 1 g uranyl acetate (SPI-CHEM, cat. 1070911) in 50 ml double-distilled water in a flask and slowly mixing until crystals were completely dissolved. The flask was covered with aluminium foil to protect from light and stored for up to 4 months at 4°C. Before use, the solution was filtered through a 0.2-µm filter.

2.1.12 Cell culture

Embryonic Kidney 293 (HEK293) cells were obtained from laboratory stocks in liquid nitrogen. Cells were cultured under sterile conditions in a level 2 biological safety cabinet (Haier Biomedical, product EN12469:2000). Surfaces were maintained in a sterile condition using UV light exposure for 30 minutes daily and 70% ethanol for cleaning purposes.

2.1.13 Cell thawing

A cryogenic vial containing the cell line was selected from the liquid nitrogen dewar and thawed using a water bath set to 37◦C. Cells were then transferred into a sterile 15 ml falcon tube and containing fresh prewarmed medium. The cells were centrifuged at 3200 xg for 5 minutes at room temperature, using the bench top centrifuge (DSC-158T; MRC, serial. 0608318). The supernatant was discarded, and cells resuspended in 1 ml SCM, 20 µl sample was removed and cells were counted using a cell counter (Invitrogen Countess 3 FL, ThermoFisher, AMQAF2000). The desired number of cells were then transferred to T75 tissue culture flasks containing 10 ml warm SCM and maintained in a 37^{o}C and 5% carbon dioxide (CO_2) incubator (ESCO, serial. 2018-124079). Adherence and cell growth was confirmed using the Olympus CKX41 brightfield microscope.

2.1.14 Cell passaging

Cells were passaged once they are 70 – 80% confluent. The medium was aspirated from the flask and cells rinsed twice with 5 ml warm PBS followed by the addition of 2 ml warm Trypsin-Versene (BioWhittaker, 17-161E) for 3 minutes in the 37°C, 5% CO_2 incubator. Once cellular detachment was confirmed using the brightfield microscope, the trypsin was inactivated by adding an equal volume (1 ml) of serum containing media and mixing thoroughly via pipetting. The mixture was pipetted into a 15 ml tube and centrifuged at 3200 xg for 5 minutes (DSC-158T). The cell pellet was resuspended in growth medium as required. A 20 µl sample was removed and cells were counted using a cell counter (Invitrogen Countess 3 FL, ThermoFisher, AMQAF2000). A dilution was preformed to achieve the required number of cells to be seeded, and the remaining cells were either frozen or divided into a new flask with fresh growth media.

2.1.15 Cryopreservation

Stocks of HEK293 cells were cryopreserved for later use. Briefly, cells (600 000 cells per 500 µl) were resuspended in freezing media containing 10% Dimethyl sulfoxide (DMSO; Sigma – Aldrich, cat. RNBK7771) and 90% FBS (Capricorn Scientific, cat. FBS-GI-12A). The resuspended cell volume was then transferred into labelled cryogenic vial and immediately placed in Mr Frosty freezing container filled with isopropyl alcohol to freeze overnight at -80^{o}C before being transferred to liquid nitrogen for long-term storage.

2.2. Extracellular vesicles

2.2.1. Generation and isolation

Extracellular vesicles were generated from HEK293 cells using a protocol adapted from previously (Lobb et al., 2015) with modification as illustrated in Figure 2.1. Cultured cells (T175 culture flask; cat.709001) were washed twice with 10 ml PBS, followed by trypsinization with 2 ml Trypsin-Versene (1X; BioWhittaker, cat. 17-161E) for 10 minutes at 37°C in a CO_2 incubator (ESCO; 170L). Trypsin was then neutralized with an equal volume of SCM and 20 µl removed for cell counting (Countess^{TM} 3 FL Automated Cell Counter, AMQAF2000) so that the required cell number (minimum 40 x10^{6} cells) could be pelleted by centrifugation at 3200 xg for 10 minutes. The cell pellet was then resuspended in serum-free medium (SFM; 1 ml) and incubated using a rotating mixer (Revolver Rotator, Labnet, H5600) for 20 hours under hypoxic conditions to generate conditioned media (CM). The CM was then centrifuged for 10 minutes at 300 x g to pellet cells and the supernatant transferred to a new tube and centrifuged at 13 000 x g (Beckman Coulter Allegra X-22R centrifuge; F2402H rotator) at 4^{o}C for 1 hour to eliminate large EVs (microvesicles and apoptotic bodies) and remaining cell debris. This was followed by addition of PEG 6000 (20% stock; uniLAB, 504018) to the supernatant to a final concentration of 5% (v/v), which was gently mixed for 5 seconds and incubated on ice for 1 hour. The mixture was then centrifuged at 10 000 x g for 1 hour at 4^{o}C to isolate EVs. The resulting pellet was resuspended in 1X warm PBS (250 µl) or lysis buffer (100 µl) and then aliquoted in 50 µl volumes and stored at -20°C until needed. Samples were named as conditioned media (CM) 1-7, designating seven separate HEK293-generated EV isolations.

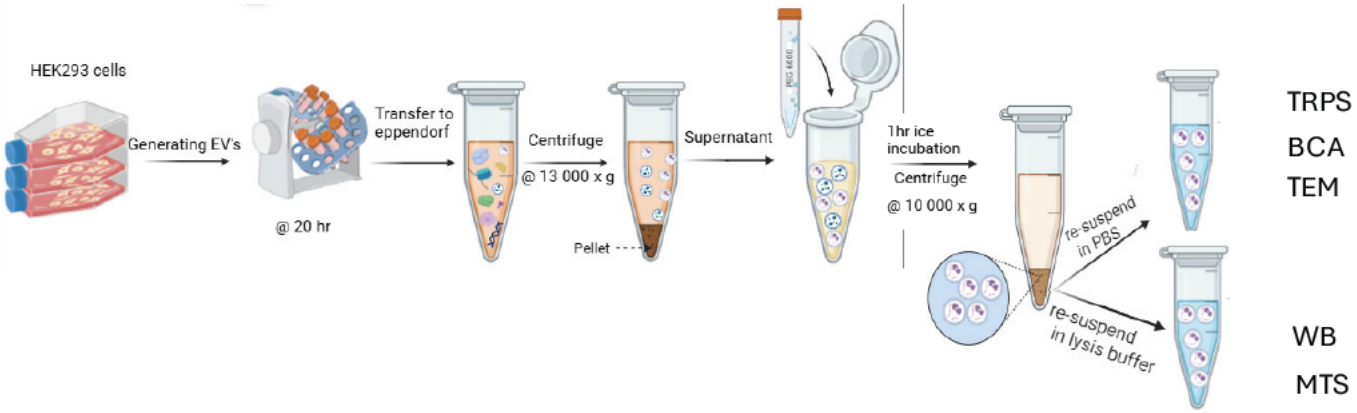

Figure 2. 1: A schematic diagram illustrating the generation and isolation of EVs from HEK293 cells. EVs were generated over 20 hours in SFM. The sample was then centrifuged before adding PEG 6000 to the supernatant which was then incubated on ice for 1 hour. EVs were concentrated to the pellet via centrifugation at 10 000 x g and the pellet is then resuspended in either PBS or lysis buffer as required.

All collected samples were assessed for protein concentration using the BCA assay, for size and particle number using TRPS, for morphology using TEM and analysed to detect specific markers using Western blotting (WB). MTS assays were also carried out to determine cytotoxicity (Figure 2.1).

2.2.2. Protein quantification - BCA Assay

Protein concentration was measured using the bicinchoninic acid (BCA) assay according to Smith (Smith P.K. et al, 1985). A standard curve was prepared using bovine serum albumin (BSA) protein standards (0, 25, 125, 250, 500, 700, 1000, 1500 µg/ml) in triplicate. The standard was prepared from a 2 mg/ml BSA stock (Sigma, cat. P0834-10X) and the BCA working reagents (WR) (Pierce™ BCA Protein Assay kit, Thermo Fisher Scientific, #23227) were prepared by mixing 50 parts BCA reagent A with 1 part of BCA Reagent B. From each standard, 25 µl was pipetted into the well of a 96-well plate and 200 µl of the WR was added to each well. The plate was then incubated at 37°C, 5% CO_2 for 30 minutes and then cooled for 10 minutes at room temperature (RT). The absorbance was measured at 562 nm using a SpectreMax ABS Plus spectrophotometer and a BSA standard curve constructed (Figure 2.2). The same protocol was then utilised to measure 25 µl of EV samples that had been lysed at a 1:4 ratio using Bio-Plex cell lysis buffer (Bio-Rad, #171304011) and determine protein concentration, in accordance with the Pierce BCA protein assay kit.

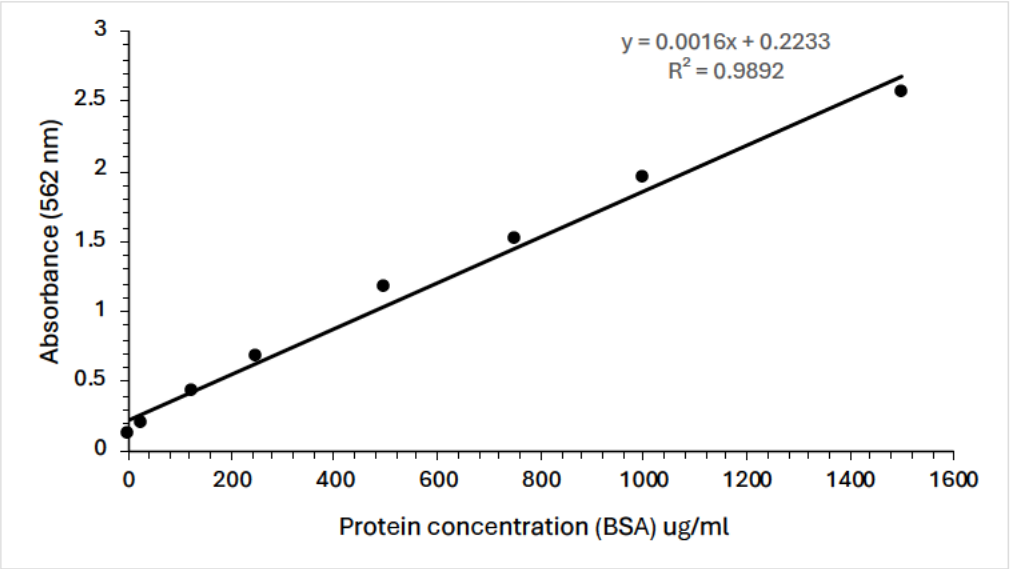

Figure 2. 2: Standard curve of BCA protein assay. Bovine serum albumin concentrations ranging from 0 – 1500 µg/ml were added to the BCA reagent and the absorbance values measured at 562 nm. The protein concentration of EV samples was then determined using the equation y=0,016x + 0,2233 with correlation coefficient value of 0,9892 (n=3).

2.2.3. Tunable Resistive Pulse Sensing (TRPS)

The concentration and size of isolated vesicles was determined using TRPS (EXOID; Version 1.0, serial. EXOID-062-R; Izon Science, France) previously described from Izon (www.izon.com) with modification (Kis et al., 2022). All samples and reagents were kept on ice throughout analysis. Prior to analysis of biological samples, a wetting procedure Izon wetting reagent diluted to 1:100 and nanopore characterisation are carried out to ensure a stable baseline is achieved (Appendix 1). Calibration using Izon CPC100 polystyrene beads of known diameter and concentration (100 nm; 1.2 x 10^{13} particles/ml) was achieved prior to each sample run at three different pressures (Appendix 1). Once run, samples were calibrated at selected pressures to generate data on particle diameter (nm) and included maximum size, minimum size, mode, mean, d90, d90/d10 as well as particle concentrations (raw and measured concentration) (Figure 2.3).

Analysis Report

IZON

Sample: **EXOPBS 15-07-23_P2**
Measurement date: 15 July 2023 14:07

Sample Statistics

Particle diameter (nm)

Mean:	90 (Std Dev=34.3)	d50:	78		
Mode:	60	d10:	59	d90:	142
Maximum:	260	d90/d10:	2.39		
Minimum:	55	Span:	1.06		

Concentration [0-∞] (particles/ml)

Measured Concentration:	1.08e+10
Raw Concentration:	1.08e+12

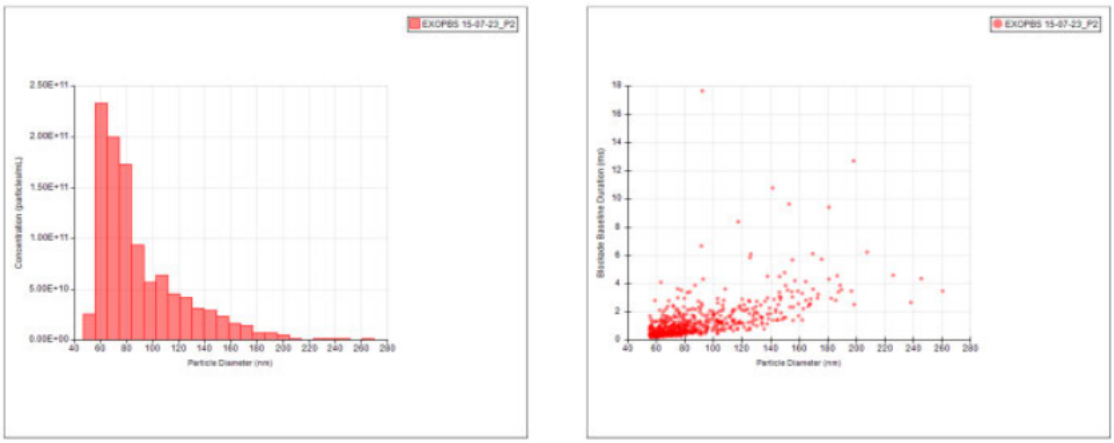

Figure 2. 3: Particle size distribution and concentration of EVs derived from HEK293 cells. Data shown is from sample CM 1 and includes mean, mode, range and d-values. The raw concentration represents the concentration of the sample prior to dilution. The histogram and dotted line show particle diameter (nm) against particle concentration (particles/ml) of samples measured using the EXOID.

The raw concentration refers to the final concentration of particles once the dilution factor (to generate the measured concentration) has been considered; in Figure 2.3, the final concentration of the sample is 1.08 x 10^{12} particles/ml, while the diluted sample (run on the Izon EXOID) is 1.08 x 10^{10} particles/ml. The d-values (d90, d50, d10) represent the minimum diameter that a specific percentage of measured particles fall within. For example, in Figure 2.3, the d90 value of 142 indicates that 90% of the particles have a diameter of 142 nm and less, while the d10 value of 59 indicates that 10% of the particles have a diameter of 59 nm and less. The d90/d10 value measures particle distribution and is directly proportional to particle heterogeneity, the larger this value, the great the size heterogeneity of the sample. The mean diameter of the detected vesicles was 90 nm, with a standard deviation of ±34.3 nm, indicating a moderate degree of size variability within sample. This suggests that while most vesicles are close to the average size, some are significantly smaller or larger. The mode

diameter, representing the most frequently occurring vesicle size, was 60 nm, suggesting that a majority of vesicles fall within the smaller size range. The vesicle diameter ranged from 55 nm to 260 nm, highlighting the board distribution of particle sizes in the sample. This range is consistent with extracellular vesicles, such as sEVs.

To analyse our biological samples, filtered PBS was used to dilute our samples 1:100; the diluted sample was then filtered through a 0,22 µm filter (Pall Corporation, FL4758) to remove any larger particle and thereby avoid nanopore clogging. To the lower fluid cell 75 µl filtered PBS was added, while 35 µl of the diluted biological sample was added to the upper fluid cell. Pressure and voltage were adjusted until particles were observed to pass through the nanopore. The first pressure is set by the user and must be above 400 Pa to achieve optimum particle rate (>100 particle/minute); the system then sets the next pressure value at 200 Pa less and subsequently the third pressure is set at 400 Pa above the first pressure. The system then applies the same settings to measure 500 particles of the diluted sample, using the same conditions that were used for calibration with CPC100 beads; this ensures compatibility between the calibration step and the sample analysis. The data is then analysed using the IZON Data Suit Software; an analysis report (Figure 2.3) is generated for each sample, at each pressure.

2.2.4. SDS PAGE and Western blotting

SDS PAGE and Western blotting was used to analyse samples as described previously (Towbin et al., 1979) with modifications for the presence of specific proteins using antibodies listed in Table 2.2 below.

Table 2. 2: Details of primary and secondary antibodies used for Western blotting.

Primary Antibodies	**Dilutions**	**Suppliers**	**Catalogue Number**
Mouse monoclonal flotillin-1	1:100	Santa Cruz Biotechnology	sc-74566
Mouse monoclonal TSG 101	1:100	Santa Cruz Biotechnology	sc-7964
Alpaca Anti-human CD63 (His tagged)	1:500	Afrobodies	AFB-CD63-2
Secondary Antibodies	**Dilutions**	**Suppliers**	**Catalogue Number**
HRP–conjugated Rabbit anti-mouse secondary antibody	1:16 000	DAKO	20039216
HRP–conjugated Mouse anti-His Tag secondary antibody	1:500	Roche	11965085001

EVs in lysis buffer (Bio-Plex Cell Lysis kit, #171304012), were vortexed and incubated on ice for 1 hour before quantification of protein using BCA (section 2.2.2). Subsequently, the sample (30 µg protein) was mixed (1:1) with bromophenol blue and reducing buffer (125 mM Tris-HCl, pH 6.8, 4% (m/v) SDS, 20% (v/v) Glycerol, 0.03% Bromophenol Blue and 10% (v/v) β-mercaptoethanol), and boiled for 5 minutes. Samples and Spectra Multicolour Broad Range Protein Ladder (3 µL, Thermo Scientific, #2632508) were then loaded onto and separated using 12.5% Sodium Dodecyl Sulphate Polyacrylamide Gel Electrophoresis (SDS-PAGE) at 140 V for 2 hours. Gels were stained with 1% Coomassie Brilliant Blue R-250 Dye for 1 hour and destained for 30 minutes to visualise proteins. Proteins were transferred onto nitrocellulose membrane by semi-dry transfer method for 1 hour. The nitrocellulose membrane was then blocked for 1 hour with 5% skim milk powder in Tris-buffered saline containing 0,01% Tween-20 (TBS-T). The membranes were washed with TBS-T (3 times, 5 minutes each) and probed with appropriate primary antibody diluted in TBS-T (either anti-human CD63, mouse monoclonal TSG101 IgG2a or mouse monoclonal flotillin-1 IgG) overnight at 4^{o}C (Table 2.2). After washing with TBS-T (3 times for 5 minutes each), the membranes were then incubated for 1 hour with the appropriate secondary antibody, either polyclonal rabbit anti-mouse immunoglobulin-horseradish peroxidase or anti-His-horseradish peroxidase, at room temperature (Table 2.2). The membranes were then washed with TBS-T (3 times for 5 minutes each), incubated with Clarity TM Western ECL Substrate (Bio-Rad, #170-5060) and visualized using the Syngene G: Box.

2.2.5. Transmission Electron Microscopy (TEM)

To study EV morphology using TEM, samples (5 µl diluted in 1/100 with PBS) were loaded onto a Formvar-coated copper grids. After 5 minutes, excess sample was removed using Whatman's filter paper. Once dried, negative staining was performed using 2% Uranyl acetate for 30 seconds and excess liquid removed using Whatman's filter paper. The grid was allowed to dry completely at RT before viewing the sample using the JEM 1400 transmission electron microscope (JOEL, serial. EM18480030). Images were generated using the Gatan Microscopy Suite software.

2.2.6. MTS Assay

The MTS toxicity assay was used to evaluate the effect of EVs on cellular proliferation. To construct a standard curve (Figure 2.4), increasing numbers of HEK293 cells (0, 5000, 10000, 20000, 40000, and 80000; each in triplicate) were plated in a 96-well plate. The cells were allowed to adhere for 3 hours at 37°C in a CO_2 incubator in a final volume of 200 µl/well in serum containing media (SCM). The cells were then incubated with 20 µl MTS reagent (Cell Titer 96® Aqueous One, cat. G3580) for 3 hours to allow for the colour formation and absorbance measured at 490 nm using a SpectraMax Spectrophotometer with SoftMax Pro 7.

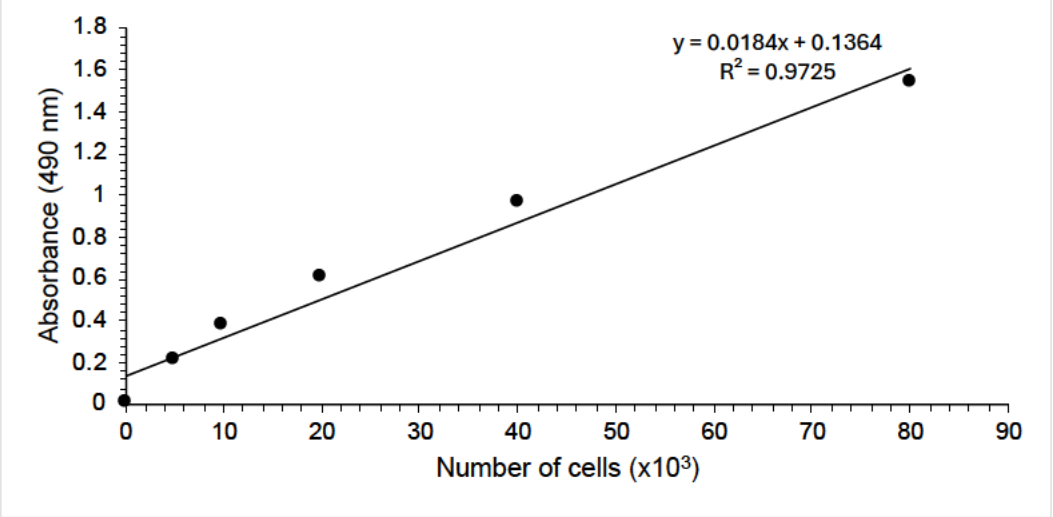

Figure 2. 4: MTS assay standard curve. An increasing number of HEK293 cells (0–80x10^3 cells) were plated in a final volume of 200 µl/well and incubated for 3 hours at 37°C and 5% CO_2. MTS reagent (20 µl) was added and absorbance measured at 490 nm. The equation of the trendline is given by y = 0,0184x + 0,1364 with a correlation coefficient of 0.9725 (n=3).

To assess the proliferation of HEK293 cells in response to EVs, 10 000 cells were plated in 96 well plates in triplicate in SCM. The cells were allowed to adhere for 4 h, after which the wells were washed gently and 200 µl of SCM, SFM, or SFM-containing EVs added Cells were incubated for 24 hours, after which 20 µl of MTS reagent was added for 3 hours and absorbance measured at 490 nm.

2.3. Cargo Loading

2.3.1. mRNA

The eGFP mRNA used in this study was a gift from Prof Patrick Arbuthnot (University of Witwatersrand, South Africa). The full mRNA sequence is provided in Appendix 2. The mRNA was received at a concentration of 1.2 ng/µl and stored at -80^{o}C until use. Prior to loading into sEVs, the mRNA was thawed on ice and diluted to a working concentration of 1.2 ng/µl in 50 µl OptiMEM (Gibco, 31985-062).

2.3.2. Lipofectamine complex

To prepare the lipofectamine complex, 1.2 µL of Lipofectamine MessengerMax was mixed gently with 50 µL Opti-MEM I reduced serum in a 2 ml Eppendorf.

2.3.3. Cell preparation

In preparation for transfection experiments, 2.5 × 10^4 HEK293 cells were plated on coverslips in a volume of 500 µL SCM per well of 24-well plate (Nest Biotechnology, cat. 112720BA01). The cells were incubated overnight at 37^{o}C, 5% CO_2.

2.3.4. sEV staining

Prior to application, sEVs were stained with the red fluorescent PKH26 dye (Sigma – Aldrich, cat. MIDI26-1kt). The dye was first diluted in 250 µL diluent C to a final concentration of 20 µM. Subsequently, 25 µL sEV-containing sample (in PBS) was incubated with 25 µL dye solution for 1 minute while continuously resuspending with gentle pipetting. The unbound PKH26 dye in the sEV mixture was quenched with 1% bovine serum albumin ((BSA) Roche, cat. 107350860010) in SFM.

2.3.5. Fluorescence microscopy/Confocal microscopy

To visualise fluorescence, cells were washed twice with PBS, fixed in 100% cold methanol for 10 min, then washed twice with PBS and nuclei stained with Hoechst 33342 nuclear stain (Sigma – Aldrich, cat. B2261; 1/50 dilution of stock 10 mg/ml concentration). Cells were then washed again with PBS (twice) and mounted onto glass microscope slides, using Mowiol mounting medium. Imaging was carried out using either the Zeiss LSM 710 confocal microscope or the Olympus AX70 Fluorescence microscope.

2.3.6. Optimization of eGFP-mRNA delivery to HEK293 cells

To determine the optimal amount of eGFP mRNA to use when transfecting HEK293 cells, a standard lipofectamine protocol was applied (Figure 2.5). HEK293 cells (2.5×10^4) were prepared by plating in 24-well plates, washed with 500 µl PBS/well and subsequently incubated with 500 µl OptiMEM reduced serum media for 1 hour at 37°C and 5% CO_2. For transfection, 50 µl Opti-MEM I reduced serum media containing either 0, 0.5, 1.2 or 2.4 µg eGFP-mRNA was added to the Lipofectamine complex and gently mixed every 5 minutes for 30 minutes before being added dropwise to the cells. Cells were then incubated for 24 hours at 37°C and 5% CO_2, fixed (section 2.3.4) and viewed using fluorescence microscopy (Olympus AX70 Fluorescence microscope) to verify presence of positive eGFP expression.

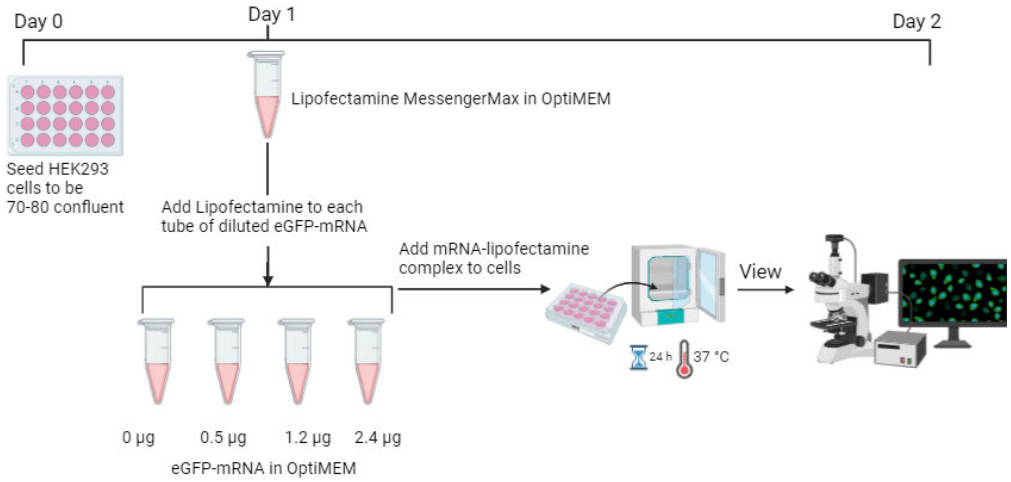

Figure 2. 5: Experimental procedure for the optimization of eGFP-mRNA delivery to HEK293 cells using Lipofectamine MessengerMax reagent.

2.3.7. Delivery of mRNA using sEVs

To determine whether sEVs can delivery eGFP-mRNA to HEK293 cells in the absence of lipofectamine, PKH-dyed sEVs (25 µl; 4 billion sEVs) were incubated with 50 µl Opti-MEM I reduced serum media containing either 0, 0.5, 1.2, 2.4 or 4.8 µg mRNA by gently mixing it every 5 minutes for 30 minutes and subsequently adding it dropwise to the HEK293 cells. Cells were incubated for 24 hours at 37°C and 5% CO_2, fixed (section 2.3.4) and viewed using fluorescence microscopy to verify eGFP expression (Figure 2.6).

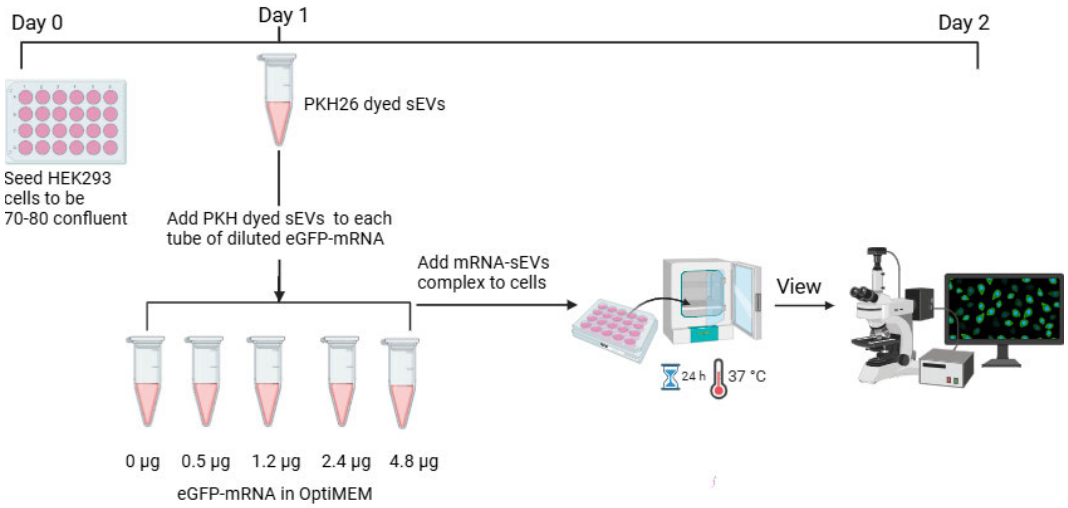

Figure 2. 6: Experimental procedure for the delivery of eGFP-mRNA to HEK293 cells using PKH26 dyed sEVs.

2.3.8. Determination of eGFP expression in transfected cells over time

To evaluate the duration of eGFP expression in cells, fluorescence was analysed daily from 1 to 4 days post-mRNA delivery. Transfection complexes were generated in 50 µl Opti-MEM I reduced serum media by adding of 2.4 µg eGFP mRNA and 25 µl PKH-dyed sEVs, which were gently mixed while incubating and added dropwise to the cells. Cells were cultured for 1, 2, 3 and 4 days in the cell incubator, fixed (section 2.3.4) and analysed using fluorescence microscopy (Figure 2.7).

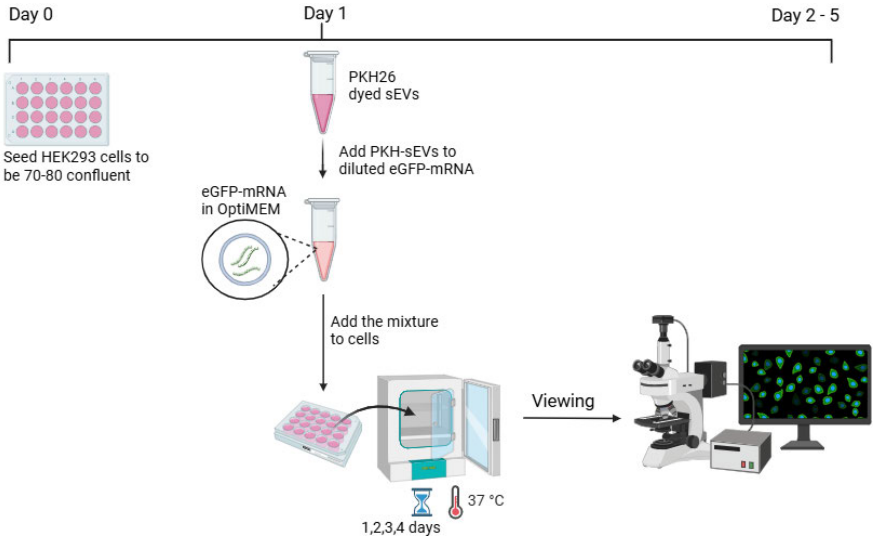

Figure 2. 7: Experimental procedure for the delivery of 2.4 µg eGFP-mRNA to HEK293 cells over time.

2.3.9. Optimization of sEV number for mRNA delivery

To determine whether fewer sEVs could be used for optimal mRNA delivery, the use of 4 x 10^9, 1 x 10^9, 400 x 10^6 and 100 x 10^6 sEVs were compared. For transfection of one well of 24-well plate, 50 µl Opti-MEM I reduced serum media containing 2.4 µg eGFP mRNA and the respective number of PKH-dyed sEVs was prepared. The transfection mixture was gently mixed and were added dropwise to the cells. Cells were incubated for 24 hours at 37°C and 5% CO_2, fixed (section 2.3.4) and using confocal, the eGFP expression in the cells was verified (Figure 2.8).

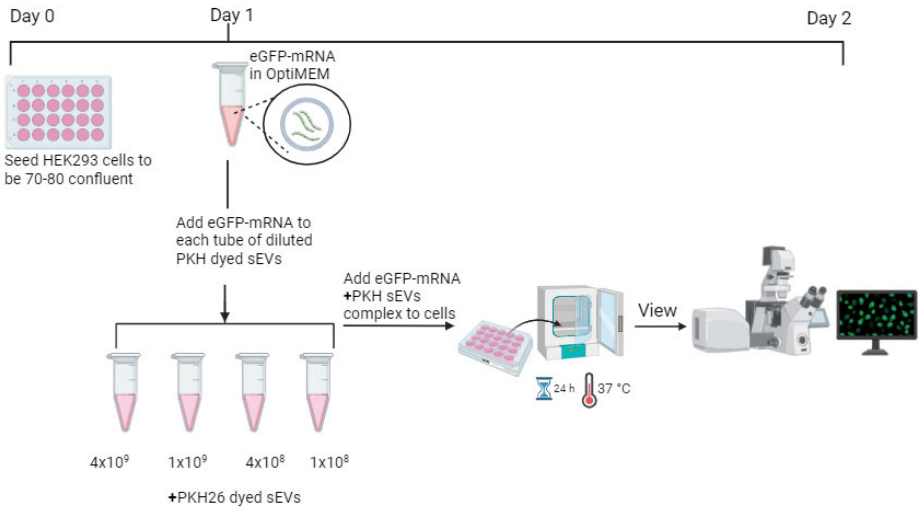

Figure 2. 8: The delivery of 2.4 µg eGFP-mRNA to HEK293 cells using different sEV numbers.

Chapter 3: Results

3.1. Isolation and characterisation of EVs

3.1.1 Size and concentration

Conditioned media (designated CM1 – CM7), generated from different HEK293 cell passages following the protocol described in Chapter 2 (section 2.2.1) was first characterized using TRPS to determine the presence of EVs. Several key parameters were analysed, including particle concentration (particles/ml), their size distribution (mean, mode, min, max), and statistical metrics (d90 and d90/d10) as presented in Table 3.1. These data provide critical insights into the characteristics and quality of the EV preparation.

Table 3. 1: Particle characteristics of EVs isolated from different HEK293 cell passages. Data generated following TRPS runs at multiple pressures and subsequent analyses.

Samples	EV Concentration (billion particles/ml)	Mean diameter (nm)	Mode (nm)	Minimum (nm)	Maximum (nm)	d90 (nm)	d90/d10 (nm)
CM 1	1 000	90	60	55	260	142	2,39
CM 2	329	116	100	94	240	141	1,45
CM 3	174	141	123	114	354	172	1,46
CM 4	125	130	95	92	421	203	2,14
CM 5	50	111	87	73	278	152	1,94
CM 6	30	122	107	99	205	153	1,5
CM 7	20	122	102	98	249	152	1,51
Average	247	119	96	89	287	159	2
SD	349,14	16,00	19,49	19,37	74,87	21,80	0,38

The concentrations of particles, measured as the number of EVs per ml, revealed significant variation across samples CM1 to CM7. CM1 exhibited the highest concentration, at 1000 x 10^9 particles/ml, while CM7 presented the lowest concentration at 20 x 10^9 particles/ml. On average, the particle concentration was 247 x 10^9 particles/ml, with a standard deviation (SD) of 349,14 x 10^9 particles/ml, indicating considerable variability in vesicle yield between samples (Table 3.1 and Figure 3.1A).

The size distribution of EVs was assessed through analysis of the mean, mode, minimum and maximum diameters, providing a comprehensive overview of particle size heterogeneity. The mean (average) diameter of particles within a CM sample ranged from 90 nm (CM1) to 141 nm (CM3), with an overall mean diameter of 119±16 nm. Similarly, the mode, indicating the most frequently observed particle diameter varied between 60 nm (CM1) and 123 nm (CM3), with an average of 96± 19 nm; therefore, all vesicles had a mode value below 150 nm which indicated that our samples comprised of vesicles within the sEV desired size range. The minimum diameter ranged from 55 nm (CM1) to 114 nm (CM3), while the maximum diameters extended from 205 nm to 421 nm. These findings highlight the presence of both small and large vesicles, with sample CM4 (421 nm) exhibiting the widest range of diameters (Table 3.1 and Figure 3.1).

To further understand the size distribution, statistical size metrics such as d90 and the d90/d10 ratio were analysed. The d90 metric, with an average of 159±22 nm, further confirms that the majority of vesicles were within the correct size-range of sEVs. Only CM 3 (d90 of 172 nm) and CM 4 (d90 of 203 nm) were observed to be substantially above this value (Table 3.1, Figure 3,1B), confirming the presence of larger vesicles in some samples. The d90/d10 ratio, used to assess the spread of particle sizes, ranged from 1.45 to 2.39, with an average of 2.0. Higher d90/d10 ratios, such as those observed in CM1 (2.39 nm) and CM4 (2.14), suggest broader heterogeneity in particle sizes whereas lower ratios (CM2, CM3, CM5, CM6, CM7) suggesting more uniform/homogeneous population of vesicles (Table 3.1).

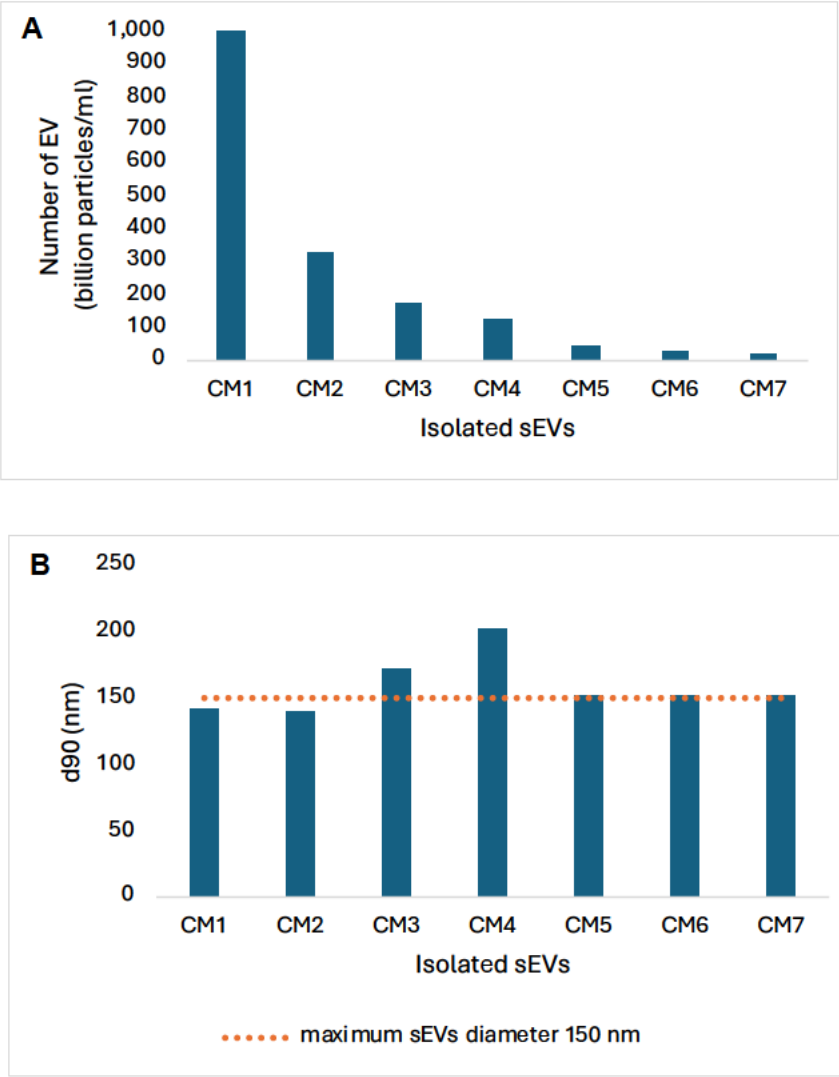

Figure 3. 1: Graphical representation of A) Particle concentration and B) d90 particle size distribution values of EVs in the CM samples. Data generated following TRPS analysis.

3.1.1.1. Analysis of protein concentrations of isolated EV samples

The analysis of the total protein content across all seven samples (CM1 -7) revealed concentrations ranging from 0.336 µg/µl to 0.614 µg/µl (Figure 3.2A). Interestingly, there was no correlation observed between total protein concentration and number of EVs (billion/ml), as indicated by poor regression correlation of 0,3385 (Figure 3.2B). For example, samples CM3 and CM5, both of which exhibited the same protein concentrations of 0,47 µg/µl (Figure 3.2A), displayed a substantial difference in the number of EVs, with CM 3 containing 174 $x10^9$/ml and CM 5 containing 46,7 $x10^9$/ml EVs (Figure 3.1A). This highlights that the total protein concentration dos not reliably predict the quantity of EVs.

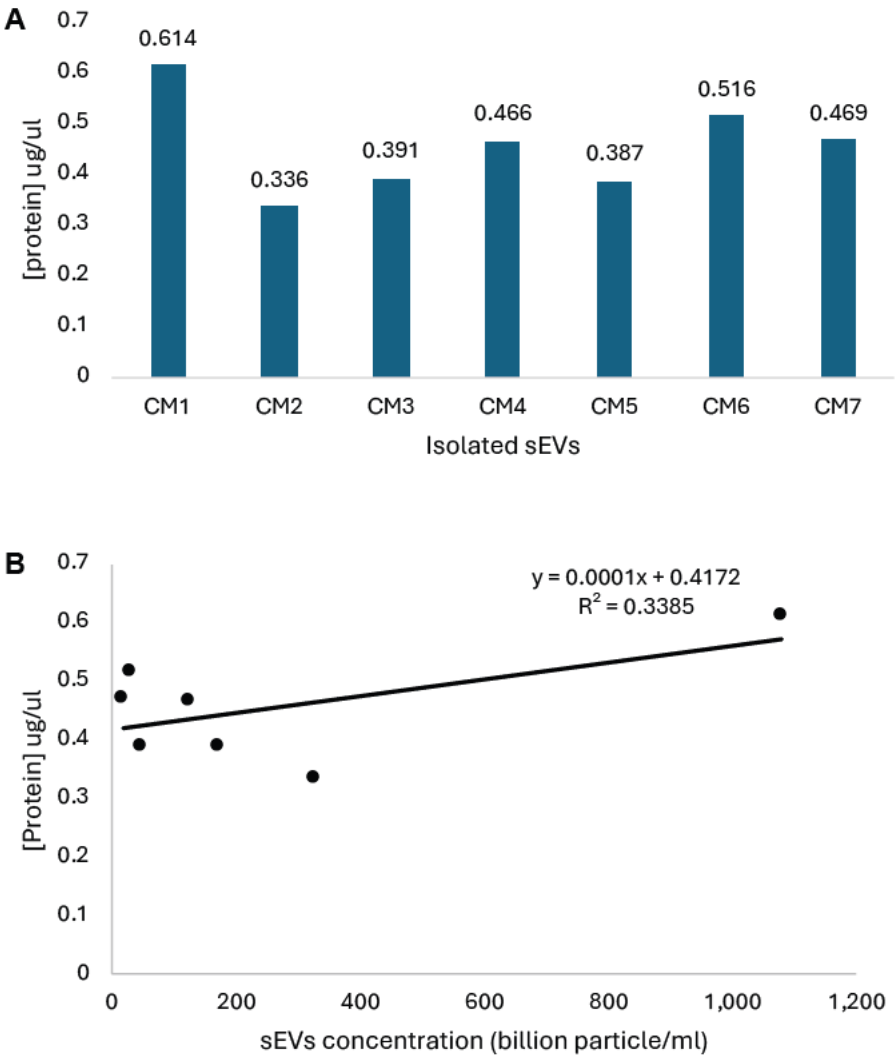

Figure 3. 2: Analysis of EV protein concentration in CM1-CM7. A) Protein concentration of isolated EVs using BCA assay. B) Relationship between EV number and total protein concentration.

3.1.2. EV Purity

To analyse the purity of EVs isolated from HEK293 cells using PEG 6000 precipitation, particle-to-protein ratio was calculated (Webber J. & Clayton A., 2013). The purity of EVs is defined by the particle-to-protein ratio and was calculated for each sample (Table 3.2). CM1 achieved the highest purity (1,63 x 10^9 particle/µg), followed by CM2 (9,70 x 10^8 particle/µg) and CM3 (4,45 x 10^8 particle/µg). The lowest purity was observed in CM7 (4,26 x 10^7 particle/µg) as shown in Table 3.2. According to Webber and Clayton, purity ratios >3.0 x 10^{10} particle/µg are indicative of high vesicular purity, suggesting that none of our samples met a high purity threshold. However, Webber and Clayton also reported that EVs from cells cultured in T75s generally yield purity ratios of approximately 1x10^7 particles/ug protein; all

our CM samples had purity levels greater than this, which is promising, but suggests that refinement is necessary.

Table 3. 2: Purity evaluation of EVs isolated from HEK293 cells using PEG 6000 precipitation.

Samples	EV concentration (billion particles/ml)	Protein content (µg/µl)	Purity ration (particles/ug)
CM 1	1 000	0,614	$1,63 \times 10^{9}$
CM 2	329	0,336	$9,70 \times 10^{8}$
CM 3	174	0,391	$4,45 \times 10^{8}$
CM 4	125	0,466	$2,68 \times 10^{8}$
CM 5	50	0,387	$1,29 \times 10^{8}$
CM 6	30	0,516	$5,81 \times 10^{7}$
CM 7	20	0,469	$4,26 \times 10^{7}$

3.1.3. Transmission Electron Microscopy (TEM)

To further characterize the isolated EVs and confirm their sEV morphology, we carried out transmission electron microscopy (TEM). Following a 1/100 dilution, samples (5 µl) of EVs were loaded onto formvar-coated copper grids, counterstained, and then viewed using TEM. TEM analysis revealed vesicles consistent with the expected size range for sEVs (Figure 3.3A). The vesicles displayed the characteristic cup-shaped morphology (Figure 3.3B, C) that is commonly associated with sEVs, in accordance with the MISEV2018 guidelines for EVs characterization (Théry et al., 2018). The use of negative staining provided clear visualization of EVs of different sizes (Figure 3.3A & B) further confirming their known structural features of sEVs (cup-shaped morphology). These findings support the successful isolation and identification of sEVs from the sample.

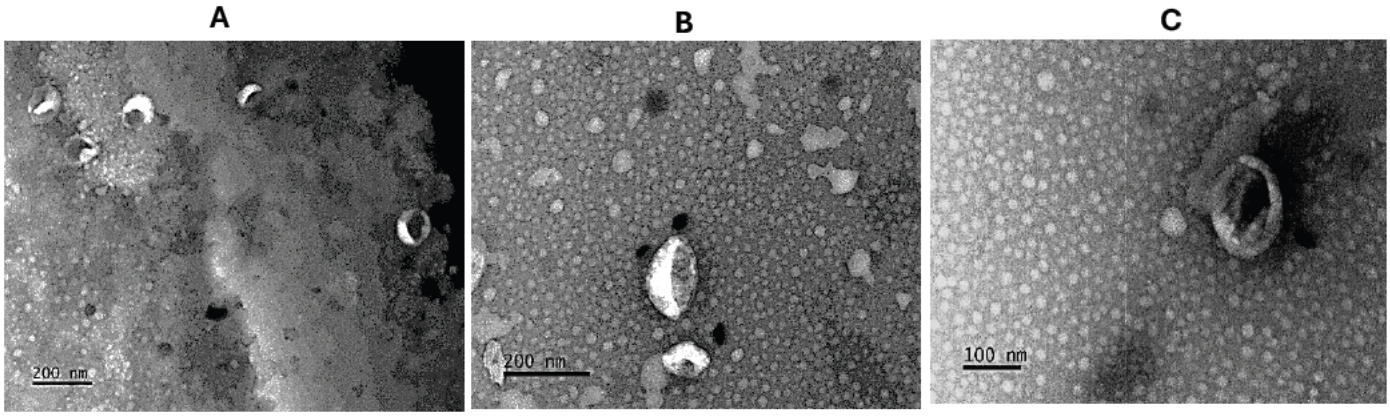

Figure 3. 3: TEM image of EVs derived from HEK293 cells. Cup-shaped structures, with 30 –150 nm diameter (blue arrows) were identified at different magnifications. Images were captured using a JEM-1400 electron microscope (20x objective). Scale bar (A & B) 200 nm and (C) 100 nm.

3.1.4. SDS-PAGE and Western blotting

The International Society for Extracellular Vesicles (ISEV's) minimal experimental requirements emphasize the analysis of specific proteins to determine the purity of the sEV isolate. SDS PAGE and Western blot analysis was therefore used to determine the presence of proteins known to be enriched on or in sEVs, including flotillin-1, TSG101 and CD63. EV samples (30 µg) were separated on a 12% SDS-PAGE gel and then transferred to a nitrocellulose membrane for protein detection using relevant primary and secondary antibodies followed by chemiluminescence. While these results suggest the presence of flotillin-1, TSG101 and CD63, the sizes of these proteins do not align exactly with the previously reported molecular mass ranges for these proteins (Figure 3.4). Flotillin-1 is typically observed at 49 kDa, TSG101 at 44 kDa and CD63 at 63 kDa (Fengyan Deng & Josh Miller, 2019). As confirmatory controls were not included, it is not possible to rule out the possibilities that some of the observed bands may represent nonspecific binding rather than true detection of the intended proteins.

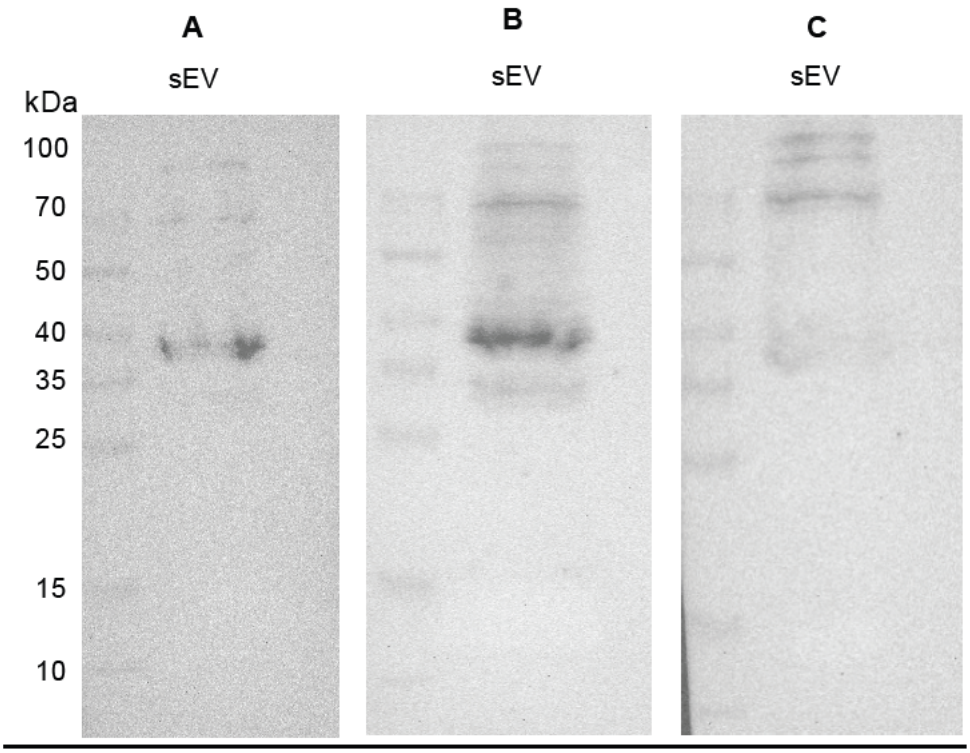

Figure 3. 4: Western blot analysis of EVs derived from conditioned media. Representative blots of membrane probed with antibodies against sEV markers flotillin-1 (A: 1/100), TSG101 (B: 1/100) and CD63 (C: 1/500).

3.1.5. Effects of sEVs on proliferation

We finally wanted to confirm the non-toxic nature of the generated sEVs on HEK293 cells, and selected CM1, CM2, CM4 and CM6 to determine the effect of sEVs on cell proliferation. To achieve this, cells were treated in either SCM (positive control), SFM (negative control) or SFM supplemented with increasing numbers of sEVs (ranging from 3×10^6 to 3×10^{10}) for 24h at 37^{o}C, 5% CO_2, after which the MTS reagent was added and absorbance measured as described in section 2.1.2. Results were expressed as a percentage relative to the SFM condition, which was set at 100% (Figure 3.5).

Cells cultured in SFM showed the lowest relative cell proliferation, confirming the adverse effect of serum deprivation on HEK293 cell growth. In contrast, cells in SCM showed significantly higher cell growth (~ 150% relative to SFM) ($p<0.01$), confirming its role as a positive proliferation control. Supplementation of SFM with increasing number of sEVs significantly increased cell proliferation in a concentration-dependent manner, when compared with SFM alone. At the highest sEV concentrations, cell proliferation increased significantly with sEV1 and SEV2 at 180% and 135% compared with SFM respectively ($p<0.05$). Importantly, sEV1 not only restored variability but also exceeded the growth observed in SCM, suggesting a significant growth-promoting effect at this concentration. Moderate concentrations (sEV3) resulted in 120% cell growth, partially restoring proliferation to levels comparable to SFM, whereas the lowest concentrations (sEV4 and sEV5) resulted in 111% and 103% cell growth, respectively, maintaining viability close to SFM. Importantly, incubation with sEVs from CM1, CM2, CM4 and CM6 showed no negative effects on cell proliferation at any concentration, suggesting that these sEVs do not induce any toxicity in these cells. Therefore, these findings suggest that sEVs from CM1, CM2, CM4 and CM6 do not inhibit HEK293 cell proliferation, even at the lowest concentration tested. Furthermore, at higher concentrations of sEVs can enhance growth, suggesting their potential to promote cell viability under serum-free conditions.

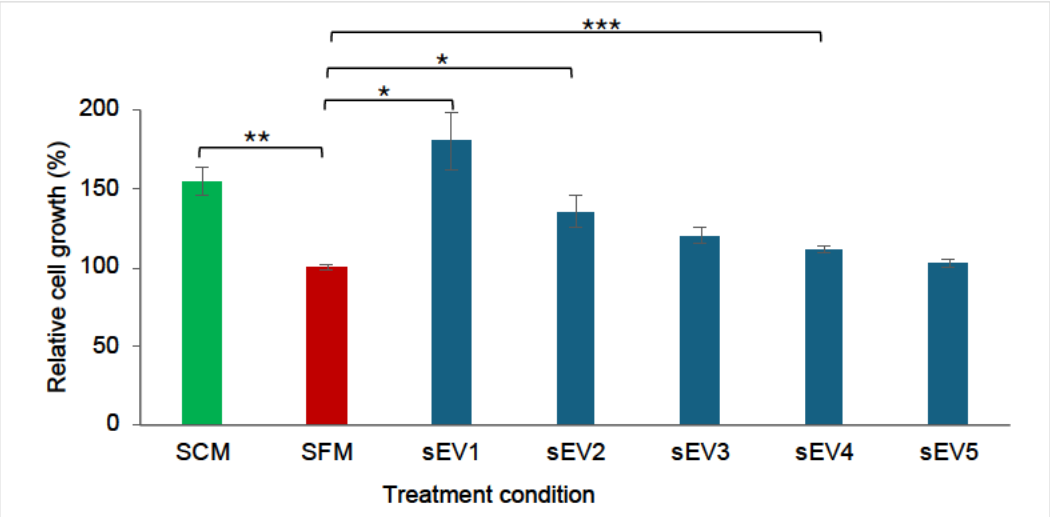

Figure 3. 5: MTS assay analysing cell growth in response to an increasing number of sEVs. Average effect of sEVs from CM1, CM2 and CM4 on HEK293 cell growth. Cells were treated either in SCM, SFM or SFM containing increasing numbers of sEVs $3x10^{10}$ (sEV1), $3x10^{9}$ (sEV2), $3x10^{8}$ (sEV3), $3x10^{7}$ (sEV4) and $3x10^{6}$ (sEV5) sEVs. n=4; each repeat in duplicate. * = $p<0.05$; ** = $p<0.01$; *** = $p<0.001$.

3.2. mRNA cargo-loading

3.2.1. Delivery of eGFP mRNA to HEK293 cells using Lipofectamine

To establish a positive control for eGFP-mRNA delivery and expression in HEK293 cells, we used Lipofectamine MessengerMax as a transfection reagent, as it has been successfully employed for mRNA delivery in previous studies (Avci-Adali M. et al., 2014). Different amounts of eGFP-mRNA (0, 0.5, 1.2 or 2.4 µg) were then incubated with lipofectamine and added to HEK293 cells, which were then allowed to incubate for 24 hours at 37°C. Strong expression of GFP protein (as indicated by green fluorescence) following transfection with either 0.5 ug mRNA or 1.2 ug mRNA was not evident, particularly when compared with the controls which lacked either mRNA or lipofectamine (Figure 3.6A-C, E). However, following transfection with 2.4 µg mRNA, cells with higher fluorescence intensity (Figure 3.6D) were observed when compared to control. Importantly, in the absence of lipofectamine MessengerMax, the resulting absence of GFP within cells (Figure 3.6E), confirmed the essential role of lipofectamine in facilitating mRNA delivery under these conditions.

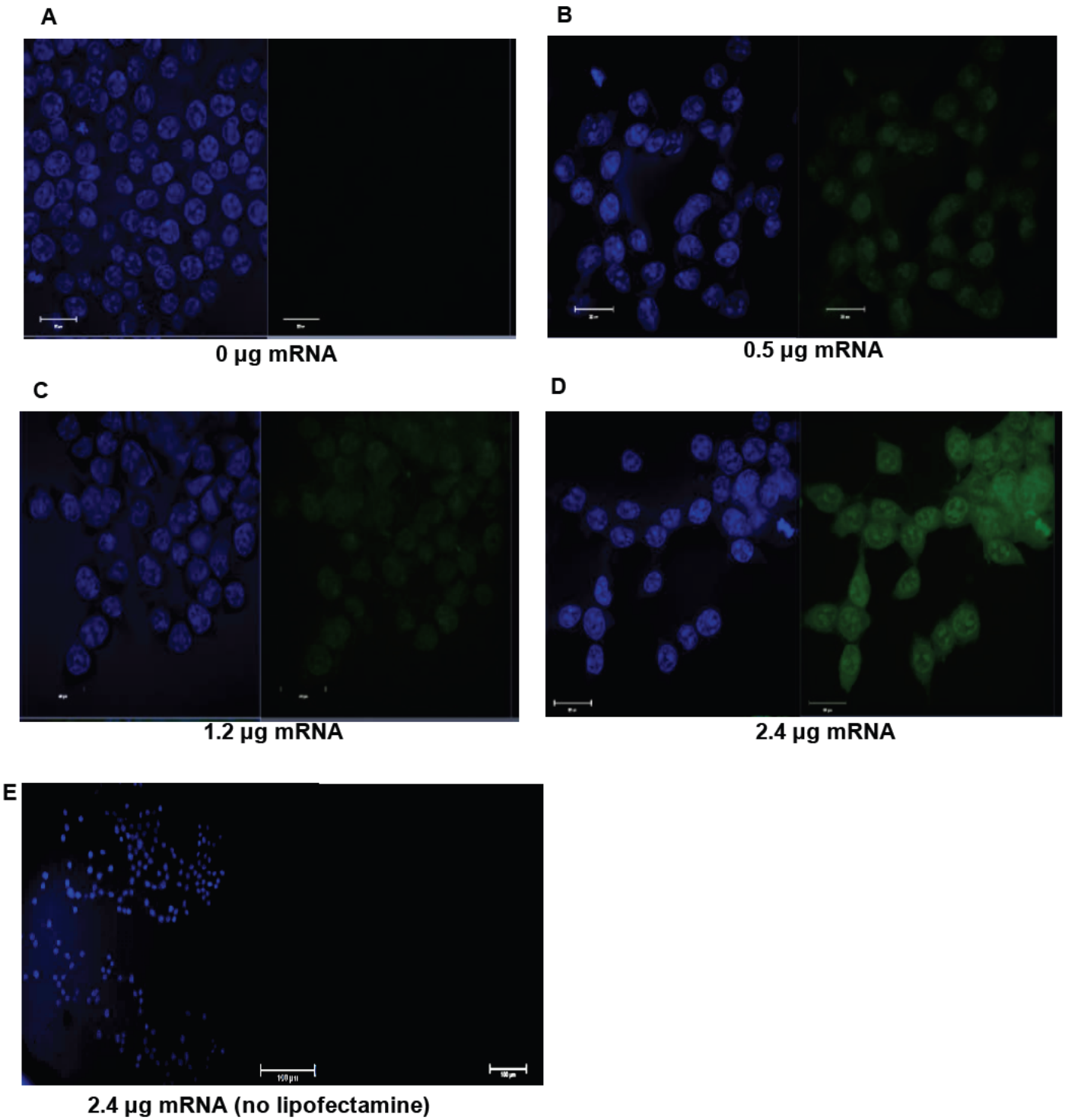

Figure 3. 6:HEK293 cells following transfection with Lipofectamine MessengerMax and different amounts of eGFP mRNA. HEK293 cells were transfected in the presence of Lipofectamine and either A) 0 µg mRNA, B) 0.5 µg mRNA, C) 1.2 µg mRNA, D) 2.4 µg mRNA, or in the absence of Lipofectamine with E) 2.4 µg mRNA with no lipofectamine for 24 hours in OptiMEM. GFP expression is indicated by the green staining. Nuclei stained with Hoechst (blue). Images were obtained using a confocal microscope. Scale bar = 20 µm (A-D) and 100 µm (E).

3.2.2. Delivery of mRNA to HEK293 cells using sEVs

To determine whether sEVs can be used to effectively deliver mRNA into cells, an incubation technique was employed based on a method escribed by Avci-Adali M et al., (2014). In this study, the protocol was adapted by first incubating the cells with Opti-MEM for 1 hour, followed by a 24-hours incubation with the sEV-mRNA mixture. The transfection complexes were generated by incubating eGFP mRNA (0, 0.5, 1.2, or 2.4 µg) with 25 µL PKH-stained sEVs (CM3, CM4 and CM7); these were subsequently incubated with HEK293 cells for 24 hours. As expected, incubation of cells with sEVs in the absence of eGFP mRNA did not result in detectable green fluorescence, while PKH staining (red) was evident, confirming the presence of sEVs (Figure 3.7A). Incubation of cells with sEVs and 0.5 µg mRNA led to detection of eGFP positive cells (Figure 3.7B), confirming that sEVs can indeed deliver mRNA into cells. Increasing the amount of mRNA to 1.2 µg or 2.4 ug further increased the intensity of the GFP fluorescence, while the PKH fluorescence remained relatively unchanged (Figure 3.7C & D), indicating a dose-dependent relationship with respect to the delivery of mRNA. Despite this, transfecting cells with more than 2.4 µg did not increase the eGFP expression to a large degree (Figure 3.7E), suggesting that there may be a saturation point beyond which increasing eGFP-mRNA quantity no longer result in a significant increase in transfection efficiency. Overall, this data demonstrates that sEVs are capable of delivering mRNA into cells, and as the amount of mRNA increases, a corresponding increase in eGFP expression is observed, with 2.4 µg reaching the highest expression.

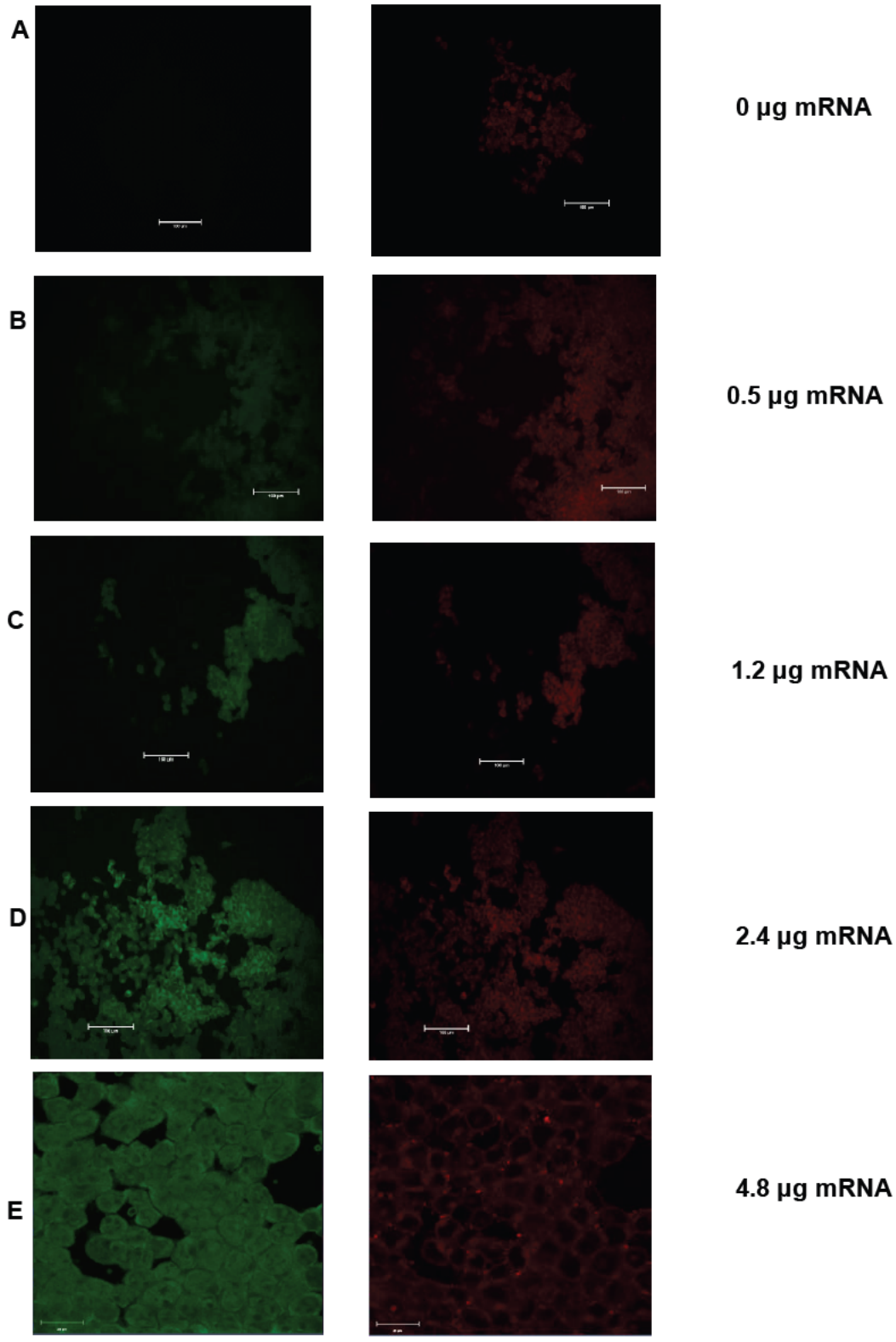

Figure 3. 7: HEK293 cells following incubation with 25 µl PKH-stained sEVs and increasing amounts of eGFP mRNA. HEK293 cells were incubated with either A) 0 µg mRNA, B) 0.5 µg mRNA, C) 1.2 µg mRNA, D) 2.4 µg mRNA (green) and sEVs (CM7) stained with PKH26 (red) for 24 hours in OptiMEM. After treatment fluorescent images were obtained using a fluorescence/confocal microscopy. Scale bar = 100 µm (A-D) and 20 µm (E).

3.2.3. Duration of GFP expression following delivery of mRNA using sEVs

The duration of eGFP-mRNA expression in HEK293 cells was then determined following transfection of cells with 2.4 µg mRNA using 25 µl PKH dyed sEVs (CM3 or CM4) with approximately 150 x 10^9 particles/ml of sEVs (Figure 3.8). The eGFP expression in cells was monitored at 1-, 2-, 3- and 4-days post-delivery, using a fluorescence microscope. On day 1, the cells exhibited the highest fluorescence intensity (Figure 3.8A), indicating strong eGFP expression shortly after transfection. GFP fluorescence was still easily detected by day 2 (Figure 3.8B), however by day 3 and 4, very little eGFP expression remained visible (Figure 3.8C, D). This time-dependent decline in fluorescence is consistent with expected kinetics of mRNA expression following on integrative delivery by extracellular vesicles. As sEVs deliver mRNA into the cytoplasm without integrating into the genome, the mRNA is subjected to natural degradation by RNAses and dilution through cell division (Andaloussi et al., 2013; Kalluri & LeBleu, 2020). Over time, the delivered eGFP expression therefore reached a maximum between day 1 and 3, gradually decreased beyond that with minimal expression detected by day 4, reflects the typical transient nature of exogenously delivered mRNA via sEVs.

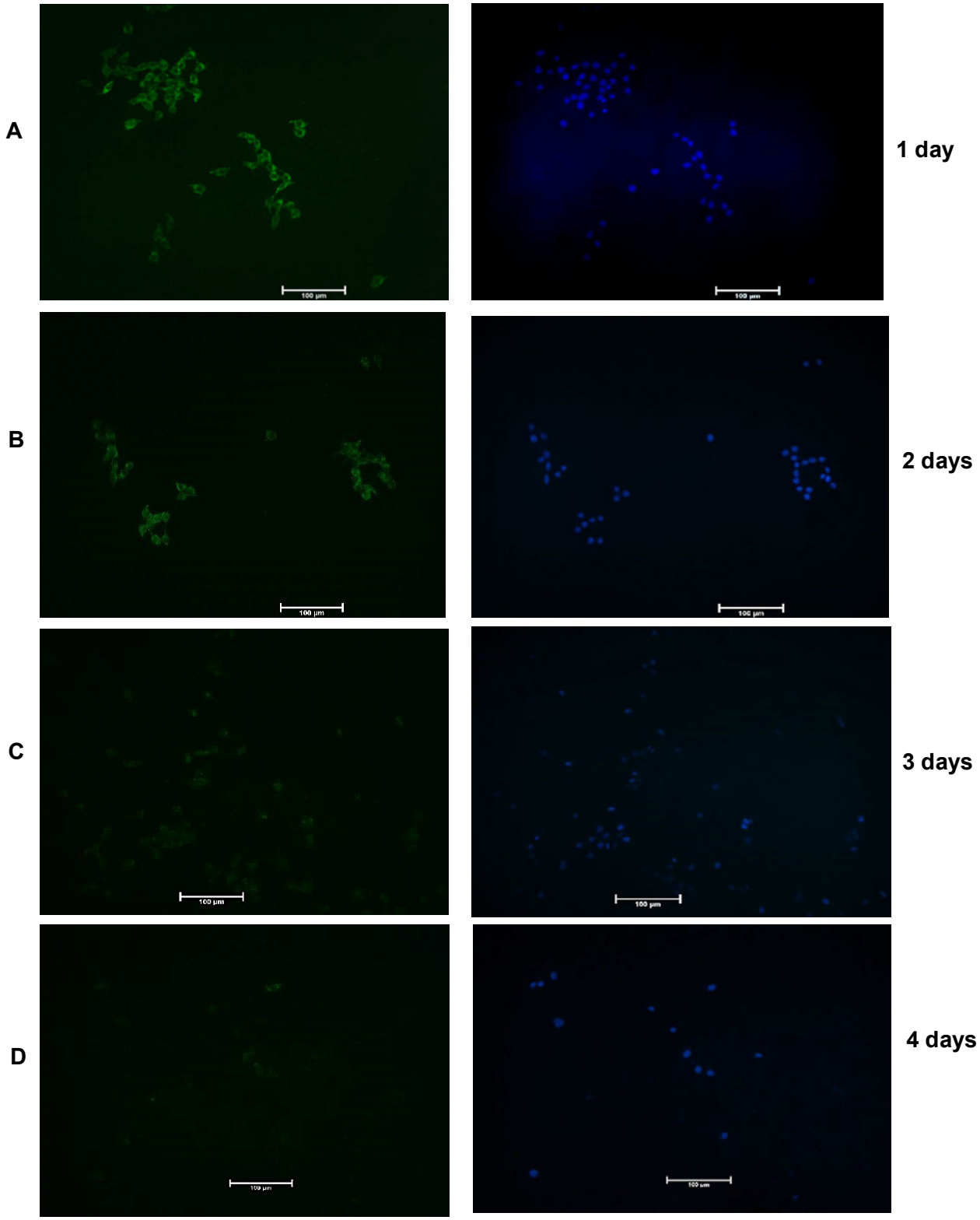

Figure 3. 8: HEK293 cells following delivery of eGFP mRNA via sEVs to determine eGFP expression over 4 days. HEK293 cells were incubated with sEVs (CM3) and either A) 2.4 µg mRNA for 1 day, B) 2.4 µg mRNA for 2 days, C) 2.4 µg mRNA for 3 days, D) 2.4 µg mRNA for 4 days in OPTIMEM. The cell nucleus stained with the Hoechst (blue). After treatment fluorescent images were obtained using a fluorescence microscopy. Scale bar = 100 µm.

To determine whether GFP expression reached a maximum earlier than 24 hours, HEK293 cells were subsequently assessed after delivery using PKH dyed sEVs incubated with 0.5, 1.2 and 2.4 μg mRNA at 6 hours and 24 hours (Figure 3.9). The eGFP-mRNA transfected cells at 24 hours showed significantly higher eGFP expression compared to cells transfected at 6 hours, regardless of the amount of eGFP-mRNA used. Specifically, cells incubated with 2.4 μg eGFP-mRNA-sEVs for 24 hours showed the greatest eGFP expression (Figure 3.9F), with much higher fluorescence intensity than those transfected with lower amount of eGFP-mRNA. At 6 hours, GFP was not easily visible in HEK293 cells (Figure 3.9A-C), indicating that 6 hours is not sufficient time to facilitate significant mRNA GFP expression in these cells. However, at 24 hours an increase of fluorescence intensity was observed as the amount of mRNA increase (Figure 3.9D-F), suggesting that 24 hours allows for more efficient expression, especially at higher mRNA concentrations. This data highlights that both the amount of mRNA and the transfection duration are important factors in determining the level of eGFP expression in cells, with a longer incubation period (at least 24 hours) and higher mRNA load (2.4 μg) yielding the best results.

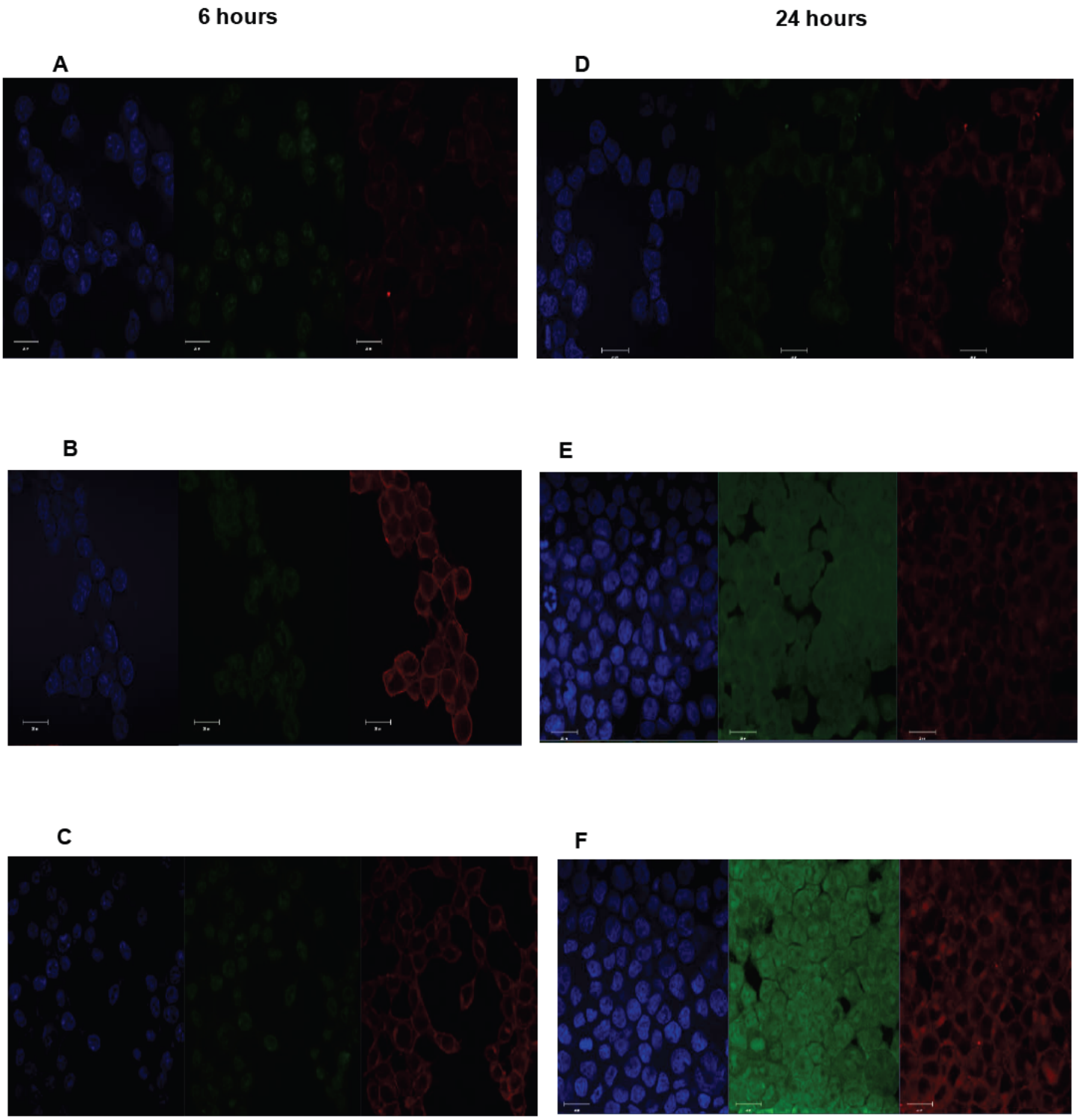

Figure 3. 9: HEK293 cells following sEV delivery of eGFP mRNA and analysis of expression at 6h and 24h. PKH-dyed sEVs (CM3) delivered either A, D) 0.5 µg mRNA, B, E) 1.2 µg mRNA or C, F) 2.4 µg mRNA to HEK293 cells and expression was analysis at were 6 hours (A, B, C) or 24 h (D, E, F) in OptiMEM. Images were obtained using a confocal microscope. Scale bar = 20 µm.

3.2.3. Analysis of sEV number related to mRNA delivery efficiency

We finally wanted to determine whether the delivery of mRNA to HEK293 cells is affected by the number of sEVs used. HEK293 cells were incubated with complexes containing 2.4 µg eGFP mRNA using 4 x 10^9, 1 x 10^9 and 0.4 x 10^9 PKH-dyed sEVs for generation (Figure 3.10). The use of 4 x 10^9 PKH stained EVs revealed higher fluorescence intensity in HEK293 cells than incubation with 1 x 10^9 PKH stained or 0.4 x 10^9 PKH sEVs (Figure 3.10 A-C). This suggest that the use of higher sEV numbers (4 x 10^9) sEVs are needed to generate eGFP positive cells.

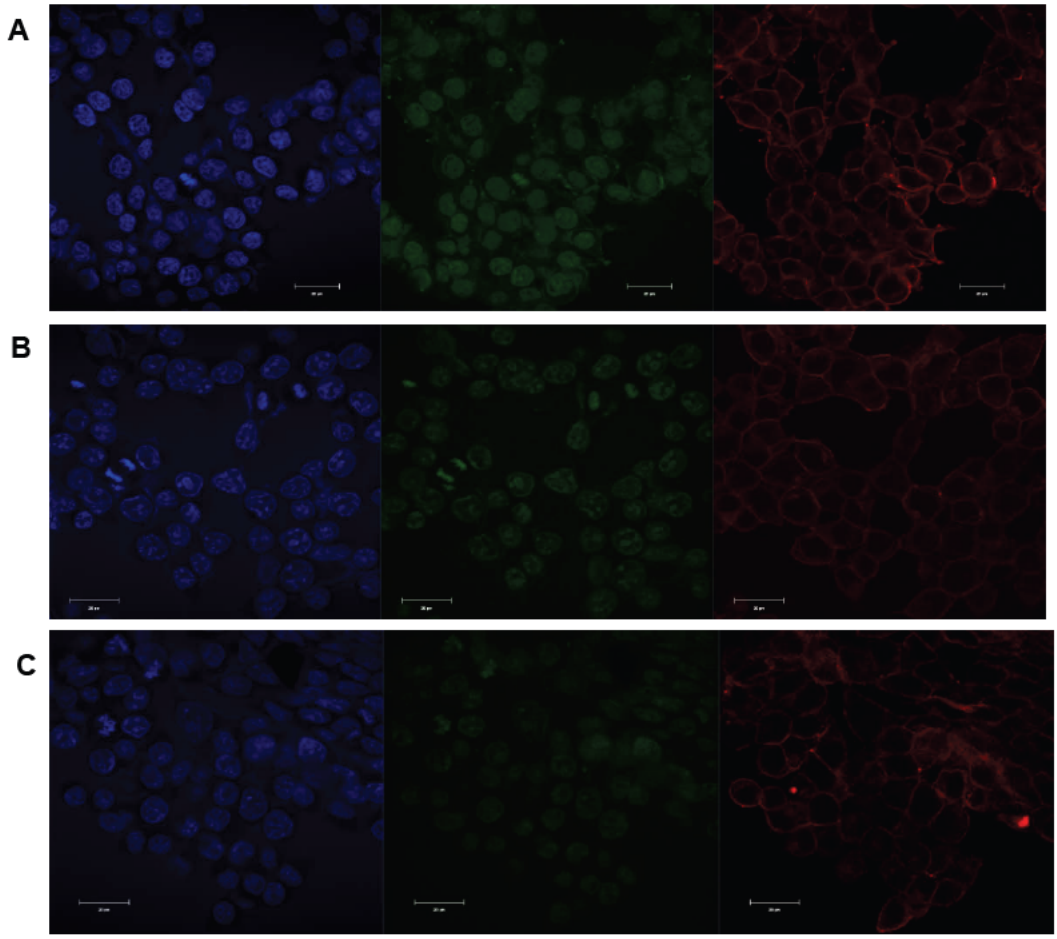

Figure 3. 10: HEK293 cells following incubation with 2.4 µg eGFP mRNA and different amounts of PKH-dyed sEVs. HEK293 cells were incubated with either A) 4 x10^9 PKH dyed sEVs, B) 1 x10^9 PKH dyed sEVs or C) 0.4 x10^9 PKH dyed sEVs for 24 hrs in OptiMEM. Nuclei stained with Hoechst (blue). After treatment fluorescent images were obtained using a confocal microscope. Scale bar = 20 µm.

Chapter 4: Discussion

Small extracellular vesicles (sEVs), a subclass of extracellular vesicles, have emerged as critical mediators of intercellular communication and hold immense potential in therapeutic applications, including targeted drug and mRNA delivery (Andaloussi et al., 2013; Théry et al., 2018). Their nanoscale size, lipid bilayer composition, and cargo-carrying capacity enable them to transport bioactive molecules such as proteins, lipids, and nucleic acids, enable them to influence diverse cellular processes (Lobb et al., 2015). Notably, sEVs offer advantages over synthetic delivery systems (such as LNPs), including enhanced biocompatibility, reduced immunogenicity, and the ability to cross biological barriers, making them a promising candidate for gene therapy and regenerative medicine (Théry et al., 2018). This study provides a comprehensive review of small extracellular vesicles (sEVs), highlighting their significance in therapeutic applications, including mRNA delivery. Vesicles were then successfully generated from HEK293 cells, isolated using PEG 6000, characterised as sEVs, and subsequently investigated for their ability to deliver mRNA in vitro.

The characterization of HEK293-generated EVs using TRPS revealed particles within the correct diameter, but with vary variable concentrations. TRPS itself is technically challenging as it requires the establishment and maintenance of a stable baseline for successful sample analysis. The conditions for an acceptable baseline are different for each new nanopore and are time-consuming. Once established, particle analysis can be further disrupted due to nanopore clogging, which requires further extensive intervention to resolve. Such challenges can affect the accuracy of the measurement of particle size and concentration. To mitigate nanopore clogging, we implemented a pre-filtration step and optimized dilution of EV samples as part of preparation process, ensuring that the particle concentration was within the optimal range of TRPS measurement. TRPS successfully confirmed that the majority of vesicles had a diameter of 159 nm or less as indicated by the average d90 value. These findings align with established criteria for exosome-like EVs (i.e. sEVs), which are optimal for therapeutic delivery due to their efficient cellular uptake and prolonged circulation times (Théry et al., 2018). Particle concentrations ranged from 20×10^9 to $1{,}000 \times 10^9$ particles/mL, with variability across samples likely reflecting the passage of the HEK293 cells used, variations in isolation efficiency or inherent sEV production heterogeneity (Witwer et al., 2013). These findings underscore the importance of refining isolation protocols to ensure reproducible and high-quality sEV preparations for therapeutic applications.

One advantage of TRPS is its ability to detect individual particles with high sensitivity, enabling precise quantification of size and concentration even in heterogeneous samples. Compared to bulk methods, such as nanoparticle tracking analysis (NTA), TRPS provides higher resolution, allowing for the identification of minor variations in vesicle populations (Vogel et al., 2016). However, TRPS is highly sensitive to sample purity, requiring careful preparation to minimize artefacts such as aggregates or co-isolated debris. Furthermore, a range of nanopore sizes are available (e.g. NP100, NP150, NP250), each accommodating particle characterisation across a specific size range. In our studies, the NP100 and NP150 were utilised; these nanopores accommodate analysis across approximate size ranges of 50-330 nm (NP100) and 70-420 nm (NP150). This could result in the underestimation of the smaller sEVs (below 50 nm). Complementing TRPS with additional techniques, such as NTA would enhance the accuracy of size and concentration data while providing insights into vesicle heterogeneity (Lobb et al., 2015). Such multi-technique approaches are essential for ensuring that sEVs are consistently characterized, particularly when they are used for applications like mRNA delivery, where precise particle size and concentration are critical for therapeutic efficacy.

The EVs were further characterized using TEM, confirming the characteristic cup-shaped morphology of sEVs, consistent with their biogenesis from multivesicular bodies (Théry et al., 2018). This morphology, coupled with the absence of large aggregates or debris, highlights the structural integrity of the vesicles and validates the isolation protocol. TEM analysis also confirmed the relatively narrow particle size distribution observed in TRPS, emphasizing the reliability of the combined analytical approach to ensure comprehensive vesicle characterization (Théry et al., 2018). Western blot analysis detected hallmark sEV markers, including CD63, TSG101, and flotillin-1, further confirming the successful isolation of vesicles enriched in exosomal markers. These markers are integral to vesicle membrane structure and biogenesis, validating the purity and functionality of the isolated sEVs (Yáñez-Mó et al., 2015). The enrichment of markers such as CD63 and TSG101 further supports the vesicles' potential to encapsulate and deliver therapeutic molecules, including mRNA (S et al., 2013). Western blotting proved to be one of the more technically challenging aspects of this study. Although bands were detected for CD63, flotillin-1, and TSG 101, the observed molecular weight did not consistently match standard values reported in the literature. However, similar findings have been described in previous studies where these EV markers exhibited a range of molecular weight due to factors such as post translation modification, protein degradation and alternative isoforms. As confirmatory controls were not included it is

not possible to rule out the possibilities that some of the observed bands may represent nonspecific binding rather than true detection of the intended proteins.

For instance, a band presumed to represent TSG101 appeared around 40 kDa-lower than the expected range of 43 to 48 kDa (Praja et al., 2021). While such shifts have been attributed to post translation modifications like ubiquitination or phosphorylation, it is possible that the bands were non-specific. Additionally, variation have been reported that TSG101 molecular weight could shift depending on sample type and experimental conditions (Théry et al., 2006). We also observed a higher molecular weight band (70kDa), which is likely due to ubiquitin conjugation or complexed form of TSG101, as previously reported (Bache et al., 2003; Cheng et al., 2014). However, the specificity of this band remains uncertain without supporting evidence from positive control lysates, knockdown experiments or mass spectrometry, it is not possible to confidently verify its identity. Flotillin-1, is another commonly used marker for EVs. It typically appears at 45-50 kDa (Berrone et al., 2015). Our result shows approximately 40kDa which is slightly lower than the expected size, and a lower observation could be due to post-translation or partial degradation of flotillin-1 produced smaller fragments that are detectable. CD63 marker is heavily glycosylated tetraspanin, and its glycosylation status can significantly affect its molecular weight and detection. Therefore, it is common to have multiple isoforms of the protein at different sizes based on their glycosylation state. Researchers have reported observing CD63 bands at various molecular weights, ranging from 30 kDa to as high as 80 kDa (Bobrie et al., 2012; Le et al., 2017; Mathieu et al., 2021; van Niel et al., 2011), depending on the sample source and antibody used (Fordjour et al., 2022). I'm not familiar with this but some have mentioned glycan extension such as polyactosamine of CD63 is known (Latysheva et al., 2006; Yáñez-Mó et al., 2015). Polyactosamine is disaccharide unit of N-acetyllactosamine that can extend from N-linked or O-linked glycans on glycoproteins and since CD63 is a heavily glycosylated protein and its glycan structure can be attached to polylactosamine chain, potentially influencing its function, interaction and stability (Ageberg & Lindmark, 2003; Kavanagh et al., 2021).

Despite repeated optimization-adjusting antibody dilutions, protein loading, and transfer conditions-the TSG101 signal remained inconsistent and non-specific. These challenges were likely compounded by low sample purity, a known limitation of PEG-based EV isolation. If additional time and resources had been available, future validation strategies such as testing different commercial antibodies, optimizing lysis buffer composition, using protease inhibitors and enriching EV fraction using density gradient ultracentrifugation or size-exclusion chromatography.

Protein concentration analysis revealed levels ranging from 0.336 to 0.614 µg/µL. Notably, no direct correlation was observed between protein concentration and vesicle number, as exemplified by CM3 and CM5, which had identical protein levels but completely different particle concentrations. This discrepancy suggests the potential presence of co-isolated non-vesicular proteins, emphasizing the need for advanced purification methods, such as size-exclusion chromatography or ultrafiltration, to ensure sample purity (Kowal et al., 2016). The use of PEG 6000 to isolate sEVs is often challenging due to the co-isolation of non-associated proteins. Analysis of purity revealed a potential positive correlation between particle concentration and purity ratios, with CM1 yielding the highest particle concentration (1 000 x 10^9 particles/mL) and purity (1.63 x 10^9 particles/µg), and CM7 the lowest. These findings align with prior studies by Webber and Clayton, which reported that EVs from cell culture in T75s generate purity ratios of approximately 1x10^7 particles/ug protein (Webber & Clayton, 2013). Although Webber and Clayton (2013) used the particle-to-protein ratio to indicate EV purity by relating particle number to the amount of contaminant proteins external to the vesicles. Other studies have used this type of approach to measure EV purity as well (Yang et al., 2021). To quantify total protein and prepare samples for western blotting, we lysed our EVs, which allowed detection of both surface-associated protein and internal cargo. While for purity assessment the protein measurement should ideally reflect only external contamination, we compared lysed and unlysed EV samples and found no significant difference in total protein concentration between the two.

This observation suggests that the EVs contained very little internal protein, and that most of the proteins detected likely originated from the external source or surface associated contaminants. Therefore, although this is not strictly correct method for assessing impurity- since the internal content is included- our findings still speak to purity, because the vesicles appear to be mostly “empty” inside, and the measured protein likely reflects external contamination. This interpretation provides useful insight and supports the continued use of the particle-to-particle ratio in this context. Nonetheless, this approach is not strictly the way one should do it for proper external contamination measurements going forward, and with more time and resources this analysis would be repeated. Incorporating size-exclusion chromatography (SEC) as a secondary purification step could further refine sEV purity by selectively removing non-vesicular contaminants and large aggregates (Yang et al., 2021). A combined PEG 6000-SEC approach may help balance high yield with improved purity, ensuring more consistent results across all samples (Yang et al., 2020).

The study then explored two distinct approaches for mRNA delivery into HEK293 cells: Lipofectamine MessengerMax was compared with the use of sEVs as delivery vehicles.

While both methods demonstrated the ability to facilitate mRNA delivery and subsequent eGFP expression, they exhibited differences in transfection efficiency, dose-dependent behaviour, and operational requirements, providing complementary insights into optimizing mRNA delivery systems. Lipofectamine MessengerMax, a lipid-based transfection reagent, achieved good transfection efficiency, with eGFP expression peaking at 2.4 µg of mRNA. A dose-dependent increase in fluorescence intensity was observed up to this concentration, after which no further significant enhancement was detected, indicating a plateau effect. sEVs, a biologically derived delivery system, showed a dose-dependent increase in eGFP expression, with 2.4 µg of mRNA also achieving the highest transfection efficiency. Transfection efficiency generally increases with mRNA dosage until saturation of cellular machinery or the delivery reagent's capacity is reached; it would therefore be interesting to extend the analysis to higher mRNA amounts and to further measure the green fluorescence to achieve a quantifiable measure of transfection; this would allow us to compare the two methods of mRNA delivery in a quantifiable manner (Zhu et al., 2020). The absence of eGFP expression in cells transfected without Lipofectamine MessengerMax underscores its critical role in facilitating cellular uptake and cytoplasmic release of mRNA (Moradian et al., 2020). Its reliance on lipid-based chemistry may limit its use in certain in vivo applications due to potential toxicity and off-target effects; in this regard, the use of natural lipid-based nanoparticles such as sEVs is beneficial (Zhang X. et al., 2021). Notably, the use of PKH26 staining confirmed the internalization of sEVs into HEK293 cells, further validating their role as delivery vehicles. The presence of sEVs within cells was consistent across all tested mRNA dosages, highlighting their capability for cargo delivery. However, while sEVs are a promising alternative to synthetic reagents, further optimization, such as improving loading efficiency or engineering vesicles for enhanced delivery, is needed (Elsharkasy et al., 2020).

In conclusion, this study provides valuable insights into the isolation and characterization of sEVs from HEK293 cells using PEG-based precipitation and employed the delivery of eGFP mRNA to recipient cells, marking an initial step towards developing a non-viral, EV-based mRNA deliver platform. While the results are promising, this study was limited to a single isolation approach and passive mRNA loading techniques. Given more time and resources, several enhancements could have strengthened the study's robustness. For instance, repeating key experiments such as mRNA delivery assay and analysing sEVs protein markers with additional biological and technical replicates would improve statistical robustness. Incorporating ELISA to validate EV-associated protein markers could have strengthened the conclusion regarding characterisation. While sEVs offer key advantages such as low immunogenicity and endogenous targeting, they face limitation in scalability and loading capacity. Consideration of alternative platforms such as lipid nanoparticles, viral

vectors, or virus like particle could provide useful context for optimizing delivery efficiency (Albanese et al., 2021; Lu et al., 2023). Combining sEVs with these platforms or integrating them into hybrid delivery system may represent a future direction for enhancing functionality (Mendt et al., 2018). Notably, although EV research has been widely published in the field, this study represents the first time that EVs isolation and mRNA delivery using sEVs were implemented and optimized within our laboratory. This work marks the initial setup of this platform, establishing protocol that can now be used by future students and researchers in the lab for EV based applications.

Introducing size exclusion chromatography such as qEV columns alongside PEG precipitation could enable more selective isolation of sEV subpopulations with higher purity (Lobb et al., 2015). Further optimization is necessary to enhance the loading efficiency of sEVs and improve their mRNA delivery capabilities. Future studies could explore engineering vesicles to increase their loading capacity or modify their surface properties for more targeted delivery, thereby advancing their therapeutic potential (Elsharkasy et al., 2020; Iqbal et al., 2024). Alternative loading techniques such as electroporation, sonication, or biomaterials-assisted encapsulation (e.g. hydrogels) could also be explored in future experiments to improve mRNA encapsulation efficiency and loading uniformity (Xie et al., 2022; Zeng, H. et al., 2023).

The successful isolation of sEVs with well-defined size, morphology, and protein marker profiles, combined with their ability to efficiently deliver mRNA to target cells, establishes sEVs as a promising alternative to synthetic delivery systems. Vesicles within the 70–150 nm range are preferentially taken up by cells via endocytosis or membrane fusion, facilitating efficient cargo delivery (Manzanares & Ceña, 2020). sEVs therefore offer unique advantages, including biocompatibility and reduced immunogenicity, and hold great potential for targeted delivery, which are particularly valuable for therapeutic applications. Ultimately, while this research provides foundational insight into the potential of HEK293 derived sEVs as mRNA delivery vehicles, much work remains to optimize and standardize isolation, loading and analytical methods. The findings of this study lay important groundwork for the ongoing development of sEV-based drug and gene delivery platforms, offering a potential avenue for future therapeutic applications.

Appendix 1: TRPS Optimisation

A standard operating procedure (SOP) had to be established using 100 nm nanoparticles (CPC100; 1.2 x 10^{13} particles/ml). To establish this, a nanopore membrane (NP100 or NP150) was loaded onto the EXOID and stretched to 47 mm. The surfactant-containing wetting solution (Izon Science Ltd.), which allows contact between upper and lower fluid cell through the nanopore, was prepared by diluting it at 1:100 (v/v) with filtered PBS. A volume of this wetting solution (75 µl) was then loaded in the lower fluid cell, while 35 µl was loaded in the upper fluid cell. A pressure of 2500 Pa was then applied for 10 minutes. After removing the wetting solution 10% (w/v) filtered Izon coating solution in filtered electrolyte-PBS was loaded in the upper and lower fluid and applied 2500 Pa pressure for 10 minutes this avoids contamination binding to the nanopore. The nanopore membrane as well as the upper and lower fluid cells (loading chambers) were rinsed with filtered electrolyte-PBS and dried using lint-free paper towels. After assembling the loading chambers back, characterisation of the nanopore was done using CPC100 (1.2x10^{13}particles/ml) which was diluted 1:5000 in filtered PBS initial applied pressure was set to 1000 Pa.

Prior to subsequent EV sample analysis, one needs to ensure that the pressure, voltage and nanopore membrane stretch are set such that:

- The baseline current is maintained between 100 nA to 140 nA
- RMS noise is below 15 pA
- Particle rate is between 100 particles/minute to 1500 particles/minute to obtain accurate results.

After optimization and baseline establishment, analysis can begin. The Izon Data Suit Software generates a particle rate plot for both the sample and the calibration. The rate plot below reflects the results for a CPC100 sample run at three different pressures: 400 Pa, 600 Pa and 1000 Pa; it is critical to check this rate plot to determine the best pressures at which to calibrate unknown samples (Figure A1). As the pressure increases, the rate should also increase (in other words the time taken to measure at least 500 particles should decrease as the pressure increases (Figure A1).

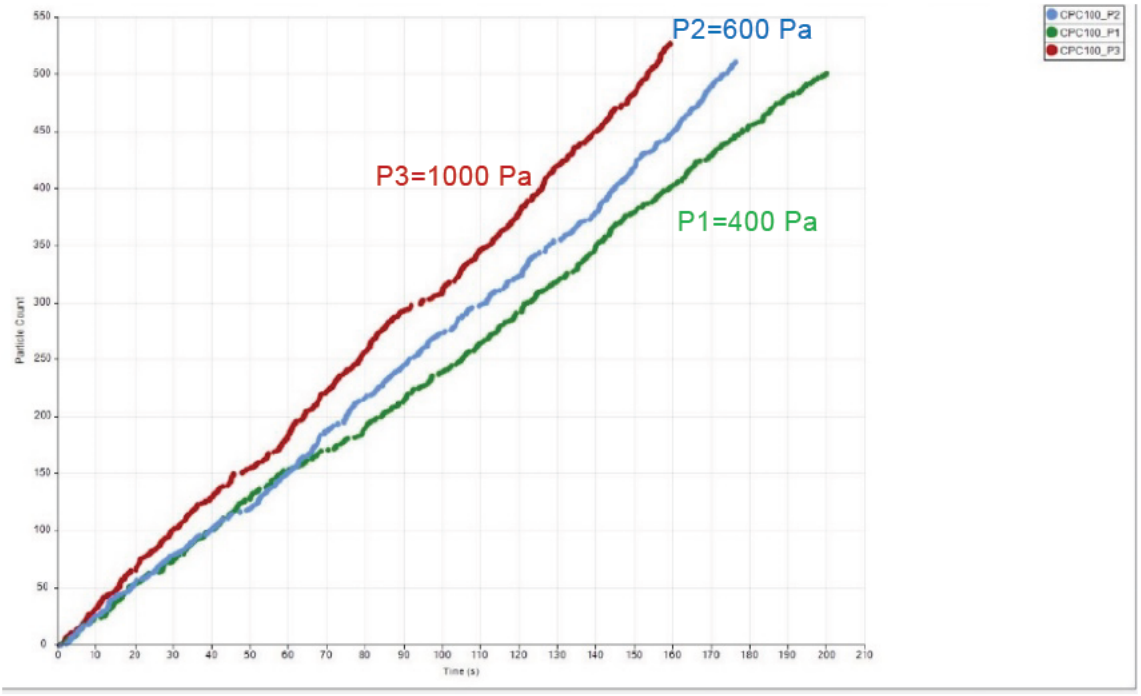

Figure A 1: Particle rate plots for sample analysis run at 3 different pressures. Pressure 1 at 400 Pa (green), pressure 2 at 600 Pa (blue) and pressure 3 at 1000 Pa (red). The analysis was carried out using NP100 nanopore and calibrated with 110 nm polystyrene beads (CPC100).

Appendix 2: eGFP DNA sequence

GACGCGCCCTGTAGCGGCGCAT(T7
promoter)TAAGCGCGGCGGGTGTGGTGGTTACGCGCAGCGTGACCGCTACACTTGCCAGCGCCCTAGCGCCCGCTCCTTTC
GCTTTCTTCCCTTCCTTTCTCGCCACGTTCGCCGGCTTTCCCCGTCAAGCTCTAAATCGGGGGCTCCCTTTAGGGTTCCGATT
TAGTGCTTTACGGCACCTCGACCCCAAAAAACTTGATTAGGGTGATGGTTCACGTAGTGGGCCATCGCCCTGATAGACGGTTT
TTCGCCCTTTGACGTTGGAGTCCACGTTCTTTAATAGTGGACTCTTGTTCCAAACTGGAACAACACTCAACCCTATCTCGGTC
TATTCTTTTGATTTATAAGGGATTTTGCCGATTTCGGCCTATTGGTTAAAAAATGAGCTGATTTAACAAAAATTTAACGCGAA
TTTTAACAAAATATTAACGCTTACAATTTCCATTCGCCATTCAGGCTGCGCAACTGTTGGGAAGGGCGATCGGTGCGGGCCTC
TTCGCTATTACGCCAGCTGGACATTGATTATTGACTAGTTATTAATAGTAATCAATTACGGGGTCATTAGTTCATAGCCCATA
TATGGAGTTCCGCGTTACATAACTTACGGTAAATGGCCCGCCTGGCTGACCGCCCAACGACCCCCGCCCATTGACGTCAATAA
TGACGTATGTTCCCATAGTAACGCCAATAGGGACTTTCCATTGACGTCAATGGGTGGACTATTTACGGTAAACTGCCCACTTG
GCAGTACATCAAGTGTATCATATGCCAAGTACGCCCCCTATTGACGTCAATGACGGTAAATGGCCCGCCTGGCATTATGCCCA
GTACATGACCTTATGGGACTTTCCTACTTGGCAGTACATCTACGTATTAGTCATCGCTATTACCATGGTGATGCGGTTTTGGC
AGTACATCAATGGGCGTGGATAGCGGTTTGACTCACGGGGATTTCCAAGTCTCCACCCCATTGACGTCAATGGGAGTTTGTTT
TGGCACCAAAATCAACGGGACTTTCCAAAATGTCGTAACAACTCCGCCCCATTGACGCAAATGGGCGGTAGGCGTGTACGGTG
GGAGGTCTATATAAGCAGAGCTCTCTGGCTAACTAGAGAACCCACTGCTTACTGGCTTATCGAAATTAATACGACTCACTATA
GGGACATTTGCTTCTGACACAACTGTGTTCACTAGCAACCTCAAACAGACACCGCC (5’UTR)GCCACC(ORF-eGFP
region)ATGGTGAGCAAGGGCGAGGAGCTGTTCACCGGGGTGGTGCCCATCCTGGTCGAGCTGGACGGCGACGTAAACGGCC
ACAAGTTCAGCGTGTCCGGCGAGGGCGAGGGCGATGCCACCTACGGCAAGCTGACCCTGAAGTTCATCTGCACCACCGGCAAG
CTGCCCGTGCCCTGGCCCACCCTCGTGACCACCCTGACCTACGGCGTGCAGTGCTTCAGCCGCTACCCCGACCACATGAAGCA
GCACGACTTCTTCAAGTCCGCCATGCCCGAAGGCTACGTCCAGGAGCGCACCATCTTCTTCAAGGACGACGGCAACTACAAGA
CCCGCGCCGAGGTGAAGTTCGAGGGCGACACCCTGGTGAACCGCATCGAGCTGAAGGGCATCGACTTCAAGGAGGACGGCAAC
ATCCTGGGGCACAAGCTGGAGTACAACTACAACAGCCACAACGTCTATATCATGGCCGACAAGCAGAAGAACGGCATCAAGGT
GAACTTCAAGATCCGCCACAACATCGAGGACGGCAGCGTGCAGCTCGCCGACCACTACCAGCAGAACACCCCCATCGGCGACG
GCCCCGTGCTGCTGCCCGACAACCACTACCTGAGCACCCAGTCCGCCCTGAGCAAAGACCCCAACGAGAAGCGCGATCACATG
GTCCTGCTGGAGTTCGTGACCGCCGCCGGGATCACTCTCGGCATGGACGAGCTGTACAAGTAAGCTCGCTTTCTTGCTGTCCA
ATTTCTATTAAAGGTTCCTTTGTTCCCTAAGTCCAACTACTAAACTGGGGGATATTATGAAGGGCCTTGAGCATCTGGATTCT
GCCTAATAAAAAACATTTATTTTCATTGC (poly (A) tail)
AAAAAAAAAAAAAAAAAAAAAAAAAAAAAAAAAAAAAAAAAAAAAAAAAAAAAAAAAAAAAAAAAAAAAAAAAAAAAAAAA
AAAAAAAAAAAAAAAAAAAAAAAAAAAAAAAAAAAAAAGAGACCATAGCAGGTGCATACACCTGCATATAGACGGCTAGCCCGC
TGATCAGCCTCGACTGTGCCTTCTAGTTGCCAGCCATCTGTTGTTTGCCCCTCCCCCGTGCCTTCCTTGACCCTGGAAGGTGC
CACTCCCACTGTCCTTTCCTAATAAAATGAGGAAATTGCATCGCATTGTCTGAGTAGGTGTCATTCTATTCTGGGGGGTGGGG
TGGGGCAGGACAGCAAGGGGGAGGATTGGGAAGAAAATAGCAGGCATGCTGGGGATGCGGTGGGCTCTATGGGCGGCCGCCAT
GTGAGCAAAAGGCCAGCAAAAGGCCAGGAACCGTAAAAAGGCCGCGTTGCTGGCGTTTTTCCATAGGCTCCGCCCCCCTGACG
AGCATCACAAAAATCGACGCTCAAGTCAGAGGTGGCGAAACCCGACAGGACTATAAAGATACCAGGCGTTTCCCCCTGGAAGC
TCCCTCGTGCGCTCTCCTGTTCCGACCCTGCCGCTTACCGGATACCTGTCCGCCTTTCTCCCTTCGGGAAGCGTGGCGCTTTC
TCATAGCTCACGCTGTAGGTATCTCAGTTCGGTGTAGGTCGTTCGCTCCAAGCTGGGCTGTGTGCACGAACCCCCCGTTCAGC
CCGACCGCTGCGCCTTATCCGGTAACTATCGTCTTGAGTCCAACCCGGTAAGACACGACTTATCGCCACTGGCAGCAGCCACT
GGTAACAGGATTAGCAGAGCGAGGTATGTAGGCGGTGCTACAGAGTTCTTGAAGTGGTGGCCTAACTACGGCTACACTAGAAG
AACAGTATTTGGTATCTGCGCTCTGCTGAAGCCAGTTACCTTCGGAAAAAGAGTTGGTAGCTCTTGATCCGGCAAACAAACCA
CCGCTGGTAGCGGTGGTTTTTTTGTTTGCAAGCAGCAGATTACGCGCAGAAAAAAAGGATCTCAAGAAGATCCTTTGATCTTT
TCTACGGGGTCTGACGCTCAGTGGAACGAAAACTCACGTTAAGGGATTTTGGTCATGAGATTATCAAAAAGGATCTTCACCTA
GATCCTTTTAAATTAAAAATGAAGTTTTAAATCAATCTAAAGTATATATGAGTAAACTTGGTCTGACAGTTACCAATGCTTAA
TCAGTGAGGCACCTATCTCAGCGATCTGTCTATTTCGTTCATCCATAGTTGCCTGACTCCCCGTCGTGTAGATAACTACGATA
CGGGAGGGCTTACCATCTGGCCCCAGTGCTGCAATGATACCGCGAGATCCACGCTCACCGGCTCCAGATTTATCAGCAATAAA
CCAGCCAGCCGGAAGGGCCGAGCGCAGAAGTGGTCCTGCAACTTTATCCGCCTCCATCCAGTCTATTAATTGTTGCCGGGAAG
CTAGAGTAAGTAGTTCGCCAGTTAATAGTTTGCGCAACGTTGTTGCCATTGCTACAGGCATCGTGGTGTCACGCTCGTCGTTT
GGTATGGCTTCATTCAGCTCCGGTTCCCAACGATCAAGGCGAGTTACATGATCCCCCATGTTGTGCAAAAAAGCGGTTAGCTC
CTTCGGTCCTCCGATCGTTGTCAGAAGTAAGTTGGCCGCAGTGTTATCACTCATGGTTATGGCAGCACTGCATAATTCTCTTA
CTGTCATGCCATCCGTAAGATGCTTTTCTGTGACTGGTGAGTACTCAACCAAGTCATTCTGAGAATAGTGTATGCGGCGACCG
AGTTGCTCTTGCCCGGCGTCAATACGGGATAATACCGCGCCACATAGCAGAACTTTAAAAGTGCTCATCATTGGAAAACGTTC
TTCGGGGCGAAAACTCTCAAGGATCTTACCGCTGTTGAGATCCAGTTCGATGTAACCCACTCGTGCACCCAACTGATCTTCAG
CATCTTTTACTTTCACCAGCGTTTCTGGGTGAGCAAAAACAGGAAGGCAAAATGCCGCAAAAAAGGGAATAAGGGCGACACGG
AAATGTTGAATACTCATACTCTTCCTTTTTCAATATTATTGAAGCATTTATCAGGGTTATTGTCTCATGAGCGGATACATATT
TGAATGTATTTAGAAAAATAAACAAATAGGGGTTCCGCGCACATTTCCCCGAAAAGTGCCACCT -3’

References

Abramowicz, A., Marczak, L., Wojakowska, A., Zapotoczny, S., Whiteside, T. L., Widlak, P., & Pietrowska, M. (2018). Harmonization of exosome isolation from culture supernatants for optimized proteomics analysis. *PLoS One*, *13*(10), e0205496. https://doi.org/10.1371/journal.pone.0205496

Abramowicz, A., Widlak, P., & Pietrowska, M. (2016). Proteomic analysis of exosomal cargo: the challenge of high purity vesicle isolation. *Mol Biosyst*, *12*(5), 1407-1419. https://doi.org/10.1039/c6mb00082g

Adrian, M., Dubochet, J., Lepault, J., & McDowall, A. W. (1984). Cryo-electron microscopy of viruses. *Nature*, *308*(5954), 32-36. https://doi.org/10.1038/308032a0

Ageberg, M., & Lindmark, A. (2003). Characterisation of the biosynthesis and processing of the neutrophil granule membrane protein CD63 in myeloid cells. *Clin Lab Haematol*, *25*(5), 297-306. https://doi.org/10.1046/j.1365-2257.2003.00541.x

Albanese, M., Chen, Y. A., Hüls, C., Gärtner, K., Tagawa, T., Mejias-Perez, E., Keppler, O. T., Göbel, C., Zeidler, R., Shein, M., Schütz, A. K., & Hammerschmidt, W. (2021). MicroRNAs are minor constituents of extracellular vesicles that are rarely delivered to target cells. *PLoS Genet*, *17*(12), e1009951. https://doi.org/10.1371/journal.pgen.1009951

Alvarez-Erviti, L., Seow, Y., Yin, H., Betts, C., Lakhal, S., & Wood, M. J. (2011). Delivery of siRNA to the mouse brain by systemic injection of targeted exosomes. *Nat Biotechnol*, *29*(4), 341-345. https://doi.org/10.1038/nbt.1807

Alzhrani, G. N., Alanazi, S. T., Alsharif, S. Y., Albalawi, A. M., Alsharif, A. A., Abdel-Maksoud, M. S., & Elsherbiny, N. (2021). Exosomes: Isolation, characterization, and biomedical applications. *Cell Biol Int*, *45*(9), 1807-1831. https://doi.org/10.1002/cbin.11620

Andaloussi, SEL., Mäger, I., Breakefield, X. O., & Wood, M. J. (2013). Extracellular vesicles: biology and emerging therapeutic opportunities. *Nat Rev Drug Discov*, *12*(5), 347-357. https://doi.org/10.1038/nrd3978

Andreu, Z., Rivas, E., Sanguino-Pascual, A., Lamana, A., Marazuela, M., González-Alvaro, I., Sánchez-Madrid, F., de la Fuente, H., & Yáñez-Mó, M. (2016). Comparative analysis of EV isolation procedures for miRNAs detection in serum samples. *J Extracell Vesicles*, *5*, 31655. https://doi.org/10.3402/jev.v5.31655

Andreu, Z., & Yáñez-Mó, M. (2014). Tetraspanins in extracellular vesicle formation and function. *Front Immunol*, *5*, 442. https://doi.org/10.3389/fimmu.2014.00442

Arakawa, T., & Timasheff, S. N. (1985). Mechanism of poly(ethylene glycol) interaction with proteins. *Biochemistry*, *24*(24), 6756-6762. https://doi.org/10.1021/bi00345a005

Arraud, N., Gounou, C., Linares, R., & Brisson, A. R. (2015). A simple flow cytometry method improves the detection of phosphatidylserine-exposing extracellular vesicles. *J Thromb Haemost*, *13*(2), 237-247. https://doi.org/10.1111/jth.12767

Auber, M., Fröhlich, D., Drechsel, O., Karaulanov, E., & Krämer-Albers, E. M. (2019). Serum-free media supplements carry miRNAs that co-purify with extracellular vesicles. *J Extracell Vesicles*, *8*(1), 1656042. https://doi.org/10.1080/20013078.2019.1656042

Bache, K. G., Raiborg, C., Mehlum, A., & Stenmark, H. (2003). STAM and Hrs are subunits of a multivalent ubiquitin-binding complex on early endosomes. *J Biol Chem*, *278*(14), 12513-12521. https://doi.org/10.1074/jbc.M210843200

Baden, L. R., El Sahly, H. M., Essink, B., Kotloff, K., Frey, S., Novak, R., Diemert, D., Spector, S. A., Rouphael, N., Creech, C. B., McGettigan, J., Khetan, S., Segall, N., Solis, J., Brosz, A., Fierro, C., Schwartz, H., Neuzil, K., Corey, L., . . . Zaks, T. (2021). Efficacy and Safety of the mRNA-1273 SARS-CoV-2 Vaccine. *N Engl J Med*, *384*(5), 403-416. https://doi.org/10.1056/NEJMoa2035389

Baixauli, F., López-Otín, C., & Mittelbrunn, M. (2014). Exosomes and autophagy: coordinated mechanisms for the maintenance of cellular fitness. *Front Immunol*, *5*, 403. https://doi.org/10.3389/fimmu.2014.00403

Baranyai, T., Herczeg, K., Onódi, Z., Voszka, I., Módos, K., Marton, N., Nagy, G., Mäger, I., Wood, M. J., El Andaloussi, S., Pálinkás, Z., Kumar, V., Nagy, P., Kittel, Á., Buzás, E. I., Ferdinandy, P., & Giricz, Z. (2015). Isolation of Exosomes from Blood Plasma: Qualitative and Quantitative Comparison of Ultracentrifugation and Size Exclusion Chromatography Methods. *PLoS One*, *10*(12), e0145686. https://doi.org/10.1371/journal.pone.0145686

Bebelman, M. P., Smit, M. J., Pegtel, D. M., & Baglio, S. R. (2018). Biogenesis and function of extracellular vesicles in cancer. *Pharmacol Ther*, *188*, 1-11. https://doi.org/10.1016/j.pharmthera.2018.02.013

Becker, A., Thakur, B. K., Weiss, J. M., Kim, H. S., Peinado, H., & Lyden, D. (2016). Extracellular Vesicles in Cancer: Cell-to-Cell Mediators of Metastasis. *Cancer Cell*, *30*(6), 836-848. https://doi.org/10.1016/j.ccell.2016.10.009

Bellavia, D., Raimondo, S., Calabrese, G., Forte, S., Cristaldi, M., Patinella, A., Memeo, L., Manno, M., Raccosta, S., Diana, P., Cirrincione, G., Giavaresi, G., Monteleone, F., Fontana, S., De Leo, G., & Alessandro, R. (2017). Interleukin 3- receptor targeted exosomes inhibit in vitro and in vivo Chronic Myelogenous Leukemia cell growth. *Theranostics*, *7*(5), 1333-1345. https://doi.org/10.7150/thno.17092

Berrone, E., Corona, C., Mazza, M., Costassa, E. V., Faro, M. L., Properzi, F., Guglielmetti, C., Maurella, C., Caramelli, M., Deregibus, M. C., Camussi, G., & Casalone, C. (2015). Detection of cellular prion protein in exosomes derived from ovine plasma. *J Gen Virol*, *96*(12), 3698-3702. https://doi.org/10.1099/jgv.0.000291

Bobrie, A., Colombo, M., Krumeich, S., Raposo, G., & Théry, C. (2012). Diverse subpopulations of vesicles secreted by different intracellular mechanisms are present in exosome preparations obtained by differential ultracentrifugation. *J Extracell Vesicles*, *1*. https://doi.org/10.3402/jev.v1i0.18397

Bobrie, A., Colombo, M., Raposo, G., & Théry, C. (2011). Exosome secretion: molecular mechanisms and roles in immune responses. *Traffic*, *12*(12), 1659-1668. https://doi.org/10.1111/j.1600-0854.2011.01225.x

Born, L. J., Chang, K. H., Shoureshi, P., Lay, F., Bengali, S., Hsu, A. T. W., Abadchi, S. N., Harmon, J. W., & Jay, S. M. (2022). HOTAIR-Loaded Mesenchymal Stem/Stromal Cell Extracellular Vesicles Enhance Angiogenesis and Wound Healing. *Adv Healthc Mater*, *11*(5), e2002070. https://doi.org/10.1002/adhm.202002070

Borniego, M. L., & Innes, R. W. (2023). Extracellular RNA: mechanisms of secretion and potential functions. *J Exp Bot*, *74*(7), 2389-2404. https://doi.org/10.1093/jxb/erac512

Bryzgunova, O. E., Zaripov, M. M., Skvortsova, T. E., Lekchnov, E. A., Grigor'eva, A. E., Zaporozhchenko, I. A., Morozkin, E. S., Ryabchikova, E. I., Yurchenko, Y. B., Voitsitskiy, V. E., & Laktionov, P. P. (2016). Comparative Study of Extracellular Vesicles from the Urine of Healthy Individuals and Prostate Cancer Patients. *PLoS One*, *11*(6), e0157566. https://doi.org/10.1371/journal.pone.0157566

Chang, P. K. C., Prestidge, C. A., & Bremmell, K. E. (2022). PAMAM versus PEI complexation for siRNA delivery: interaction with model lipid membranes and cellular uptake. *Pharm Res*, *39*(6), 1151-1163. https://doi.org/10.1007/s11095-022-03229-7

Chargaff, E., & West, R. (1946). The biological significance of the thromboplastic protein of blood. *J Biol Chem*, *166*(1), 189-197.

Chen, Y. W., Lin, Y. H., Ho, C. C., Chen, C. Y., Yu, M. H., Lee, A. K., Chiu, S. C., Cho, D. Y., & Shie, M. Y. (2024). High-yield extracellular vesicle production from HEK293T cells encapsulated in 3D auxetic scaffolds with cyclic mechanical stimulation for effective drug carrier systems. *Biofabrication*, *16*(4). https://doi.org/10.1088/1758-5090/ad728b

Cheng, L., Sharples, R. A., Scicluna, B. J., & Hill, A. F. (2014). Exosomes provide a protective and enriched source of miRNA for biomarker profiling compared to intracellular and cell-free blood. *J Extracell Vesicles*, *3*. https://doi.org/10.3402/jev.v3.23743

Cocucci, E., & Meldolesi, J. (2011). Ectosomes. *Curr Biol*, *21*(23), R940-941. https://doi.org/10.1016/j.cub.2011.10.011

Colombo, M., Raposo, G., & Théry, C. (2014). Biogenesis, secretion, and intercellular interactions of exosomes and other extracellular vesicles. *Annu Rev Cell Dev Biol*, *30*, 255-289. https://doi.org/10.1146/annurev-cellbio-101512-122326

Contreras-Naranjo, J. C., Wu, H. J., & Ugaz, V. M. (2017). Microfluidics for exosome isolation and analysis: enabling liquid biopsy for personalized medicine. *Lab Chip*, *17*(21), 3558-3577. https://doi.org/10.1039/c7lc00592j

de Gassart, A., Geminard, C., Fevrier, B., Raposo, G., & Vidal, M. (2003). Lipid raft-associated protein sorting in exosomes. *Blood*, *102*(13), 4336-4344. https://doi.org/10.1182/blood-2003-03-0871

Deville, S., Garcia Romeu, H., Oeyen, E., Mertens, I., Nelissen, I., & Salvati, A. (2022). Macrophages Release Extracellular Vesicles of Different Properties and Composition Following Exposure to Nanoparticles. *Int J Mol Sci*, *24*(1). https://doi.org/10.3390/ijms24010260

Didiot, M. C., Hall, L. M., Coles, A. H., Haraszti, R. A., Godinho, B. M., Chase, K., Sapp, E., Ly, S., Alterman, J. F., Hassler, M. R., Echeverria, D., Raj, L., Morrissey, D. V., DiFiglia, M., Aronin, N., & Khvorova, A. (2016). Exosome-mediated Delivery of Hydrophobically Modified siRNA for Huntingtin mRNA Silencing. *Mol Ther*, *24*(10), 1836-1847. https://doi.org/10.1038/mt.2016.126

Doherty, G. J., & McMahon, H. T. (2009). Mechanisms of endocytosis. *Annu Rev Biochem*, *78*, 857-902. https://doi.org/10.1146/annurev.biochem.78.081307.110540

Du, S., Guan, Y., Xie, A., Yan, Z., Gao, S., Li, W., Rao, L., Chen, X., & Chen, T. (2023). Extracellular vesicles: a rising star for therapeutics and drug delivery. *J Nanobiotechnology*, *21*(1), 231. https://doi.org/10.1186/s12951-023-01973-5

Duan, L., Ouyang, K., Wang, J., Xu, L., Xu, X., Wen, C., Xie, Y., Liang, Y., & Xia, J. (2021). Exosomes as Targeted Delivery Platform of CRISPR/Cas9 for Therapeutic Genome Editing. *Chembiochem*, *22*(24), 3360-3368. https://doi.org/10.1002/cbic.202100359

Elsharkasy, O. M., Nordin, J. Z., Hagey, D. W., de Jong, O. G., Schiffelers, R. M., Andaloussi, S. E., & Vader, P. (2020). Extracellular vesicles as drug delivery systems: Why and how? *Adv Drug Deliv Rev*, *159*, 332-343. https://doi.org/10.1016/j.addr.2020.04.004

Fordjour, F. K., Guo, C., Ai, Y., Daaboul, G. G., & Gould, S. J. (2022). A shared, stochastic pathway mediates exosome protein budding along plasma and endosome membranes. *J Biol Chem*, *298*(10), 102394. https://doi.org/10.1016/j.jbc.2022.102394

French, K. C., Antonyak, M. A., & Cerione, R. A. (2017). Extracellular vesicle docking at the cellular port: Extracellular vesicle binding and uptake. *Semin Cell Dev Biol*, *67*, 48-55. https://doi.org/10.1016/j.semcdb.2017.01.002

Fuhrmann, G., Serio, A., Mazo, M., Nair, R., & Stevens, M. M. (2015). Active loading into extracellular vesicles significantly improves the cellular uptake and photodynamic effect of porphyrins. *J Control Release*, *205*, 35-44. https://doi.org/10.1016/j.jconrel.2014.11.029

Gao, X., Wan, Z., Wei, M., Dong, Y., Zhao, Y., Chen, X., Li, Z., Qin, W., Yang, G., & Liu, L. (2019). Chronic myelogenous leukemia cells remodel the bone marrow niche via exosome-mediated transfer of miR-320. *Theranostics*, *9*(19), 5642-5656. https://doi.org/10.7150/thno.34813

García-Romero, N., Madurga, R., Rackov, G., Palacín-Aliana, I., Núñez-Torres, R., Asensi-Puig, A., Carrión-Navarro, J., Esteban-Rubio, S., Peinado, H., González-Neira, A., González-Rumayor, V., Belda-Iniesta, C., & Ayuso-Sacido, A. (2019). Polyethylene glycol improves current methods for circulating extracellular vesicle-derived DNA isolation. *J Transl Med*, *17*(1), 75. https://doi.org/10.1186/s12967-019-1825-3

Gardiner, C., Ferreira, Y. J., Dragovic, R. A., Redman, C. W., & Sargent, I. L. (2013). Extracellular vesicle sizing and enumeration by nanoparticle tracking analysis. *J Extracell Vesicles*, *2*. https://doi.org/10.3402/jev.v2i0.19671

Gebeyehu, A., Kommineni, N., Meckes, D. G., Jr., & Sachdeva, M. S. (2021). Role of Exosomes for Delivery of Chemotherapeutic Drugs. *Crit Rev Ther Drug Carrier Syst*, *38*(5), 53-97. https://doi.org/10.1615/CritRevTherDrugCarrierSyst.2021036301
Gézsi, A., Kovács, Á., Visnovitz, T., & Buzás, E. I. (2019). Systems biology approaches to investigating the roles of extracellular vesicles in human diseases. *Exp Mol Med*, *51*(3), 1-11. https://doi.org/10.1038/s12276-019-0226-2
Glaeser, R. M., & Hall, R. J. (2011). Reaching the information limit in cryo-EM of biological macromolecules: experimental aspects. *Biophys J*, *100*(10), 2331-2337. https://doi.org/10.1016/j.bpj.2011.04.018
Goh, W. J., Lee, C. K., Zou, S., Woon, E. C., Czarny, B., & Pastorin, G. (2017). Doxorubicin-loaded cell-derived nanovesicles: an alternative targeted approach for anti-tumor therapy. *Int J Nanomedicine*, *12*, 2759-2767. https://doi.org/10.2147/ijn.S131786
Gong, C., Tian, J., Wang, Z., Gao, Y., Wu, X., Ding, X., Qiang, L., Li, G., Han, Z., Yuan, Y., & Gao, S. (2019). Functional exosome-mediated co-delivery of doxorubicin and hydrophobically modified microRNA 159 for triple-negative breast cancer therapy. *J Nanobiotechnology*, *17*(1), 93. https://doi.org/10.1186/s12951-019-0526-7
Greening, D. W., Xu, R., Ji, H., Tauro, B. J., & Simpson, R. J. (2015). A protocol for exosome isolation and characterization: evaluation of ultracentrifugation, density-gradient separation, and immunoaffinity capture methods. *Methods Mol Biol*, *1295*, 179-209. https://doi.org/10.1007/978-1-4939-2550-6_15
Gudbergsson, J. M., Johnsen, K. B., Skov, M. N., & Duroux, M. (2016). Systematic review of factors influencing extracellular vesicle yield from cell cultures. *Cytotechnology*, *68*(4), 579-592. https://doi.org/10.1007/s10616-015-9913-6
Gudbergsson, J. M., Jønsson, K., Simonsen, J. B., & Johnsen, K. B. (2019). Systematic review of targeted extracellular vesicles for drug delivery - Considerations on methodological and biological heterogeneity. *J Control Release*, *306*, 108-120. https://doi.org/10.1016/j.jconrel.2019.06.006
Guevara, M. L., Persano, F., & Persano, S. (2020). Advances in Lipid Nanoparticles for mRNA-Based Cancer Immunotherapy. *Front Chem*, *8*, 589959. https://doi.org/10.3389/fchem.2020.589959
Guo, J., Wu, C., Lin, X., Zhou, J., Zhang, J., Zheng, W., Wang, T., & Cui, Y. (2021). Establishment of a simplified dichotomic size-exclusion chromatography for isolating extracellular vesicles toward clinical applications. *J Extracell Vesicles*, *10*(11), e12145. https://doi.org/10.1002/jev2.12145
Gurunathan, S., Kang, M. H., Jeyaraj, M., Qasim, M., & Kim, J. H. (2019). Review of the Isolation, Characterization, Biological Function, and Multifarious Therapeutic Approaches of Exosomes. *Cells*, *8*(4). https://doi.org/10.3390/cells8040307
Gurung, S., Perocheau, D., Touramanidou, L., & Baruteau, J. (2021). The exosome journey: from biogenesis to uptake and intracellular signalling. *Cell Commun Signal*, *19*(1), 47. https://doi.org/10.1186/s12964-021-00730-1
Gussoni, E., Soneoka, Y., Strickland, C. D., Buzney, E. A., Khan, M. K., Flint, A. F., Kunkel, L. M., & Mulligan, R. C. (1999). Dystrophin expression in the mdx mouse restored by stem cell transplantation. *Nature*, *401*(6751), 390-394. https://doi.org/10.1038/43919
Haney, M. J., Klyachko, N. L., Zhao, Y., Gupta, R., Plotnikova, E. G., He, Z., Patel, T., Piroyan, A., Sokolsky, M., Kabanov, A. V., & Batrakova, E. V. (2015). Exosomes as drug delivery vehicles for Parkinson's disease therapy. *J Control Release*, *207*, 18-30. https://doi.org/10.1016/j.jconrel.2015.03.033
Haney, M. J., Zhao, Y., Jin, Y. S., Li, S. M., Bago, J. R., Klyachko, N. L., Kabanov, A. V., & Batrakova, E. V. (2020). Macrophage-Derived Extracellular Vesicles as Drug Delivery Systems for Triple Negative Breast Cancer (TNBC) Therapy. *J Neuroimmune Pharmacol*, *15*(3), 487-500. https://doi.org/10.1007/s11481-019-09884-9
Hannafon, B. N., Trigoso, Y. D., Calloway, C. L., Zhao, Y. D., Lum, D. H., Welm, A. L., Zhao, Z. J., Blick, K. E., Dooley, W. C., & Ding, W. Q. (2016). Plasma exosome microRNAs are indicative of breast cancer. *Breast Cancer Res*, *18*(1), 90. https://doi.org/10.1186/s13058-016-0753-x

Harding, C., Levy, M. A., & Stahl, P. (1985). Morphological analysis of ligand uptake and processing: the role of multivesicular endosomes and CURL in receptor-ligand processing. *Eur J Cell Biol*, *36*(2), 230-238.
Hessvik, N. P., & Llorente, A. (2018). Current knowledge on exosome biogenesis and release. *Cell Mol Life Sci*, *75*(2), 193-208. https://doi.org/10.1007/s00018-017-2595-9
Hessvik, N. P., Øverbye, A., Brech, A., Torgersen, M. L., Jakobsen, I. S., Sandvig, K., & Llorente, A. (2016). PIKfyve inhibition increases exosome release and induces secretory autophagy. *Cell Mol Life Sci*, *73*(24), 4717-4737. https://doi.org/10.1007/s00018-016-2309-8
Hong, C. S., Muller, L., Boyiadzis, M., & Whiteside, T. L. (2014). Isolation and characterization of CD34+ blast-derived exosomes in acute myeloid leukemia. *PLoS One*, *9*(8), e103310. https://doi.org/10.1371/journal.pone.0103310
Hoo, C. M., Starostin, N., West, P., & Mecartney, M. L. (2008). A comparison of atomic force microscopy (AFM) and dynamic light scattering (DLS) methods to characterize nanoparticle size distributions. *Journal of Nanoparticle Research*, *10*(1), 89-96. https://doi.org/10.1007/s11051-008-9435-7
Hoo, C. M., Starostin, N., West, P., & Mecartney, M. L. (2008). A comparison of atomic force microscopy (AFM) and dynamic light scattering (DLS) methods to characterize nanoparticle size distributions. *Journal of Nanoparticle Research*, *10*, 89-96. https://doi.org/10.1007/s11051-008-9435-7
Huang, S. H., Li, Y., Zhang, J., Rong, J., & Ye, S. (2013). Epidermal growth factor receptor-containing exosomes induce tumor-specific regulatory T cells. *Cancer Invest*, *31*(5), 330-335. https://doi.org/10.3109/07357907.2013.789905
Hurley, J. H. (2015). ESCRTs are everywhere. *Embo j*, *34*(19), 2398-2407. https://doi.org/10.15252/embj.201592484
Iqbal, Z., Rehman, K., Mahmood, A., Shabbir, M., Liang, Y., Duan, L., & Zeng, H. (2024). Exosome for mRNA delivery: strategies and therapeutic applications. *J Nanobiotechnology*, *22*(1), 395. https://doi.org/10.1186/s12951-024-02634-x
Jeong, K., Yu, Y. J., You, J. Y., Rhee, W. J., & Kim, J. A. (2020). Exosome-mediated microRNA-497 delivery for anti-cancer therapy in a microfluidic 3D lung cancer model. *Lab Chip*, *20*(3), 548-557. https://doi.org/10.1039/c9lc00958b
Jeong, M., Lee, Y., Park, J., Jung, H., & Lee, H. (2023). Lipid nanoparticles (LNPs) for in vivo RNA delivery and their breakthrough technology for future applications. *Adv Drug Deliv Rev*, *200*, 114990. https://doi.org/10.1016/j.addr.2023.114990
Jeppesen, D. K., Fenix, A. M., Franklin, J. L., Higginbotham, J. N., Zhang, Q., Zimmerman, L. J., Liebler, D. C., Ping, J., Liu, Q., Evans, R., Fissell, W. H., Patton, J. G., Rome, L. H., Burnette, D. T., & Coffey, R. J. (2019). Reassessment of Exosome Composition. *Cell*, *177*(2), 428-445.e418. https://doi.org/10.1016/j.cell.2019.02.029
Jiang, F., Ramanathan, A., Miller, M. T., Tang, G. Q., Gale, M., Jr., Patel, S. S., & Marcotrigiano, J. (2011). Structural basis of RNA recognition and activation by innate immune receptor RIG-I. *Nature*, *479*(7373), 423-427. https://doi.org/10.1038/nature10537
Jiang, Q., Tan, X. P., Zhang, C. H., Li, Z. Y., Li, D., Xu, Y., Liu, Y. X., Wang, L., & Ma, Z. (2022). Non-Coding RNAs of Extracellular Vesicles: Key Players in Organ-Specific Metastasis and Clinical Implications. *Cancers (Basel)*, *14*(22). https://doi.org/10.3390/cancers14225693
Johnsen, K. B., Gudbergsson, J. M., Skov, M. N., Pilgaard, L., Moos, T., & Duroux, M. (2014). A comprehensive overview of exosomes as drug delivery vehicles - endogenous nanocarriers for targeted cancer therapy. *Biochim Biophys Acta*, *1846*(1), 75-87. https://doi.org/10.1016/j.bbcan.2014.04.005
Johnstone, R. M. (2005). Revisiting the road to the discovery of exosomes. *Blood Cells Mol Dis*, *34*(3), 214-219. https://doi.org/10.1016/j.bcmd.2005.03.002
Johnstone, R. M., Adam, M., Hammond, J. R., Orr, L., & Turbide, C. (1987). Vesicle formation during reticulocyte maturation. Association of plasma membrane activities with released vesicles (exosomes). *J Biol Chem*, *262*(19), 9412-9420.

Kaddour, H., Tranquille, M., & Okeoma, C. M. (2021). The Past, the Present, and the Future of the Size Exclusion Chromatography in Extracellular Vesicles Separation. *Viruses*, *13*(11). https://doi.org/10.3390/v13112272

Kalluri, R., & LeBleu, V. S. (2020). The biology, function, and biomedical applications of exosomes. *Science*, *367*(6478). https://doi.org/10.1126/science.aau6977

Kamerkar, S., LeBleu, V. S., Sugimoto, H., Yang, S., Ruivo, C. F., Melo, S. A., Lee, J. J., & Kalluri, R. (2017). Exosomes facilitate therapeutic targeting of oncogenic KRAS in pancreatic cancer. *Nature*, *546*(7659), 498-503. https://doi.org/10.1038/nature22341

Karimi, N., Cvjetkovic, A., Jang, S. C., Crescitelli, R., Hosseinpour Feizi, M. A., Nieuwland, R., Lötvall, J., & Lässer, C. (2018). Detailed analysis of the plasma extracellular vesicle proteome after separation from lipoproteins. *Cell Mol Life Sci*, *75*(15), 2873-2886. https://doi.org/10.1007/s00018-018-2773-4

Kavanagh, E. L., Halasz, M., Dowling, P., Withers, J., Lindsay, S., Higgins, M. J., Irwin, J. A., Rudd, P. M., Saldova, R., & McCann, A. (2021). N-Linked glycosylation profiles of therapeutic induced senescent (TIS) triple negative breast cancer cells (TNBC) and their extracellular vesicle (EV) progeny [10.1039/D0MO00017E]. *Molecular Omics*, *17*(1), 72-85. https://doi.org/10.1039/D0MO00017E

Kis, D., Csordás, I. B., Persa, E., Jezsó, B., Hargitai, R., Szatmári, T., Sándor, N., Kis, E., Balázs, K., Sáfrány, G., & Lumniczky, K. (2022). Extracellular Vesicles Derived from Bone Marrow in an Early Stage of Ionizing Radiation Damage Are Able to Induce Bystander Responses in the Bone Marrow. *Cells*, *11*(1). https://doi.org/10.3390/cells11010155

Koh, Y. Q., Almughlliq, F. B., Vaswani, K., Peiris, H. N., & Mitchell, M. D. (2018). Exosome enrichment by ultracentrifugation and size exclusion chromatography. *Front Biosci (Landmark Ed)*, *23*(5), 865-874. https://doi.org/10.2741/4621

Konoshenko, M. Y., Lekchnov, E. A., Vlassov, A. V., & Laktionov, P. P. (2018). Isolation of Extracellular Vesicles: General Methodologies and Latest Trends. *Biomed Res Int*, *2018*, 8545347. https://doi.org/10.1155/2018/8545347

Kowal, E. J. K., Ter-Ovanesyan, D., Regev, A., & Church, G. M. (2017). Extracellular Vesicle Isolation and Analysis by Western Blotting. *Methods Mol Biol*, *1660*, 143-152. https://doi.org/10.1007/978-1-4939-7253-1_12

Kowal, J., Arras, G., Colombo, M., Jouve, M., Morath, J. P., Primdal-Bengtson, B., Dingli, F., Loew, D., Tkach, M., & Théry, C. (2016). Proteomic comparison defines novel markers to characterize heterogeneous populations of extracellular vesicle subtypes. *Proc Natl Acad Sci U S A*, *113*(8), E968-977. https://doi.org/10.1073/pnas.1521230113

Kowal, J., Tkach, M., & Théry, C. (2014). Biogenesis and secretion of exosomes. *Curr Opin Cell Biol*, *29*, 116-125. https://doi.org/10.1016/j.ceb.2014.05.004

Kuo, W. P., & Jia, S. (2017). *Extracellular vesicles: methods and protocols* (Vol. 1660). Springer.

Lai, R. C., Yeo, R. W., Tan, K. H., & Lim, S. K. (2013). Exosomes for drug delivery - a novel application for the mesenchymal stem cell. *Biotechnol Adv*, *31*(5), 543-551. https://doi.org/10.1016/j.biotechadv.2012.08.008

Latysheva, N., Muratov, G., Rajesh, S., Padgett, M., Hotchin, N. A., Overduin, M., & Berditchevski, F. (2006). Syntenin-1 is a new component of tetraspanin-enriched microdomains: mechanisms and consequences of the interaction of syntenin-1 with CD63. *Mol Cell Biol*, *26*(20), 7707-7718. https://doi.org/10.1128/mcb.00849-06

Le, M., Fernandez-Palomo, C., McNeill, F. E., Seymour, C. B., Rainbow, A. J., & Mothersill, C. E. (2017). Exosomes are released by bystander cells exposed to radiation-induced biophoton signals: Reconciling the mechanisms mediating the bystander effect. *PLoS One*, *12*(3), e0173685. https://doi.org/10.1371/journal.pone.0173685

Lener, T., Gimona, M., Aigner, L., Börger, V., Buzas, E., Camussi, G., Chaput, N., Chatterjee, D., Court, F. A., Del Portillo, H. A., O'Driscoll, L., Fais, S., Falcon-Perez, J. M., Felderhoff-Mueser, U., Fraile, L., Gho, Y. S., Görgens, A., Gupta, R. C., Hendrix, A., . . . Giebel, B. (2015). Applying extracellular vesicles based therapeutics in clinical

trials - an ISEV position paper. *J Extracell Vesicles*, *4*, 30087. https://doi.org/10.3402/jev.v4.30087
Li, Y. J., Wu, J. Y., Wang, J. M., Hu, X. B., Cai, J. X., & Xiang, D. X. (2020). Gemcitabine loaded autologous exosomes for effective and safe chemotherapy of pancreatic cancer. *Acta Biomater*, *101*, 519-530. https://doi.org/10.1016/j.actbio.2019.10.022
Liang, G., Zhu, Y., Ali, D. J., Tian, T., Xu, H., Si, K., Sun, B., Chen, B., & Xiao, Z. (2020). Engineered exosomes for targeted co-delivery of miR-21 inhibitor and chemotherapeutics to reverse drug resistance in colon cancer. *J Nanobiotechnology*, *18*(1), 10. https://doi.org/10.1186/s12951-019-0563-2
Liang, Y., Iqbal, Z., Lu, J., Wang, J., Zhang, H., Chen, X., Duan, L., & Xia, J. (2023). Cell-derived nanovesicle-mediated drug delivery to the brain: Principles and strategies for vesicle engineering. *Mol Ther*, *31*(5), 1207-1224. https://doi.org/10.1016/j.ymthe.2022.10.008
Liangsupree, T., Multia, E., & Riekkola, M. L. (2021). Modern isolation and separation techniques for extracellular vesicles. *J Chromatogr A*, *1636*, 461773. https://doi.org/10.1016/j.chroma.2020.461773
Lima Moura, S., Martì, M., & Pividori, M. I. (2020). Matrix Effect in the Isolation of Breast Cancer-Derived Nanovesicles by Immunomagnetic Separation and Electrochemical Immunosensing-A Comparative Study. *Sensors (Basel)*, *20*(4). https://doi.org/10.3390/s20040965
Lin, Y., Wu, J., Gu, W., Huang, Y., Tong, Z., Huang, L., & Tan, J. (2018). Exosome-Liposome Hybrid Nanoparticles Deliver CRISPR/Cas9 System in MSCs. *Adv Sci (Weinh)*, *5*(4), 1700611. https://doi.org/10.1002/advs.201700611
Liu, C., Guo, J., Tian, F., Yang, N., Yan, F., Ding, Y., Wei, J., Hu, G., Nie, G., & Sun, J. (2017). Field-Free Isolation of Exosomes from Extracellular Vesicles by Microfluidic Viscoelastic Flows. *ACS Nano*, *11*(7), 6968-6976. https://doi.org/10.1021/acsnano.7b02277
Livshits, M. A., Khomyakova, E., Evtushenko, E. G., Lazarev, V. N., Kulemin, N. A., Semina, S. E., Generozov, E. V., & Govorun, V. M. (2016). Corrigendum: Isolation of exosomes by differential centrifugation: Theoretical analysis of a commonly used protocol. *Sci Rep*, *6*, 21447. https://doi.org/10.1038/srep21447
Llorente, A., Skotland, T., Sylvänne, T., Kauhanen, D., Róg, T., Orłowski, A., Vattulainen, I., Ekroos, K., & Sandvig, K. (2013). Molecular lipidomics of exosomes released by PC-3 prostate cancer cells. *Biochim Biophys Acta*, *1831*(7), 1302-1309. https://doi.org/10.1016/j.bbalip.2013.04.011
Lobb, R. J., Becker, M., Wen, S. W., Wong, C. S., Wiegmans, A. P., Leimgruber, A., & Möller, A. (2015). Optimized exosome isolation protocol for cell culture supernatant and human plasma. *J Extracell Vesicles*, *4*, 27031. https://doi.org/10.3402/jev.v4.27031
Lu, M., Shao, W., Xing, H., & Huang, Y. (2023). Extracellular vesicle-based nucleic acid delivery. *Interdisciplinary Medicine*, *1*(2), e20220007. https://doi.org/https://doi.org/10.1002/INMD.20220007
Lu, M., Xing, H., Xun, Z., Yang, T., Zhao, X., Cai, C., Wang, D., & Ding, P. (2018). Functionalized extracellular vesicles as advanced therapeutic nanodelivery systems. *Eur J Pharm Sci*, *121*, 34-46. https://doi.org/10.1016/j.ejps.2018.05.001
Maas, S. L., De Vrij, J., & Broekman, M. L. (2014). Quantification and size-profiling of extracellular vesicles using tunable resistive pulse sensing. *J Vis Exp*(92), e51623. https://doi.org/10.3791/51623
Maguire, C. M., Rösslein, M., Wick, P., & Prina-Mello, A. (2018). Characterisation of particles in solution - a perspective on light scattering and comparative technologies. *Sci Technol Adv Mater*, *19*(1), 732-745. https://doi.org/10.1080/14686996.2018.1517587
Manzanares, D., & Ceña, V. (2020). Endocytosis: The Nanoparticle and Submicron Nanocompounds Gateway into the Cell. *Pharmaceutics*, *12*(4). https://doi.org/10.3390/pharmaceutics12040371

Mashouri, L., Yousefi, H., Aref, A. R., Ahadi, A. M., Molaei, F., & Alahari, S. K. (2019). Exosomes: composition, biogenesis, and mechanisms in cancer metastasis and drug resistance. *Mol Cancer*, *18*(1), 75. https://doi.org/10.1186/s12943-019-0991-5

Mathieu, M., Martin-Jaular, L., Lavieu, G., & Théry, C. (2019). Specificities of secretion and uptake of exosomes and other extracellular vesicles for cell-to-cell communication. *Nat Cell Biol*, *21*(1), 9-17. https://doi.org/10.1038/s41556-018-0250-9

Mathieu, M., Névo, N., Jouve, M., Valenzuela, J. I., Maurin, M., Verweij, F. J., Palmulli, R., Lankar, D., Dingli, F., Loew, D., Rubinstein, E., Boncompain, G., Perez, F., & Théry, C. (2021). Specificities of exosome versus small ectosome secretion revealed by live intracellular tracking of CD63 and CD9. *Nat Commun*, *12*(1), 4389. https://doi.org/10.1038/s41467-021-24384-2

Mathivanan, S., Ji, H., & Simpson, R. J. (2010). Exosomes: extracellular organelles important in intercellular communication. *J Proteomics*, *73*(10), 1907-1920. https://doi.org/10.1016/j.jprot.2010.06.006

Mendt, M., Kamerkar, S., Sugimoto, H., McAndrews, K. M., Wu, C. C., Gagea, M., Yang, S., Blanko, E. V. R., Peng, Q., Ma, X., Marszalek, J. R., Maitra, A., Yee, C., Rezvani, K., Shpall, E., LeBleu, V. S., & Kalluri, R. (2018). Generation and testing of clinical-grade exosomes for pancreatic cancer. *JCI Insight*, *3*(8). https://doi.org/10.1172/jci.insight.99263

Mohammadi, N., Fayazi Hosseini, N., Nemati, H., Moradi-Sardareh, H., Nabi-Afjadi, M., & Kardar, G. A. (2024). Revisiting of Properties and Modified Polyethylenimine-Based Cancer Gene Delivery Systems. *Biochem Genet*, *62*(1), 18-39. https://doi.org/10.1007/s10528-023-10416-7

Mol, E. A., Goumans, M. J., Doevendans, P. A., Sluijter, J. P. G., & Vader, P. (2017). Higher functionality of extracellular vesicles isolated using size-exclusion chromatography compared to ultracentrifugation. *Nanomedicine*, *13*(6), 2061-2065. https://doi.org/10.1016/j.nano.2017.03.011

Momen-Heravi, F. (2017). Isolation of Extracellular Vesicles by Ultracentrifugation. *Methods Mol Biol*, *1660*, 25-32. https://doi.org/10.1007/978-1-4939-7253-1_3

Momen-Heravi, F., Bala, S., Bukong, T., & Szabo, G. (2014). Exosome-mediated delivery of functionally active miRNA-155 inhibitor to macrophages. *Nanomedicine*, *10*(7), 1517-1527. https://doi.org/10.1016/j.nano.2014.03.014

Moradian, H., Roch, T., Lendlein, A., & Gossen, M. (2020). mRNA Transfection-Induced Activation of Primary Human Monocytes and Macrophages: Dependence on Carrier System and Nucleotide Modification. *Sci Rep*, *10*(1), 4181. https://doi.org/10.1038/s41598-020-60506-4

Morales-Kastresana, A., & Jones, J. C. (2017). Flow Cytometric Analysis of Extracellular Vesicles. *Methods Mol Biol*, *1545*, 215-225. https://doi.org/10.1007/978-1-4939-6728-5_16

Mu, W., Rana, S., & Zöller, M. (2013). Host matrix modulation by tumor exosomes promotes motility and invasiveness. *Neoplasia*, *15*(8), 875-887. https://doi.org/10.1593/neo.13786

Munagala, R., Aqil, F., Jeyabalan, J., Kandimalla, R., Wallen, M., Tyagi, N., Wilcher, S., Yan, J., Schultz, D. J., Spencer, W., & Gupta, R. C. (2021). Exosome-mediated delivery of RNA and DNA for gene therapy. *Cancer Lett*, *505*, 58-72. https://doi.org/10.1016/j.canlet.2021.02.011

Nguyen, K. G., Vrabel, M. R., Mantooth, S. M., Hopkins, J. J., Wagner, E. S., Gabaldon, T. A., & Zaharoff, D. A. (2020). Localized Interleukin-12 for Cancer Immunotherapy. *Front Immunol*, *11*, 575597. https://doi.org/10.3389/fimmu.2020.575597

Nie, H., Xie, X., Zhang, D., Zhou, Y., Li, B., Li, F., Li, F., Cheng, Y., Mei, H., Meng, H., & Jia, L. (2020). Use of lung-specific exosomes for miRNA-126 delivery in non-small cell lung cancer. *Nanoscale*, *12*(2), 877-887. https://doi.org/10.1039/c9nr09011h

O'Brien, K., Breyne, K., Ughetto, S., Laurent, L. C., & Breakefield, X. O. (2020). RNA delivery by extracellular vesicles in mammalian cells and its applications. *Nat Rev Mol Cell Biol*, *21*(10), 585-606. https://doi.org/10.1038/s41580-020-0251-y

Onódi, Z., Pelyhe, C., Terézia Nagy, C., Brenner, G. B., Almási, L., Kittel, Á., Manček-Keber, M., Ferdinandy, P., Buzás, E. I., & Giricz, Z. (2018). Isolation of High-Purity Extracellular Vesicles by the Combination of Iodixanol Density Gradient Ultracentrifugation and Bind-Elute Chromatography From Blood Plasma. *Front Physiol*, *9*, 1479. https://doi.org/10.3389/fphys.2018.01479

Ott, P. A., Hu, Z., Keskin, D. B., Shukla, S. A., Sun, J., Bozym, D. J., Zhang, W., Luoma, A., Giobbie-Hurder, A., Peter, L., Chen, C., Olive, O., Carter, T. A., Li, S., Lieb, D. J., Eisenhaure, T., Gjini, E., Stevens, J., Lane, W. J., . . . Wu, C. J. (2017). An immunogenic personal neoantigen vaccine for patients with melanoma. *Nature*, *547*(7662), 217-221. https://doi.org/10.1038/nature22991

Pan, B. T., Teng, K., Wu, C., Adam, M., & Johnstone, R. M. (1985). Electron microscopic evidence for externalization of the transferrin receptor in vesicular form in sheep reticulocytes. *J Cell Biol*, *101*(3), 942-948. https://doi.org/10.1083/jcb.101.3.942

Pang, B., Zhu, Y., Ni, J., Thompson, J., Malouf, D., Bucci, J., Graham, P., & Li, Y. (2020). Extracellular vesicles: the next generation of biomarkers for liquid biopsy-based prostate cancer diagnosis. *Theranostics*, *10*(5), 2309-2326. https://doi.org/10.7150/thno.39486

Pardi, N., Hogan, M. J., Porter, F. W., & Weissman, D. (2018). mRNA vaccines - a new era in vaccinology. *Nat Rev Drug Discov*, *17*(4), 261-279. https://doi.org/10.1038/nrd.2017.243

Patil, S. M., Sawant, S. S., & Kunda, N. K. (2020). Exosomes as drug delivery systems: A brief overview and progress update. *Eur J Pharm Biopharm*, *154*, 259-269. https://doi.org/10.1016/j.ejpb.2020.07.026

Peinado, H., Alečković, M., Lavotshkin, S., Matei, I., Costa-Silva, B., Moreno-Bueno, G., Hergueta-Redondo, M., Williams, C., García-Santos, G., Ghajar, C., Nitadori-Hoshino, A., Hoffman, C., Badal, K., Garcia, B. A., Callahan, M. K., Yuan, J., Martins, V. R., Skog, J., Kaplan, R. N., . . . Lyden, D. (2012). Melanoma exosomes educate bone marrow progenitor cells toward a pro-metastatic phenotype through MET. *Nat Med*, *18*(6), 883-891. https://doi.org/10.1038/nm.2753

Pisitkun, T., Shen, R. F., & Knepper, M. A. (2004). Identification and proteomic profiling of exosomes in human urine. *Proc Natl Acad Sci U S A*, *101*(36), 13368-13373. https://doi.org/10.1073/pnas.0403453101

Polack, F. P., Thomas, S. J., Kitchin, N., Absalon, J., Gurtman, A., Lockhart, S., Perez, J. L., Pérez Marc, G., Moreira, E. D., Zerbini, C., Bailey, R., Swanson, K. A., Roychoudhury, S., Koury, K., Li, P., Kalina, W. V., Cooper, D., Frenck, R. W., Jr., Hammitt, L. L., . . . Gruber, W. C. (2020). Safety and Efficacy of the BNT162b2 mRNA Covid-19 Vaccine. *N Engl J Med*, *383*(27), 2603-2615. https://doi.org/10.1056/NEJMoa2034577

Praja, R. K., Phoksawat, W., Tippayawat, P., Jumnainsong, A., & Leelayuwat, C. (2021). Alternative Method for HDL and Exosome Isolation with Small Serum Volumes and Their Characterizations. *Separations*, *8*(11), 204. https://www.mdpi.com/2297-8739/8/11/204

Raposo, G., Nijman, H. W., Stoorvogel, W., Liejendekker, R., Harding, C. V., Melief, C. J., & Geuze, H. J. (1996). B lymphocytes secrete antigen-presenting vesicles. *J Exp Med*, *183*(3), 1161-1172. https://doi.org/10.1084/jem.183.3.1161

Raposo, G., & Stoorvogel, W. (2013). Extracellular vesicles: exosomes, microvesicles, and friends. *J Cell Biol*, *200*(4), 373-383. https://doi.org/10.1083/jcb.201211138

Reshke, R., Taylor, J. A., Savard, A., Guo, H., Rhym, L. H., Kowalski, P. S., Trung, M. T., Campbell, C., Little, W., Anderson, D. G., & Gibbings, D. (2020). Reduction of the therapeutic dose of silencing RNA by packaging it in extracellular vesicles via a pre-microRNA backbone. *Nat Biomed Eng*, *4*(1), 52-68. https://doi.org/10.1038/s41551-019-0502-4

Rong, Y., Wang, Z., Tang, P., Wang, J., Ji, C., Chang, J., Zhu, Y., Ye, W., Bai, J., Liu, W., Yin, G., Yu, L., Zhou, X., & Cai, W. (2023). Engineered extracellular vesicles for delivery

of siRNA promoting targeted repair of traumatic spinal cord injury. *Bioact Mater*, *23*, 328-342. https://doi.org/10.1016/j.bioactmat.2022.11.011

Rosado, M., Silva, R., M, G. B., J, G. J., Manadas, B., & Anjo, S. I. (2019). Advances in biomarker detection: Alternative approaches for blood-based biomarker detection. *Adv Clin Chem*, *92*, 141-199. https://doi.org/10.1016/bs.acc.2019.04.003

Sahin, U., Derhovanessian, E., Miller, M., Kloke, B. P., Simon, P., Löwer, M., Bukur, V., Tadmor, A. D., Luxemburger, U., Schrörs, B., Omokoko, T., Vormehr, M., Albrecht, C., Paruzynski, A., Kuhn, A. N., Buck, J., Heesch, S., Schreeb, K. H., Müller, F., . . . Türeci, Ö. (2017). Personalized RNA mutanome vaccines mobilize poly-specific therapeutic immunity against cancer. *Nature*, *547*(7662), 222-226. https://doi.org/10.1038/nature23003

Saveyn, H., De Baets, B., Thas, O., Hole, P., Smith, J., & Van der Meeren, P. (2010). Accurate particle size distribution determination by nanoparticle tracking analysis based on 2-D Brownian dynamics simulation. *J Colloid Interface Sci*, *352*(2), 593-600. https://doi.org/10.1016/j.jcis.2010.09.006

Serrano-Pertierra, E., Oliveira-Rodríguez, M., Matos, M., Gutiérrez, G., Moyano, A., Salvador, M., Rivas, M., & Blanco-López, M. C. (2020). Extracellular Vesicles: Current Analytical Techniques for Detection and Quantification. *Biomolecules*, *10*(6). https://doi.org/10.3390/biom10060824

Shao, H., Im, H., Castro, C. M., Breakefield, X., Weissleder, R., & Lee, H. (2018). New Technologies for Analysis of Extracellular Vesicles. *Chem Rev*, *118*(4), 1917-1950. https://doi.org/10.1021/acs.chemrev.7b00534

Shieh, T.-M., Tseng, Y.-H., Hsia, S.-M., Wang, T.-H., Lan, W.-C., & Shih, Y.-H. (2022). Optimization Protocol of the PEG-Based Method for OSCC-Derived Exosome Isolation and Downstream Applications. *Separations*, *9*(12), 435. https://www.mdpi.com/2297-8739/9/12/435

Shtam, T. A., Kovalev, R. A., Varfolomeeva, E. Y., Makarov, E. M., Kil, Y. V., & Filatov, M. V. (2013). Exosomes are natural carriers of exogenous siRNA to human cells in vitro. *Cell Commun Signal*, *11*, 88. https://doi.org/10.1186/1478-811x-11-88

Shu, S., Yang, Y., Allen, C. L., Hurley, E., Tung, K. H., Minderman, H., Wu, Y., & Ernstoff, M. S. (2020). Purity and yield of melanoma exosomes are dependent on isolation method. *J Extracell Vesicles*, *9*(1), 1692401. https://doi.org/10.1080/20013078.2019.1692401

Sidhom, K., Obi, P. O., & Saleem, A. (2020). A Review of Exosomal Isolation Methods: Is Size Exclusion Chromatography the Best Option? *Int J Mol Sci*, *21*(18). https://doi.org/10.3390/ijms21186466

Simons, M., & Raposo, G. (2009). Exosomes--vesicular carriers for intercellular communication. *Curr Opin Cell Biol*, *21*(4), 575-581. https://doi.org/10.1016/j.ceb.2009.03.007

Simpson, R. J., Jensen, S. S., & Lim, J. W. (2008). Proteomic profiling of exosomes: current perspectives. *Proteomics*, *8*(19), 4083-4099. https://doi.org/10.1002/pmic.200800109

Sitar, S., Kejžar, A., Pahovnik, D., Kogej, K., Tušek-Žnidarič, M., Lenassi, M., & Žagar, E. (2015). Size characterization and quantification of exosomes by asymmetrical-flow field-flow fractionation. *Anal Chem*, *87*(18), 9225-9233. https://doi.org/10.1021/acs.analchem.5b01636

Skotland, T., Sandvig, K., & Llorente, A. (2017). Lipids in exosomes: Current knowledge and the way forward. *Prog Lipid Res*, *66*, 30-41. https://doi.org/10.1016/j.plipres.2017.03.001

Somiya, M., Yoshioka, Y., & Ochiya, T. (2018). Biocompatibility of highly purified bovine milk-derived extracellular vesicles. *J Extracell Vesicles*, *7*(1), 1440132. https://doi.org/10.1080/20013078.2018.1440132

Soo, C. Y., Song, Y., Zheng, Y., Campbell, E. C., Riches, A. C., Gunn-Moore, F., & Powis, S. J. (2012). Nanoparticle tracking analysis monitors microvesicle and exosome secretion from immune cells. *Immunology*, *136*(2), 192-197. https://doi.org/10.1111/j.1365-2567.2012.03569.x

Stoorvogel, W., Kleijmeer, M. J., Geuze, H. J., & Raposo, G. (2002). The biogenesis and functions of exosomes. *Traffic*, *3*(5), 321-330. https://doi.org/10.1034/j.1600-0854.2002.30502.x

Swanson, J. A., & Watts, C. (1995). Macropinocytosis. *Trends Cell Biol*, *5*(11), 424-428. https://doi.org/10.1016/s0962-8924(00)89101-1

Tao, H., Xu, H., Zuo, L., Li, C., Qiao, G., Guo, M., Zheng, L., Leitgeb, M., & Lin, X. (2020). Exosomes-coated bcl-2 siRNA inhibits the growth of digestive system tumors both in vitro and in vivo. *Int J Biol Macromol*, *161*, 470-480. https://doi.org/10.1016/j.ijbiomac.2020.06.052

Tenchov, R., Sasso, J. M., Wang, X., Liaw, W. S., Chen, C. A., & Zhou, Q. A. (2022). Exosomes─Nature's Lipid Nanoparticles, a Rising Star in Drug Delivery and Diagnostics. *ACS Nano*, *16*(11), 17802-17846. https://doi.org/10.1021/acsnano.2c08774

Ter-Ovanesyan, D., Norman, M., Lazarovits, R., Trieu, W., Lee, J. H., Church, G. M., & Walt, D. R. (2021). Framework for rapid comparison of extracellular vesicle isolation methods. *Elife*, *10*. https://doi.org/10.7554/eLife.70725

Terstappen, G. C., Meyer, A. H., Bell, R. D., & Zhang, W. (2021). Strategies for delivering therapeutics across the blood-brain barrier. *Nat Rev Drug Discov*, *20*(5), 362-383. https://doi.org/10.1038/s41573-021-00139-y

Théry, C., Amigorena, S., Raposo, G., & Clayton, A. (2006). Isolation and characterization of exosomes from cell culture supernatants and biological fluids. *Curr Protoc Cell Biol*, *Chapter 3*, Unit 3.22. https://doi.org/10.1002/0471143030.cb0322s30

Théry, C., Duban, L., Segura, E., Véron, P., Lantz, O., & Amigorena, S. (2002). Indirect activation of naïve CD4+ T cells by dendritic cell-derived exosomes. *Nat Immunol*, *3*(12), 1156-1162. https://doi.org/10.1038/ni854

Théry, C., Regnault, A., Garin, J., Wolfers, J., Zitvogel, L., Ricciardi-Castagnoli, P., Raposo, G., & Amigorena, S. (1999). Molecular characterization of dendritic cell-derived exosomes. Selective accumulation of the heat shock protein hsc73. *J Cell Biol*, *147*(3), 599-610. https://doi.org/10.1083/jcb.147.3.599

Théry, C., Witwer, K. W., Aikawa, E., Alcaraz, M. J., Anderson, J. D., Andriantsitohaina, R., Antoniou, A., Arab, T., Archer, F., Atkin-Smith, G. K., Ayre, D. C., Bach, J. M., Bachurski, D., Baharvand, H., Balaj, L., Baldacchino, S., Bauer, N. N., Baxter, A. A., Bebawy, M., . . . Zuba-Surma, E. K. (2018). Minimal information for studies of extracellular vesicles 2018 (MISEV2018): a position statement of the International Society for Extracellular Vesicles and update of the MISEV2014 guidelines. *J Extracell Vesicles*, *7*(1), 1535750. https://doi.org/10.1080/20013078.2018.1535750

Tkach, M., & Théry, C. (2016). Communication by Extracellular Vesicles: Where We Are and Where We Need to Go. *Cell*, *164*(6), 1226-1232. https://doi.org/10.1016/j.cell.2016.01.043

Towbin, H., Staehelin, T., & Gordon, J. (1979). Electrophoretic transfer of proteins from polyacrylamide gels to nitrocellulose sheets: procedure and some applications. *Proc Natl Acad Sci U S A*, *76*(9), 4350-4354. https://doi.org/10.1073/pnas.76.9.4350

Trajkovic, K., Hsu, C., Chiantia, S., Rajendran, L., Wenzel, D., Wieland, F., Schwille, P., Brügger, B., & Simons, M. (2008). Ceramide triggers budding of exosome vesicles into multivesicular endosomes. *Science*, *319*(5867), 1244-1247. https://doi.org/10.1126/science.1153124

Tran, P. H. L., Wang, T., Yin, W., Tran, T. T. D., Nguyen, T. N. G., Lee, B. J., & Duan, W. (2019). Aspirin-loaded nanoexosomes as cancer therapeutics. *Int J Pharm*, *572*, 118786. https://doi.org/10.1016/j.ijpharm.2019.118786

Trepotec, Z., Lichtenegger, E., Plank, C., Aneja, M. K., & Rudolph, C. (2019). Delivery of mRNA Therapeutics for the Treatment of Hepatic Diseases. *Mol Ther*, *27*(4), 794-802. https://doi.org/10.1016/j.ymthe.2018.12.012

Uchida, S., Perche, F., Pichon, C., & Cabral, H. (2020). Nanomedicine-Based Approaches for mRNA Delivery. *Mol Pharm*, *17*(10), 3654-3684. https://doi.org/10.1021/acs.molpharmaceut.0c00618

Valadi, H., Ekström, K., Bossios, A., Sjöstrand, M., Lee, J. J., & Lötvall, J. O. (2007). Exosome-mediated transfer of mRNAs and microRNAs is a novel mechanism of genetic exchange between cells. *Nat Cell Biol*, *9*(6), 654-659. https://doi.org/10.1038/ncb1596

van der Pol, E., Coumans, F. A., Grootemaat, A. E., Gardiner, C., Sargent, I. L., Harrison, P., Sturk, A., van Leeuwen, T. G., & Nieuwland, R. (2014). Particle size distribution of exosomes and microvesicles determined by transmission electron microscopy, flow cytometry, nanoparticle tracking analysis, and resistive pulse sensing. *J Thromb Haemost*, *12*(7), 1182-1192. https://doi.org/10.1111/jth.12602

van Niel, G., Charrin, S., Simoes, S., Romao, M., Rochin, L., Saftig, P., Marks, M. S., Rubinstein, E., & Raposo, G. (2011). The tetraspanin CD63 regulates ESCRT-independent and -dependent endosomal sorting during melanogenesis. *Dev Cell*, *21*(4), 708-721. https://doi.org/10.1016/j.devcel.2011.08.019

van Niel, G., D'Angelo, G., & Raposo, G. (2018). Shedding light on the cell biology of extracellular vesicles. *Nat Rev Mol Cell Biol*, *19*(4), 213-228. https://doi.org/10.1038/nrm.2017.125

van Niel, G., Porto-Carreiro, I., Simoes, S., & Raposo, G. (2006). Exosomes: a common pathway for a specialized function. *J Biochem*, *140*(1), 13-21. https://doi.org/10.1093/jb/mvj128

Vergauwen, G., Dhondt, B., Van Deun, J., De Smedt, E., Berx, G., Timmerman, E., Gevaert, K., Miinalainen, I., Cocquyt, V., Braems, G., Van den Broecke, R., Denys, H., De Wever, O., & Hendrix, A. (2017). Confounding factors of ultrafiltration and protein analysis in extracellular vesicle research. *Sci Rep*, *7*(1), 2704. https://doi.org/10.1038/s41598-017-02599-y

Vogel, R., Coumans, F. A., Maltesen, R. G., Böing, A. N., Bonnington, K. E., Broekman, M. L., Broom, M. F., Buzás, E. I., Christiansen, G., Hajji, N., Kristensen, S. R., Kuehn, M. J., Lund, S. M., Maas, S. L., Nieuwland, R., Osteikoetxea, X., Schnoor, R., Scicluna, B. J., Shambrook, M., . . . Pedersen, S. (2016). A standardized method to determine the concentration of extracellular vesicles using tunable resistive pulse sensing. *J Extracell Vesicles*, *5*, 31242. https://doi.org/10.3402/jev.v5.31242

Vogel, R., Willmott, G., Kozak, D., Roberts, G. S., Anderson, W., Groenewegen, L., Glossop, B., Barnett, A., Turner, A., & Trau, M. (2011). Quantitative sizing of nano/microparticles with a tunable elastomeric pore sensor. *Anal Chem*, *83*(9), 3499-3506. https://doi.org/10.1021/ac200195n

Wahlgren, J., De, L. K. T., Brisslert, M., Vaziri Sani, F., Telemo, E., Sunnerhagen, P., & Valadi, H. (2012). Plasma exosomes can deliver exogenous short interfering RNA to monocytes and lymphocytes. *Nucleic Acids Res*, *40*(17), e130. https://doi.org/10.1093/nar/gks463

Wallen, M., Aqil, F., Spencer, W., & Gupta, R. C. (2023). Exosomes as an Emerging Plasmid Delivery Vehicle for Gene Therapy. *Pharmaceutics*, *15*(7). https://doi.org/10.3390/pharmaceutics15071832

Wang, H., Sui, H., Zheng, Y., Jiang, Y., Shi, Y., Liang, J., & Zhao, L. (2019). Curcumin-primed exosomes potently ameliorate cognitive function in AD mice by inhibiting hyperphosphorylation of the Tau protein through the AKT/GSK-3β pathway. *Nanoscale*, *11*(15), 7481-7496. https://doi.org/10.1039/c9nr01255a

Wang, J., Ma, P., Kim, D. H., Liu, B. F., & Demirci, U. (2021). Towards Microfluidic-Based Exosome Isolation and Detection for Tumor Therapy. *Nano Today*, *37*. https://doi.org/10.1016/j.nantod.2020.101066

Webber, J., & Clayton, A. (2013). How pure are your vesicles? *J Extracell Vesicles*, *2*. https://doi.org/10.3402/jev.v2i0.19861

Weng, Y., Sui, Z., Shan, Y., Hu, Y., Chen, Y., Zhang, L., & Zhang, Y. (2016). Effective isolation of exosomes with polyethylene glycol from cell culture supernatant for in-depth proteome profiling. *Analyst*, *141*(15), 4640-4646. https://doi.org/10.1039/c6an00892e

Witwer, K. W., Buzás, E. I., Bemis, L. T., Bora, A., Lässer, C., Lötvall, J., Nolte-'t Hoen, E. N., Piper, M. G., Sivaraman, S., Skog, J., Théry, C., Wauben, M. H., & Hochberg, F. (2013). Standardization of sample collection, isolation and analysis methods in extracellular vesicle research. *J Extracell Vesicles*, *2*. https://doi.org/10.3402/jev.v2i0.20360

Wolf, P. (1967). The nature and significance of platelet products in human plasma. *Br J Haematol*, *13*(3), 269-288. https://doi.org/10.1111/j.1365-2141.1967.tb08741.x

Xie, Y., Guan, Q., Guo, J., Chen, Y., Yin, Y., & Han, X. (2022). Hydrogels for Exosome Delivery in Biomedical Applications. *Gels*, *8*(6). https://doi.org/10.3390/gels8060328

Xu, L., Faruqu, F. N., Lim, Y. M., Lim, K. Y., Liam-Or, R., Walters, A. A., Lavender, P., Fear, D., Wells, C. M., Tzu-Wen Wang, J., & Al-Jamal, K. T. (2021). Exosome-mediated RNAi of PAK4 prolongs survival of pancreatic cancer mouse model after loco-regional treatment. *Biomaterials*, *264*, 120369. https://doi.org/10.1016/j.biomaterials.2020.120369

Yáñez-Mó, M., Siljander, P. R., Andreu, Z., Zavec, A. B., Borràs, F. E., Buzas, E. I., Buzas, K., Casal, E., Cappello, F., Carvalho, J., Colás, E., Cordeiro-da Silva, A., Fais, S., Falcon-Perez, J. M., Ghobrial, I. M., Giebel, B., Gimona, M., Graner, M., Gursel, I., . . . De Wever, O. (2015). Biological properties of extracellular vesicles and their physiological functions. *J Extracell Vesicles*, *4*, 27066. https://doi.org/10.3402/jev.v4.27066

Yang, D., Zhang, W., Zhang, H., Zhang, F., Chen, L., Ma, L., Larcher, L. M., Chen, S., Liu, N., Zhao, Q., Tran, P. H. L., Chen, C., Veedu, R. N., & Wang, T. (2020). Progress, opportunity, and perspective on exosome isolation - efforts for efficient exosome-based theranostics. *Theranostics*, *10*(8), 3684-3707. https://doi.org/10.7150/thno.41580

Yang, Y., Wang, Y., Wei, S., Zhou, C., Yu, J., Wang, G., Wang, W., & Zhao, L. (2021). Extracellular vesicles isolated by size-exclusion chromatography present suitability for RNomics analysis in plasma. *J Transl Med*, *19*(1), 104. https://doi.org/10.1186/s12967-021-02775-9

Yerneni, S. S., Yalcintas, E. P., Smith, J. D., Averick, S., Campbell, P. G., & Ozdoganlar, O. B. (2022). Skin-targeted delivery of extracellular vesicle-encapsulated curcumin using dissolvable microneedle arrays. *Acta Biomater*, *149*, 198-212. https://doi.org/10.1016/j.actbio.2022.06.046

Yuan, X., Sun, L., Jeske, R., Nkosi, D., York, S. B., Liu, Y., Grant, S. C., Meckes, D. G., Jr., & Li, Y. (2022). Engineering extracellular vesicles by three-dimensional dynamic culture of human mesenchymal stem cells. *J Extracell Vesicles*, *11*(6), e12235. https://doi.org/10.1002/jev2.12235

Yuana, Y., Levels, J., Grootemaat, A., Sturk, A., & Nieuwland, R. (2014). Co-isolation of extracellular vesicles and high-density lipoproteins using density gradient ultracentrifugation. *J Extracell Vesicles*, *3*. https://doi.org/10.3402/jev.v3.23262

Yuyama, K., & Igarashi, Y. (2016). Physiological and pathological roles of exosomes in the nervous system. *Biomol Concepts*, *7*(1), 53-68. https://doi.org/10.1515/bmc-2015-0033

Zabeo, D., Cvjetkovic, A., Lässer, C., Schorb, M., Lötvall, J., & Höög, J. L. (2017). Exosomes purified from a single cell type have diverse morphology. *J Extracell Vesicles*, *6*(1), 1329476. https://doi.org/10.1080/20013078.2017.1329476

Zakeri, A., Kouhbanani, M. A. J., Beheshtkhoo, N., Beigi, V., Mousavi, S. M., Hashemi, S. A. R., Karimi Zade, A., Amani, A. M., Savardashtaki, A., Mirzaei, E., Jahandideh, S., & Movahedpour, A. (2018). Polyethylenimine-based nanocarriers in co-delivery of drug and gene: a developing horizon. *Nano Rev Exp*, *9*(1), 1488497. https://doi.org/10.1080/20022727.2018.1488497

Zeng, H., Guo, S., Ren, X., Wu, Z., Liu, S., & Yao, X. (2023). Current Strategies for Exosome Cargo Loading and Targeting Delivery. *Cells*, *12*(10). https://doi.org/10.3390/cells12101416

Zeng, W., Wen, Z., Chen, H., & Duan, Y. (2023). Exosomes as Carriers for Drug Delivery in Cancer Therapy. *Pharm Res*, *40*(4), 873-887. https://doi.org/10.1007/s11095-022-03224-y

Zeringer, E., Barta, T., Li, M., & Vlassov, A. V. (2015). Strategies for isolation of exosomes. *Cold Spring Harb Protoc*, *2015*(4), 319-323. https://doi.org/10.1101/pdb.top074476

Zhang, F., Parayath, N. N., Ene, C. I., Stephan, S. B., Koehne, A. L., Coon, M. E., Holland, E. C., & Stephan, M. T. (2019). Genetic programming of macrophages to perform anti-tumor functions using targeted mRNA nanocarriers. *Nat Commun*, *10*(1), 3974. https://doi.org/10.1038/s41467-019-11911-5

Zhang, H. G., & Grizzle, W. E. (2014). Exosomes: a novel pathway of local and distant intercellular communication that facilitates the growth and metastasis of neoplastic lesions. *Am J Pathol*, *184*(1), 28-41. https://doi.org/10.1016/j.ajpath.2013.09.027

Zhang, J., Li, S., Li, L., Li, M., Guo, C., Yao, J., & Mi, S. (2015). Exosome and exosomal microRNA: trafficking, sorting, and function. *Genomics Proteomics Bioinformatics*, *13*(1), 17-24. https://doi.org/10.1016/j.gpb.2015.02.001

Zhang, L., Fan, C., Hao, W., Zhuang, Y., Liu, X., Zhao, Y., Chen, B., Xiao, Z., Chen, Y., & Dai, J. (2021). NSCs Migration Promoted and Drug Delivered Exosomes-Collagen Scaffold via a Bio-Specific Peptide for One-Step Spinal Cord Injury Repair. *Adv Healthc Mater*, *10*(8), e2001896. https://doi.org/10.1002/adhm.202001896

Zhang, X., Yuan, X., Shi, H., Wu, L., Qian, H., & Xu, W. (2015). Exosomes in cancer: small particle, big player. *J Hematol Oncol*, *8*, 83. https://doi.org/10.1186/s13045-015-0181-x

Zhang, Y., Liu, D., Chen, X., Li, J., Li, L., Bian, Z., Sun, F., Lu, J., Yin, Y., Cai, X., Sun, Q., Wang, K., Ba, Y., Wang, Q., Wang, D., Yang, J., Liu, P., Xu, T., Yan, Q., . . . Zhang, C. Y. (2010). Secreted monocytic miR-150 enhances targeted endothelial cell migration. *Mol Cell*, *39*(1), 133-144. https://doi.org/10.1016/j.molcel.2010.06.010

Zhang, Y., Liu, Y., Liu, H., & Tang, W. H. (2019). Exosomes: biogenesis, biologic function and clinical potential. *Cell Biosci*, *9*, 19. https://doi.org/10.1186/s13578-019-0282-2

Zhu, L., Sun, H. T., Wang, S., Huang, S. L., Zheng, Y., Wang, C. Q., Hu, B. Y., Qin, W., Zou, T. T., Fu, Y., Shen, X. T., Zhu, W. W., Geng, Y., Lu, L., Jia, H. L., Qin, L. X., & Dong, Q. Z. (2020). Isolation and characterization of exosomes for cancer research. *J Hematol Oncol*, *13*(1), 152. https://doi.org/10.1186/s13045-020-00987-y

Zhu, X., Badawi, M., Pomeroy, S., Sutaria, D. S., Xie, Z., Baek, A., Jiang, J., Elgamal, O. A., Mo, X., Perle, K., Chalmers, J., Schmittgen, T. D., & Phelps, M. A. (2017). Comprehensive toxicity and immunogenicity studies reveal minimal effects in mice following sustained dosing of extracellular vesicles derived from HEK293T cells. *J Extracell Vesicles*, *6*(1), 1324730. https://doi.org/10.1080/20013078.2017.1324730

Zhuang, J., Tan, J., Wu, C., Zhang, J., Liu, T., Fan, C., Li, J., & Zhang, Y. (2020). Extracellular vesicles engineered with valency-controlled DNA nanostructures deliver CRISPR/Cas9 system for gene therapy. *Nucleic Acids Res*, *48*(16), 8870-8882. https://doi.org/10.1093/nar/gkaa683

Zomer, A., Vendrig, T., Hopmans, E. S., van Eijndhoven, M., Middeldorp, J. M., & Pegtel, D. M. (2010). Exosomes: Fit to deliver small RNA. *Commun Integr Biol*, *3*(5), 447-450. https://doi.org/10.4161/cib.3.5.12339